1989

Effect of electrically driven particles on air flow in a rectangular duct

Ahmed Mohie El-Din Saad Sarhan
Iowa State University

Order Number 9014950

Effect of electrically driven particles on air flow in a rectangular duct

Sarhan, Ahmed Mohie El-Din Saad, Ph.D.

Iowa State University, 1989

U·M·I
300 N. Zeeb Rd.
Ann Arbor, MI 48106

Effect of electrically driven particles on air flow in a rectangular duct

by

Ahmed Mohie El-Din Saad Sarhan

A Dissertation Submitted to the
Graduate Faculty in Partial Fulfillment of the
Requirements for the Degree of
DOCTOR OF PHILOSOPHY

Major: Mechanical Engineering

Approved:

Signature was redacted for privacy.

In Charge of Major Work

Signature was redacted for privacy.

For the Major Department

Signature was redacted for privacy.

For the Graduate College

Iowa State University
Ames, Iowa

1989

TABLE OF CONTENTS

NOMENCLATURE

A	Cross sectional area
C	Calibration factor
C_D	Drag coefficient
$\bar{C}_D$	Apparent drag coefficient
D_p	Particle diameter
D_H	Hydraulic diameter of the duct
E	Electric field strength
E_{LL}	Minimum electric field strength for sustained particle motion
E_{LO}	Minimum lift-off electric field strength
F	Force
F_D	Drag force
F_E	Force due to the electric field
G	Volumetric flow rate
L	Length
L_{ss}	Length of the duct where the steady state condition can be maintained
M	Slope
N	Number of particles per unit volume of the material
Q	Charge acquired by a particle
Re_D	Reynolds number based on the duct hydraulic diameter and the air bulk velocity
Re_p	Reynolds number based on the partcle diameter and the relative air to particle velocity

$Re_{p,lim}$	Reynolds number of the oscillating particles when the absolute air velocity tends to zero
$\bar{Re}_p$	Modified particle Reynolds number
S	Cross-sectional area of the particle
V	Velocity or volt
W	Weight
X	Variable
a	Radius of the spherical particle, or semi major axes in x-direction
b	Semi major axes in y-direction
c	Semi major axes in z-direction
d_f	Beam waist diameter of the focused laser beams
e_b, e_t	Coefficient of restitution (e_t - top, e_b - bottom)
f	Friction factor
f_D	Doppler shift frequency
f_i	Frequency of the incident light
f_s	Frequency of the scattered light
$\bar{f}$	Friction factor per unit mass flow rate of solid particles
P	Separation distance of the electrodes
m	Mass
$\dot{m}$	Mass flow rate
n	Particle number density
p	Pressure
Wp	Pressure drop
t	Time

Wt	Time difference
Wt_c	Particle wall collision time
Wt_f	Time of particle motion in the fluid
u	Horizontal velocity component
v	Vertical velocity component
x	Distance
a	Particles rotational relaxation ($0 \leq a \leq 1$)
a_p	Particles to air volume ratio
b	Slip coefficient ($0 \leq b \leq 1$)
b_1, b_2, b_3	Parameters in Equations (3.23-3.26)
q	Coefficient accounts to the charge reduction due to collision or ratio of specific heats
Wp	Pressure drop
Wt	Time difference
w_f	Fringe spacing (nm)
G	Mean interparticle spacing
e_{CD}	Expected error in the measurement of the apparent drag coefficient
e_D	Expected error in the measurement of the particle diameter
e_E	Expected error in the measurement of the electric field strength
e_F	Expected error in the measurement of the friction factor
e_G	Expected error in the measurement of the particles volumetric rates
e_L	Expected error in the measurement of the duct dimensions

$e_{\dot{m}}^{\circ}$	Expected error in the measurement of the particles mass flow rates
e_n	Expected error in the measurement of the particle number density
e_p	Expected error in the measurement of the pressure
e_{pa}	Expected error in the measurement of the pressure drop due to air flow
e_{ps}	Expected error in the measurement of the pressure drop due to solids
e_{ps-a}	Expected error in the measurement of the pressure drop due to solid air flow
e_{ReD}	Expected error in the measurement of the duct Reynolds number
$e_{Re,lim}$	Expected error in the measurement of the limiting Reynolds number
e_{Rep}	Expected error in the measurement of the particle Reynolds number
$e_{\overline{Rep}}$	Expected error in the measurement of the modified Reynolds number
e_V	Expected error in the measurement of the voltage
e_v, e_u	Expected error in the measurement of the particle velocity components v and u
e_{ua}	Expected error in the measurement of the air bulk velocity
e_u, e_h, e_z	Expected error in the measurement of the parameters u, h, z
r	Angle between the two intersecting laser beams

c	Angle of the particle velocity vector with the horizontal axes
g	Wave length of incident light (nm)
)	Dynamic viscocity of air
n	Kinematic viscocity of air
p	Mass density
u, h, z	Measure parameters
h	Loading of the line, solid to air mass ratio
w(ẇ)	Particle angular rotation before (after) collision

Subscripts

a	Air
b	Bottom
c	Contact
D	Duct
H	Hydraulic
Lim	Limiting
o	Initial
p	Particle
r	Relative
s	Solid
s-a	Solids plus air
ss	Steady state
st	At standard conditions
t	Tangential

w	Wall
(1-13)	Location of the pressure tap (see Figure 4.1)

Superscripts

'	After
-	Average quantity

1. INTRODUCTION

Pneumatic conveying has been useful in transporting, distributing, and processing of particulate materials. It takes the form of solid-gas suspension. The particulate materials are often limited to materials of large strength, such as immune to attrition or breakage by impact.

The basic elements of a pneumatic conveying system usually include a feeder for the solids, a gas blower, a pipeline covering the distance of transport, and a collector to recover the solids.

Pneumatic pipelines up to 2000 m long [1] have been designed for transporting various solids in pipes up to 360 mm in diameter handling capacities of hundreds of tons per hour. Pneumatic conveying systems cover the size range of dust down to 1 μm to coal in mine hoists up to 100 mm size. Above that size, it becomes advisable to use chutes or belt conveyers. Pneumatic conveying has the advantage of handling bulk materials in a closed system; it also belongs to means for automation.

The mass ratio of solids to gas tends to be low (dilute suspension) for transport over short distances for reliability; economy is usually gained here in the savings in labor. Long distance transport of several km may call for more dense suspensions.

One should recognize the absence of a well-founded, precise, scientific theory which would embrace all problems in detail and which has undergone verification in practice. The wide variety in the physical properties of the materials being conveyed, and the multiplicity of design possibilities hamper calculations by specific formulae. Installations have often been

designed on an empirical basis adapting the results of research or extending and scaling up based on the current practice.

Electrically augmented pneumatic conveying is a new technique aimed at the implementation of an electric field to suspend the particles in the duct in which the conveying air can have a lower velocity than that of a conventional pneumatic system. Electrically augmented pneumatic conveying can have the advantage of being more economical beside being more controllable, as the particles are uniformly suspended and the air can have a lower velocity. The electric suspension can also provide a good tool for studying the particulate behavior at velocities below the saltation velocity.

The present work is an experimental investigation into the effect of the electric field strength on conveyability of solids in a rectangular duct. A rectangular duct was constructed with upper and lower walls of brass while the side walls were of glass. The duct measured 5.25 cm in width, 1.6 cm in height, and 225 cm in length. Particles were supplied to the duct by an Auger particle feeder and collected by an air cyclone. The air bulk speed was measured by a systems of rotameters, while the particle velocity was measured by a Laser Doppler Anemometer. The investigation covered copper particles having diameters of (63-75, 74-88) μm and glass particles having diameters of (44-63, 63-74, and 74-88) μm. The Reynolds number based on the particle diameter was ranged from 5 to 32 while the Reynolds number based on the duct hydraulic diameter was ranged from 1300 to 12551 covering the lamenar, transient and turbulent regimes of flow.

The steady state pressure drop per unit length of the duct was theoretically calculated for the cases of the laminar air flow regime, and compared to the corresponding measured values.

Results of this investigation show that conveying particle in the transient air flow regime is the most economical, and the use of the electric augmentation technique can further decrease the required conveying power. Correlations of the drag coefficient for both copper and glass particles were also obtained in the range of laminar, transient, and low turbulent regimes of flow for an electric field strength of 5 kv/cm and the aforementioned duct size.

2. REVIEW OF RELATED LITERATURE

Pneumatic conveying has been useful in transporting, distributing, and processing of particulate materials. It takes the form of a solid-gas suspension. In the majority of cases, pneumatic means use of air.

The study of the particles dynamics can be classified according to the volume containing the particle into totally confined, partially confined and totally unconfined volume. Beside this classification the solid-gas mixture can be either a dense or a dilute mixture. In the dense mixtures, the particle-particle interaction plays a significant role, while in dilute mixtures the particle-particle interaction plays a secondary role or even can be ignored (in a very dilute mixture). Soo [1] took the ratio of mean free path of particle-to-particle collision (λ) to the interparticle spacing ($n^{-1/3}$) (given by the number density of the particles (n) as a dividing line between a dilute and dense mixture. The mixture is said to be dense if $\lambda/n^{-1/3} < 1$ and is said to be dilute if $\lambda/n^{-1/3} > 1$. The present work belongs to the case of very diluted mixture.

2.1. Particles in a Totally Confined Volume

In order to create the particle motion in a totally confined volume, there should be some force applied to the particle overcoming the gravity force and the drag force created by the particle motion. Colver [2] reported that if particles with diameters up to 1.5 mm of a semi-insulating or conducting material are confined between two parallel plates of capacitor with a high voltage DC source, these particles will accelerate

between the two plates creating an Electric Particulate Suspension (EPS). Mass, heat, and charge transfer will occur as a result of this motion.

Colver [3] defined the electric particulate suspension EPS as a cloud containing charged particles which is formed or sustained with an applied electric field as a direct result of electric field induced or otherwise electrically controlled particle charging at a particle wall interface. The strength of the electric field is of the order of KV/cm.

Colver [4] introduced the theoretical background, confirmed by the necessary experimental verifications, for the relations governing the particle motion, heat and charge transfer between two paralleled plates (electrodes or capacitors). This theoretical foundation was introduced for both single and multiple particle phenomena. He predicted mathematically that a single particle can not oscillate smoothly unless the electric field strength reaches some minimum value depending on the particle material and size. Consequently there is a minimum velocity corresponding to this minimum electric field strength. The experimental study in the present work confirmed this phenomenon for multiple particles, but the minimum electric field strength and the corresponding minimum velocity are found to be dependent on the material of the particle but not the particle size. That can be explained by the above theory. That is, when the electric field strength reaches some minimum value it will be able to suspend some amount of the particles corresponding to this strength but it will not necessarily suspend all of the particles contained between the two capacitor plates. If an electric field strength were defined as the minimum electric field necessary for driving all the contained mass into

smooth motion, then one expects a particle size dependence to appear. Then one expects that smooth particle motion can be obtained at lower strengths of the electric field.

Colver and Howel [5] gave a useful expression for the current intensity that can be transferred by a cloud of particles between the two parallel capacitor as a linear function of the particle number density, the average vertical velocity of the particles, the initial charge acquired by each particle, and a constant given by 0.57. They also studied the diffusion motion of the particles due to particle collisions (in the case of multiple particles) and due to particle wall collisions (in the case of single particle).

In a later paper, Colver and Ehlinger [6] measured the most probable speed, the mean speed, and the root mean square of electrically suspended particles by making a pin hole in the upper electrode for leaking particles. The diameter of the sampling hole was chosen large enough to accommodate the passage of the particles with a minimum of interference on the path of the particles, while it was small enough so as not to appreciably disturb the dynamics of the suspension itself. Particles were collected at different heights above the test hole and the time of exposure at each height was recorded. From the height, the vertical speed of the particles leaving the suspension could be calculated. From the number of particles collected and the time of the exposure the number of particles having speed greater than the calculated speed from the height could be obtained. The measured speeds were reported as (0.77, 0.86, 68 and 0.68) m/s for particle diameters of (44-53, 63-75, and 105-125) μm at an electric

field strength of (11.7, 12.8, and 12.0)KV/cm respectively. These values were measured for a capacitor separation distance of 1 cm. These results were of the same order as results obtained in the present work.

Colver [2-4], Colver and Howel [5], Colver and Ehlinger [6], Cotroneo and Colver [7], and Rudinger [8] used the technique of light attenuation measurement of a laser beam passing through the test section to measure the particle number density n.

2.2. Particle Transport in a Partially Confined Volume

One example of a particle in partially confined volume can be regarded as the solid-gas flow in a duct. The gas flow itself can convey the solid particles if it has a speed greater than the saltation velocity of the conveyed particle. The electric augmentation technique in the pneumatic conveying of solid particles may also be thought of as a method for decreasing the power consumption required for solid-gas transportation.

While there is great number of publications on pneumatic conveying, very few of them have dealt with the principle of electric augmentation as in the case of Catroneo and Colver [7], Colver [4], and Soo [9].

The study of the pneumatic conveying of solid particles can be classified into three main approaches.

The early approaches assumed dynamic and thermal equilibrium between the solid and the fluid phases, which corresponded to a single phase, homogeneous fluid with modified properties Farber [10], Wallis [11], and Rudenger [8]. Such an approach can handle the case of a very dilute solid-gas mixture (i.e., the solid particles are very fine and from material with a low specific mass).

The mathematical modeling approach depends on the numerical solution of a mathematical model of the forces acting on the particles taking into consideration the particle-wall interaction and particle-fluid interaction Soo [9] and Cotroneo and Colver [7]. Many investigators numerically solved the differential equation of motion, for example, Neilson and Gilchrist [12], Hogland [13], and Sharma and Crowe [14]. Later Arastoopour et al. [15, 16] and Doss [17] added the particle-particle interaction to the mathematical model and solved it mathematically. The solution of these models are difficult due to lack of available data, specifically the particle-particle interaction, particle-wall interaction, and the drag coefficient of a particle in a cloud of particles.

As a useful contribution facilitating the solution of the mathematical models Soo [18] introduced averaging theorems for solving the differential-integral equation of multiphase flow. Also Matsumoto et al. [19] introduced a model for solving the case of a non-spherical particles. Assuming that the particle can have a shape of an ellipsoid rather than that of a sphere.

The practical approach is the most common and widely used approach because of the large accumulation of data and numerous correlations, developed over a long period of time. Soo [1] discussed investigations of grains and other particulate material pneumatically transported that were first reported by Gasterstadt [20] and Cramp and Priestly [21] in 1924. Dukler et al. [22] reported that by 1964, over 20,000 experiments from various sources had been employed for obtaining correlations and a

generalization of the friction factor, pressure drop, particle saltation velocity, and particle velocity.

Hariu and Molstad [23], Konno and Saito [24], Capes and Nakamura [25], Yousfi and Gau [26], Hinkle [27], Wen and Galli [28], and Yang [29-33] presented correlations for the friction factor of solid-gas flow, each of them related the pressure drop in the duct to his correlated friction factor using his own definition. In the present work, a friction factor per unit mass flow rate of the conveyed particles was adapted and related to the pressure drop by the conventional equation of single phase fluid flow in a duct.

The reported correlation for the pressure drop of solid-gas flow in a duct can be generally classified into correlations for a vertical duct and a horizontal duct.

Vogt and White [34], Belden and Kassel [35], Korn [36], Mehta et al. [37], Razumov [38], Stemerding [39], EEUA Handbook [40], Hinkle [27], Chowdhury et al. [41], Boothroyd [42], Jones et al. [43], Curran and Gorin [44], Rose and Duckworth [45], Konno and Saito [24], Richards and Wiersma [46], Khan and Pei [47], Knowlton and Bachovchin [48], Leung and Wiles [49], and Yang [31, 33] presented correlations for the pressure drop of a solid-air flow in a vertical duct, where the flow moves against the gravity.

Modie et al. [50] used data of coal-air flow reported by Curran and Gorin [44] and Konchesky et al. [51] and Knowlton [48] to evaluate the pressure drop correlations published by Curran and Gorin [44], Rose and Duckworth [45], Konno and Saito [24], Richards and Wiersma [46], Knowlton

and Bachovchin [48], Yang [33], Leung and Wiles [49], and Hinkle [27]. As a result of the evaluation Modie et al. [50] concluded that on an overall basis a modified Konno and Saito's correlation is the best and is, therefore, recommended for designing gas-solid transport lines for coal and related materials at low as well as high pressure. Therefore, the Konno and Saito correlation is presented in detail in the theoretical part of the present work.

Vogt and White [34], Korn [36], Lapple [52], Culgan [53], Clark et al. [54], Hinkle [27], Mehta et al. [37], Richardson and McLeman [55], EEUA Handbook [40], Rose and Duckworth [45], Duckworth and Kokka [56], Curran and Gorin [44], and Yang [33] presented correlations of pressure drop of solid-air flow in a horizontal duct. It should be noted that the conveying air speed must be greater than the saltation velocity, otherwise the particles will not be suspended in the flow. However, the technique of electrically augmented pneumatic transportation presented in the present work, particles can be conveyed with air speeds below the saltation speed.

Arastroopour et al. [57] used experimental data of a coal-air flow published by Konchesky et al. [51] and Clark et al. [54] to evaluate the correlations of pressure drop of a dilute solid-air flow in a horizontal duct presented by Culgan [53], Hinkle [27], EEUA Handbook [40], Curran and Gorin [44], Rose and Duckworth [45] and Yang [33]. Arastoopour et al. [57] concluded that the correlations of Hinkle [27] and Yang [33] give the best results for solid-air flow in a horizontal duct.

Doing and Roper [58], Rose and Duckworth [45], Matsumoto et al. [59], Thomas [60], and Zenz [61] prescribed different methods for the calculation

of the saltation velocity. Arastoopour et al. [57] compared the results of each method with the available data for coal-air flow, and concluded that the Zenz [61] method is the best of them, with a relative average deviation of 31%. The Zenz method compared with test data in the present study gave considerable errors for glass particles (which has a mean density close to that of coal), and even poorer results for copper particles which has a high density compared with that of coal.

Arastoopour et al. [57] gave a correlation of the velocity of the conveyed particle as a function of the velocity of the conveying air and the particle density and diameter. Results of the present work are in a good agreement with the Arastoopour correlation. Therefore, this correlation is presented in the theoretical part of the present work in the English units, as it was reported, and modified for SI units.

The method of the electrically augmented pneumatic transportation of solid particle was reported by Cotroneo and Colver [7]. They used a fluidized bed feeder to supply a rectangular duct with copper particles having a diameter of 85 μm. The particles were suspended by supplying a high volt DC potential difference to the electrodes of the duct. They used the electric field strength as a new independent variable to control the vertical motion of the particle. They introduced a mathematical model for the forces acting on a single particle as it moves along the duct. They used a modified Stokes drag as was recommended by Soo [9] to calculated the drag force. Particle-particle collisions were ignored. The test data were obtained for low Reynolds number based on the equivalent duct diameter and the particle relative velocity. They predicted that the needed conveying

power may be reduced at some value of the electric field strength. The present work is an extension of the study of Cotroneo and Colver to cover laminar and turbulent regimes of the flow. An apparent drag coefficient for a cloud of particles will include both the particle-particle and the particle-wall interactions. The predicted reduction in the conveying power has been observed for glass particles at an electric field strength of 2.5 kv/cm.

2.3. Particle Transport in an Unconfined Volume

It is the study of the particle motion in our surrounding space. Particles suspended in the air is an example of an unconfined suspension which is manifested as one type of pollution. There are other kinds of waste pollution, such as chemical, biological, thermal and radiational pollution. The main concerns regarding particles in the environment is to understand the dynamics of a cloud of particles (particle suspension, diffusion, and fall-out), the methods of collecting the airborne dust, and the methods of preventing airborne dust formation.

Sutton [62], Stern [63], and Soo [9] studied particle diffusion and fall-out from a point source located at a given altitude. The Richardson number of the atmosphere, the Grashof number relating to gas buoyancy, and the Reynolds number of the stack exhaust gases were taken as the governing parameters to evaluate the diffusivity in the direction of the cross flow and in a perpendicular direction. They also introduced a method for the calculation of the flux of the particle fall-out near ground including the effects of drift and diffusion. Later, Chen and Soo as reported by Soo [9] extended their model to treat the transient dispersion by wind from a

nonpoint source. Noll and Fang [64], and McCready [65] reported laboratory measurements of the atmospheric inertial deposition of coarse particle having diameters of (5-100) μm. They used a fan to control the air speed, and a plate with sharp edge to collect the deposited particles in both the lower and upper surface of the plate. The study demonstrated that there is both a downward and upward flux for atmospheric coarse particles. The two fluxes are related to the inertial deposition velocity and increase with particle size and wind speed. Wind direction, speed and vorticity as well as the humidity and chances of rain are very decisive factors in planning for building industries producing dust. In some cases artificial water spray is used for the collection of airborne dust Cheng [66]. In the same time air filters should be used to minimize the amount of dust ejected to the atmosphere. Air cyclone like that which is used in the present test rig is a typical example of the air filters. A design procedure based on data obtained by Rietema [67] is presented by Soo [9].

3. THEORETICAL STUDY

For the sake of simplicity the theoretical study of an electrically driven particle in an air flow can be divided into a study of the particle electric suspension phenomenon, and a study of the mutual effect of the particle on the air flow and of air flow on the particle.

3.1. The Particle Electric Suspension

The electric (particulate) suspension or EPS has been defined by Colver [5] as a cloud containing charged particles which is formed or sustained with an applied electric field as a direct result of electric field induced or otherwise electrically controlled particle charging at a particle-wall interference. Particles charged triboelectrically by contacting a wall, or charged by spraying the environment with ions, as in electrostatic precipitation, can also be controlled by electric fields.

The present study is directed at the determination of the vertical velocity of particles suspended between two electrically charged, copper plates, as a function of the applied field strength. Single particle theory is used in helping to understand particle-wall encounters. Multiple particle interaction lead to a variety of phenomena including particle diffusion and upper limits on the number density of the cloud at a fixed electric field strength [5].

3.1.1. Single particle phenomena

The theoretical equilibrium charge, Q, induced on a single conducting sphere in contact with an infinite flat plate in the presence of a uniform electric field, E, is the Maxwell charge [4, 68] given by (see Figure 3.1)

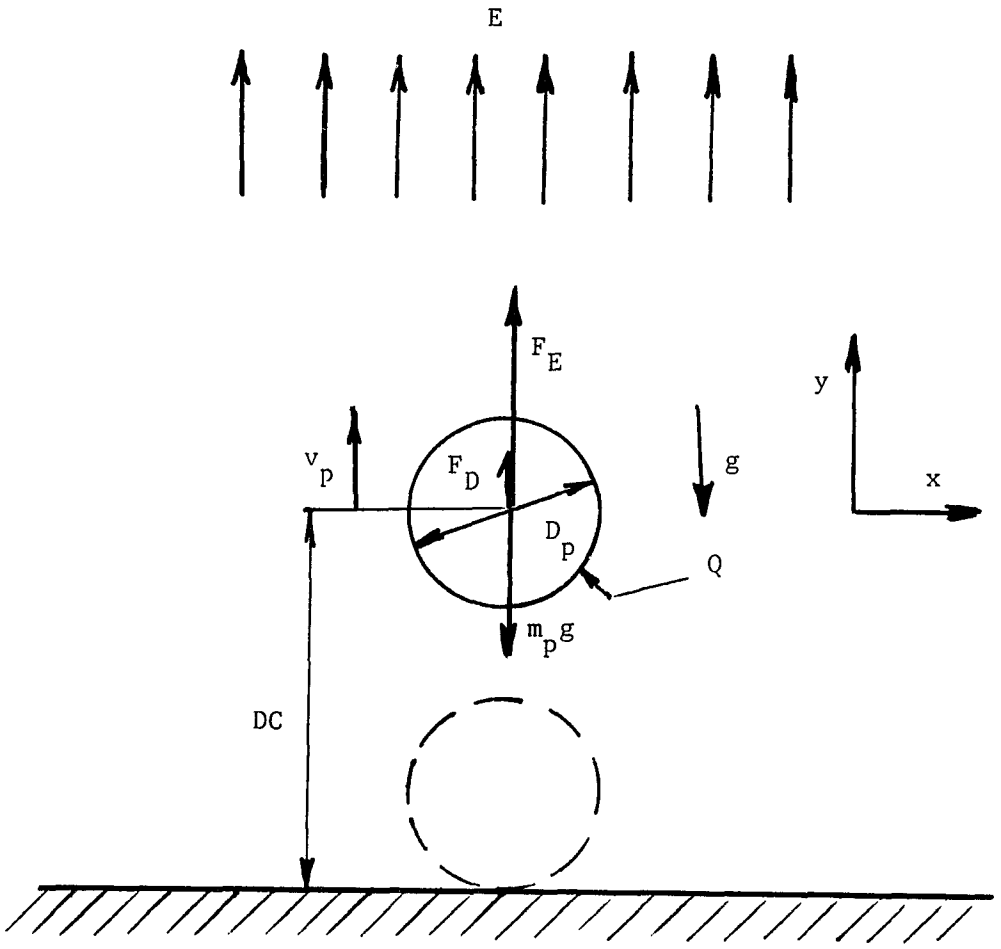

Figure 3.1. Model of a single particle

$$Q = \frac{\pi}{6} \varepsilon_o D_p^2 E \tag{3.1}$$

where ε_o and D_p are the permitivity and particle diameter respectively. For copper particles up to 1.5 mm diameter. Equation (3.1) was found to be valid for particles in dynamic contact with flat conducting surface even with an oxide coating in both surfaces [4, 69].

The mean particle velocity $\bar{v}_p$ for a single particle oscillating between parallel plates separated by distance, ℓ, with uniform electric field strength, E, [4, 5, 69] is

$$\bar{v}_p = \left[\frac{\ell/8}{1-e_b^2 e_t^2}\right]^{1/2} \left\{\left[(1+e_t^2)\left(\frac{Q_o E}{m_p}\right) + (1-e_t^2)g\right]^{1/2} (1+e_b) + \left[(1+e_b^2)\left(\frac{Q_o E}{m_p}\right) - (1-e_b^2)g\right]^{1/2} (1+e_t)\right\}, \left[\frac{3\pi\mu D_p \ell}{2(1-e)m_p \bar{v}_p}\right] \ll 1 \tag{3.2}$$

where Q_o, m_p, E, g, e_b and e_t are respectively the charge and mass per particle,[1] apparent electric field strength, gravity, and coefficient of restriction at bottom and top plates. To account for the particle drag force replace QE by $(QE-F_D)$ in Equation (3.2) where

$$F_D = 3\pi\mu D_p \bar{v}_p (1+3D_p\rho\bar{v}_p/16\mu)^{1/2}, \quad (Re_p < 100) \tag{3.3}$$

and where F_D, D_p, μ, ρ are drag force per particle, particle diameter, fluid viscosity and density respectively and $Re_p = \rho\bar{v}_p D_p/\mu$ is the particle Reynolds number.

---

[1] $Q = Q_o$. For more accurate value see [70-74].

From Equations (3.1), (3.2), and (3.3) the minimum electric field strength for sustained particle motion is given by [4]

$$E_{L.L} = \left\{ \left[\frac{(1-e_b^2)}{(1+e_b^2)} m_p g + F_D \right] \frac{6}{\pi^3 \varepsilon_o D_p^2} \right\}^{1/2} \tag{3.4}$$

which leads in Equation (3.2) to

$$\bar{v}_{L.L} = \left[\frac{(1+e_b)^2}{(1+e_b^2)} \left(\frac{\ell g}{4} \right) \right]^{1/2} \tag{3.5}$$

The theoretical equilibrium force required to lift a single conducting sphere in a uniform electric field from a plane is [75]

$$F_E = \pi \varepsilon_o D_p^2 E^2 \ (1.37) \tag{3.6}$$

which when combined with Equation (3.1) gives the lift-off criteria of a spherical particle

$$E_{L.O} = \left[\frac{m_p g}{\pi \varepsilon_o D_p^2 (1.37)} \right]^{1/2} \tag{3.7}$$

when compared with Equation (3.10) it follows that $E_{L.L} < E_{LO}$, that is, the required electric field strength to just sustain particle motion is less than that field strength to initiate motion of a static particle from a conducting plate if $(F_D/m_p g < 0.2)$ [4].

From Equation (3.2) we note that the particle cannot oscillate smoothly unless

$$\frac{Q_o E (1+e_b^2)}{m_p g (1-e_b^2)} \geq 1$$

This is the condition for having real roots of the second term in Equation (3.2) leading to a real velocity. This implies that a restriction exists on Equation (3.1) in the allowable magnitude of Q_o. If this condition was not satisfied the particle will oscillate in a jumpy or irregular manner. Also for each material (ρ, ε_o) there is a maximum diameter D_p that can be lifted by a specified electric field strength (E).

3.1.2. Multiple particle phenomena

There are three test categories of EPS. The particulate cloud be either totally confined, i.e., contained in a closed volume, unconfined, i.e., there are no side walls restricting the horizontal motion of the particles oscillating between the two parallel electrodes, or partially confined, i.e., there are walls restricting the horizontal motion in some direction while it is opened in some other direction (the case of a rectangular duct with open ends).

For either partially or totally confined PES, the mean interparticle spacing Λ is given by the particle number density n as

$$\Lambda = n^{-1/3} \tag{3.8}$$

In the present work, Λ was found to be in the range of 1178 → 2342 μm.

The mean interparticle spacing is related to the volume fraction solid ϕ Soo [1] as

$$n^{-1/3}/D_p = (\pi/6\phi)^{1/3} \tag{3.9}$$

In the present work, ϕ was found to be in the range of 0.000012 → 0.00012.

The mean free path for particle to particle collision λ given by Colver and Ehlinger [6] and Colver and Howell [76] as

$$\lambda = 1/(\pi D_p^2 n) \tag{3.10}$$

In the present work, λ was found to be in the range of 0.1134 → 0.7106 m.

The ratio of mean free path of particle to particle collision λ to the interparticle spacing, given by

$$\lambda/n^{-1/3} = \phi^{-2/3}(36\pi)^{-1/3} \tag{3.11}$$

In the present work $\lambda/n^{-1/3}$ was found to be in the range of 95.9 → 380.6. The solid-gas suspension is said to be diluted if $\lambda/n^{-1/3} \geq 1$ or $\phi \leq 0.1$ Soo [1]. The present work belongs to the case of very diluted mixture.

3.2. Solid-Gas Flow in a Duct

The design of a solid particle transport line should lead to the knowledge of the pressure drop through the line and the mass flow rate of the conveying air necessary to convey the required mass flow rate of particles. With this information, the needed conveying power can be determined. Besides this economical aspect, the designer should also satisfy some safety and reliability requirements. In general, the designer can adopt either theoretical or empirical methods. While the idea of theoretical methods can give detailed analysis of the transport line, the simplicity of the solution and the availability of great amounts of reported experimental data often invoke the empirical method.

3.2.1. Theoretical model of a particle in a duct

A theoretical model for a particle transported in a duct in the presence of an electric field was given by Cotroneo and Colver [7]. The model is based on the assumption that a particle alternately strikes the upper and then the lower wall (plate) as it drifts along the duct. The

upper and lower wall collisions are completely symmetrical, producing identical impulses, rotations, velocities, etc. Gravitational effects are neglected and air slug flow is assumed. A modified Stoke's drag is assumed for low Reynolds number based on the particle diameter.

3.2.1.1. Particle-wall mechanism During a particle-wall collision a tangential impulse (wall drag) exists according to

$$\int_{\Delta t_c} F_t dt = I(\omega'-\omega)/a = m_p(u'_s - u_s) \tag{3.12}$$

$$= -m_p\left[\frac{I(1+\alpha)\ \beta/m_p a^2}{1+I(1+\alpha)\beta/2m_p a^2}\right]\bar{u}_s \tag{3.13a}$$

$$= -m_p\left[\frac{2(1+\alpha)\ \beta/5}{1+(1+\alpha)\ \beta/5}\right]\ \bar{u}_s \quad \text{(sphere)} \tag{3.13b}$$

where

Rotational slip condition $\omega' = -u'_s\beta/a$, $(0 \leq \beta \leq 1)$.

Rotational relaxation condition $\omega = -\alpha\omega'$, $(0 \leq \alpha \leq 1)$.

Mean particle (slip) velocity $\bar{u}_s = (u'_s + u_s)/2$.

The later condition gives an estimated error of less than 1% compared to the more realistic logarithmic velocity average Cotroneo and Colver [7].

α is a measure of the particle rotational relaxation in stagnant fluid [7, 77] given by $\alpha = \exp(-\Delta t_f\ 8\pi\mu a^3/I)$.

β is to be experimenally determined as the degree of particle rotational slippage relative to the wall immediately following a particle-wall encounter.

F_t tangential force on a wall due to a particle.

Δt_c particle-wall collision time ($\sim 10^{-5}$S).

$\omega(\omega')$ particle angular velocity before (after) collision.

t time of particle motion in the fluid.

a radius of the particle.

Advantage has been taken, above, of the rotational and velocity change symmetry (in steady state motion) expected during particle collision and particle traverse of the duct [i.e., $(u'_s - u_s)$ (wall collision) = Δu (traverse), and $(\omega'-\omega)$ (wall collision) = $\Delta\omega$ (traverse)]. An alternative discussion of a particle-wall encounter can be found in Conno and Saito [24].

3.2.1.2. Particle-fluid mechanics A spherical particle subjected to a sequence of forces (i.e., wall interaction over Δt_f) will undergo an average horizontal acceleration (neglecting particle-particle collision) over the total time, Δt, given by

$$m_p(\Delta\bar{u}/\Delta t) = (\sum_i \int_{\Delta t_i} F_i dt)/\Delta t, \quad \Delta t = \sum_i \Delta t_i \tag{3.14}$$

$$= 6\pi\mu a\bar{u}_r[1+3\rho a\ V_r/8\mu]^{1/2} + \pi a^3\rho\bar{\omega}\bar{v}_s \tag{3.15}$$

$$- m_p\bar{u}_s\bar{v}_s\ [\frac{2(1+\alpha)\ \beta/5}{1+(1+\alpha)\ \beta/5}]/\ell$$

where

$\bar{u}_r = \bar{u}_a - \bar{u}_s$

$\bar{V}_r^{\,2} = \bar{u}_r^{\,2} + \bar{v}_s^{\,2}$ (relative fluid-particle velocity)

$|\bar{\omega}| = [\frac{(1+\alpha)\ \beta}{1+(1+\alpha)\ \beta/5}]\bar{u}_s/2a$

$\Delta t = \Delta t_f + \Delta t_c \simeq \ell/\bar{v}_s$, $\Delta t_c << \Delta t_f$

The r.h.s. terms are, respectively, the fluid drag force, fluid lift force (Magnus effect), and the wall drag forces. The ratio of the particle lift to wall drag (or fluid drag) forces from Equation (3.23) is approximately $5\pi a^2\rho\ell/4m_p \sim 3\%$ (for further discussion, see Soo [9], p. 28).

The additional particle drag effects of presure gradient, apparent fluid mass, temperature gradient, and particle history (Basset term) are neglected due to the large particle-to-fluid mass ratio [9]. The effects of walls fluid velocity profile and particle collisions across the duct have also not been considered.

3.2.1.3. Fluid mechanics From the conservaton of momentum principles, the steady state additional pressure drop Δp_s due to the presence of a uniform distribution of particles (i.e., besides the viscuss boundary layer effects) can be written as [7, 78]

$$\Delta p_s/L_{ss} = n\bar{F}_p \tag{3.16}$$

where $\bar{F}_p$ is the average force per particle, and L_{ss} is the length of the duct in which the particle moves in a steady state motion.

3.2.2. Empirical methods

Due to the lack of available basic data necessary for the theoretical solution, the empirical methods appears as an alternative method and offers considerable accuracy. The pressure drop of the transporting line can be determined by one of the available pressure drop correlation, which can be classified into two main cases.

Correlation of the pressure drop in a vertical duct without electric field. The correlation of Conno and Saito [24] was recommended as the best method by Modi et al. [50] and is expressed in English units as

$$\Delta p_{s-a} = \frac{2f_a u^2 L \rho_a}{g D_H} + 0.057 \frac{u_a L}{\sqrt{g D_H}} \eta \rho_a + L \frac{W_s}{V_r} \tag{3.17}$$

where

$V_r = u_a - u_s$

f_a friction factor of the air flow in the duct

η loading of the line, solid to air weight ratio

D_H hydraulic diameter of the duct

W_s weight of the solid particles in the line

Correlation of the pressure drop in a horizontal duct without electric field. The correlation of Hinkle [27] as the best method chosen by Arastoopour et al. [57] is expressed in English unit as

$$\Delta p_{s-a} = \frac{u_a^2 \rho_a}{2g} + \frac{W_s u_s}{g} + \frac{2f_a \rho_a u_a^2 L}{g D_H} \left[1 + \frac{f_s u_s}{f_a u_a} \frac{W_s}{u_a \rho_a}\right] \tag{3.18}$$

where

$$u_s/u_a = (1-0.179\ D_p^{0.3} \rho_s^{0.5}) \tag{3.19}$$

$$f_s = \frac{3}{8} \frac{\rho_a}{\rho_s} \cdot C_D \frac{D_H}{D_p} \left(\frac{u_a - u_s}{u_s}\right)^2 \tag{3.20}$$

The solid to air velocity ratio Equation (3.19) was corrected by Arastoopour et al. [57] and expressed in English units as

$$u_s/u_a = (1-0.1233\ D_p^{0.3}\ \rho_s^{0.5}) \tag{3.21}$$

which can be expressed in SI units as

$$u_s/u_a = (1-0.044029\ D_p^{0.3}\ \rho_s^{0.5}) \tag{3.22}$$

The available pressure drop correlations may be broadly classified into the following two categories:

1. Type 1 in which the ratio of total pressure drop to the pressure drop due to gas (air) alone is correlated.
2. Type 2 in which the total pressure drop is expressed as the summation of pressure drops due to acceleration, wall friction, and static head.

One will notice that the correlations which were chosen as the best for vertical and horizontal conveying were of type 2.

The saltation velocity of a cloud of particles on a duct according to Zenz's [61], which was evaluated by Arastoopour et al. [57] as the most accurate method for coal. It can be calculated as follows:

$$\beta_1 = \left[\frac{4g\mu_a(\rho_s-\rho_a)}{3\ \rho_a^2}\right]^{1/3} \tag{3.23}$$

$$\beta_2 = \left[\frac{3\ \mu_a^2}{4g\rho_a(\rho_s-\rho_a)}\right]^{1/3} \tag{3.24}$$

From Figure 2, in Zenz [61], according to the duct diameter, find $(u_{cs,ref}/\beta_1)$ and the slope M.

$$\beta_3 = 0.32 \times 10^{-2},\ (M \leq 0.05) \tag{3.25}$$

or $$\beta_3 = 21.4 \times 10^{-2}\ M,\ (M > 0.05) \tag{3.26}$$

Correction of the duct diameter.

$$(u_{cs}/u_{cs,ref}) = (D_H/D_{H,ref})^{0.4} \tag{3.27}$$

The multiple particle particle saltation speed is

$$\frac{G_s}{\rho_s} \simeq \frac{W_s}{W_a}\left(\frac{\rho_a}{\rho_s}\right) u_{sm} = \beta_3 \frac{(u_{sm} - u_{cs})}{u_{cs}} \tag{3.28}$$

where

$u_{cs,ref}$ saltation velocity of a single particle in the reference duct.

u_{cs} saltation velocity of single particle in a duct.

u_{cm} saltation velocity of a multiple particle in a duct.

$D_{H,ref}$ hydraulic diameter of the reference duct.

One of the most important and basic parameters needed is the drag coefficient of a cloud of particles. Unlike the drag coefficient of a single particle, which is very well known, the drag coefficient of multi particle is not well defined, because it is influenced by the particle-particle interaction which is function of the particle mass density, particle number density, particle size, and particle size distribution. The available correlations for a multiple particle drag coefficient are:

Ingebo [79] drag coefficient

$$C_D = 27/Re_p^{0.84}, \quad (6 < Re < 400) \tag{3.29}$$

where $Re_p = V_r D_p/\nu$

V_r is the relative air to particle velocity.

Rudinger [80, 81] drag coefficient

$$C_D = 6000/Re_p^{1.7}, \quad (5 < Re < 200) \tag{3.30}$$

Rowe and Henwood [82] drag coefficient

$$C_D = 0.44, \quad (Re_p > 1000) \tag{3.31}$$

or

$$C_D = (24/Re_p)\ (1 + 0.15\ Re_p^{0.687}), \quad (Re_p < 1000) \tag{3.32}$$

Rudinger [8] introduced a correlation of the drag coefficient as

$$C_D = (24/Re_p)\ [1 + \tfrac{1}{6}\ Re^{2/3}\ (1 + \alpha_p^{\,2})^{1/3}] \tag{3.33}$$

where α_p is the volume of solid to air ratio.

The present experimental work includes a correlation of an apparent drag coefficient for copper and glass spherical particles. The term apparent drag coefficient is used because the particle-particle and particle-wall interactions have great effect on the aerodynamic drag coefficient in the case of electrically suspended particles as a result of the vertical velocity of the particle.

4. EXPERIMENTAL STUDY

This section includes a description of the experimental investigation of the effect of an electrically suspended cloud of particles in ducted flow. The particle velocity, particle number density and the flow pressure drop were measured along the duct, for copper spherical particles (63-74 and 74-88) μm and glass spherical particles (44-63, 63-74, and 74-88) μm. The measurements were taken at different flow speeds ranging from 0.8 m/s up to 8.0 m/s which give a duct Reynolds number Re_D in the range of (1300 up to 12551) covering the laminar, transient and low turbulent regimes of flow. The particle Reynolds number Re_p based on relative velocity of the particle flow was found to be in the range of (5 up to 32). The effect of the electric field strength on the flow parameters was also investigated for the case of glass particles. The vertical velocities of the copper and glass particles were measured for different values of electric field strength, in both a confined and partially confined volume.

The test data were analyzed for the following results:

1. The friction factor per unit mass flow rate of conveyed particles vs. the duct Reynolds number, for copper and glass particles.
2. The pressure gradient of solid-air per unit mass flow rate of the conveyed particles vs. the duct Reynolds number, for the copper and glass particles.
3. The apparent drag coefficient for each size the copper and glass particles vs. the particle Reynolds number.

4. The apparent drag coefficient vs. a newly defined particle Reynolds number. Correlations for both copper and glass particles were reduced to a single curve.

4.1. Test Facility

A rectangular duct Figures 4.1 and 4.2 having a cross section measuring (5.25 x 1.6) cm and a length of 225 cm was produced. Its upper and lower walls (electrodes) were produced from brass strips 10 cm in width and 8 mm in thickness. The side walls were fabricated from glass strips 1.6 cm in height and 3 mm in thickness. The particles were fed to the duct by an Auger, driven by a DC servomotor and a system of gears designed to feed the particles with a controlled volumetric rates (Appendix A). The solid particles were separated from the air and collected in a reservoir using a specially designed cyclone. The air was fed to the duct at various mass flow rates and measured by a system of rotameters (Appendix B). Before entering the duct, the air was passed through an air straightener. The particle velocity was measured by a DISA 55x modular Laser Doppler Anemometer LDA (Appendix C). The LDA output was displayed on a Tektronix 434 oscilloscope. The pressure of the solid-air flow was measured by a Barocel pressure sensor type 570D-100T.1A1-V1 in 13 pressure taps located along the center of the upper plate of the duct, with a distance of 15 cm between each tap (see Figure 4.1). The pressure sensor was connected to the different pressure taps thorugh a scana valve. The pressure measurements started after a very short distance from the duct exit section without having fully developed flow since in fact two phase flows are rarely fully developed Hewitt [83, 84]. If the effect of the particle

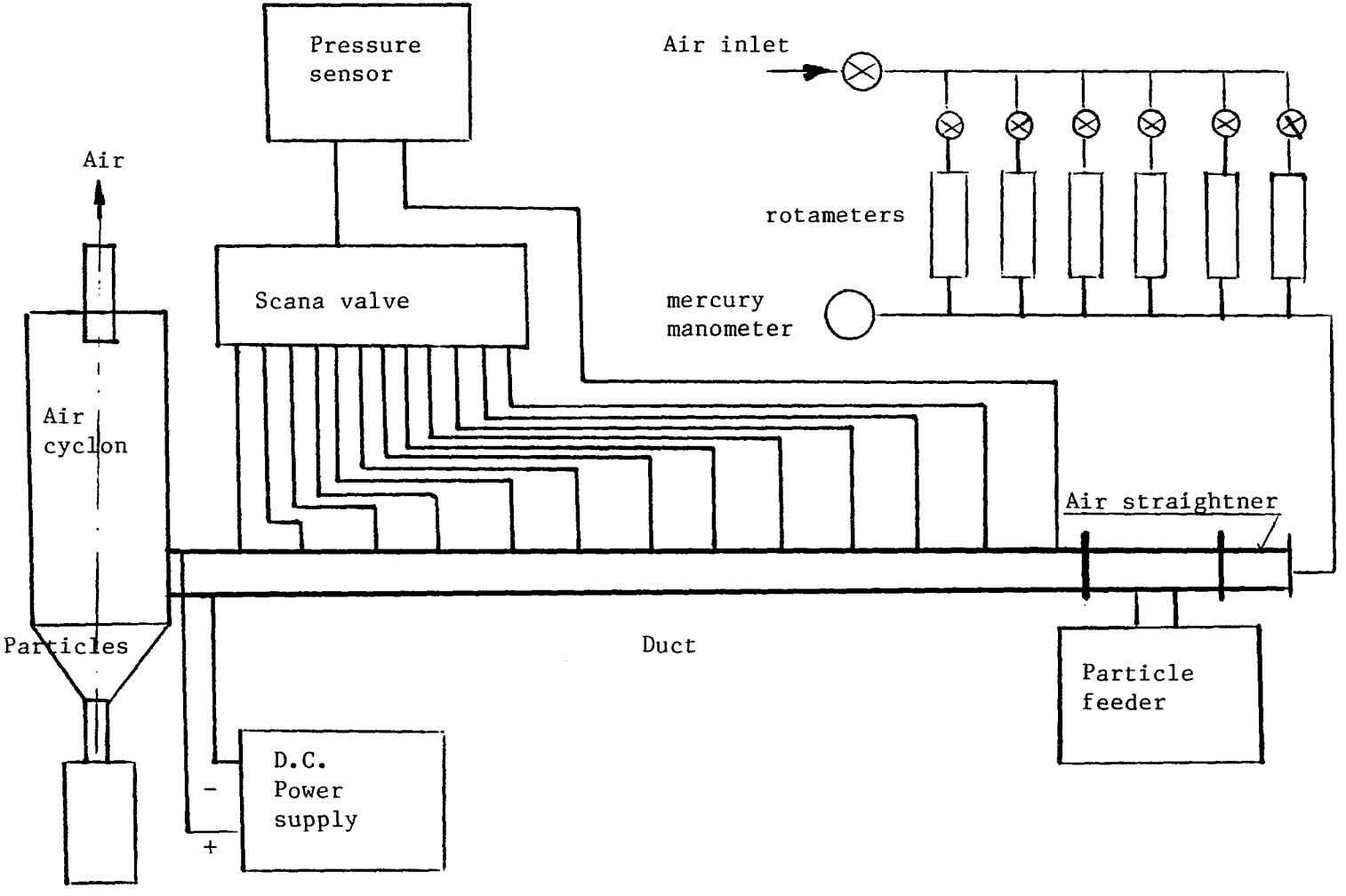

Figure 4.1. Diagram of experimental system

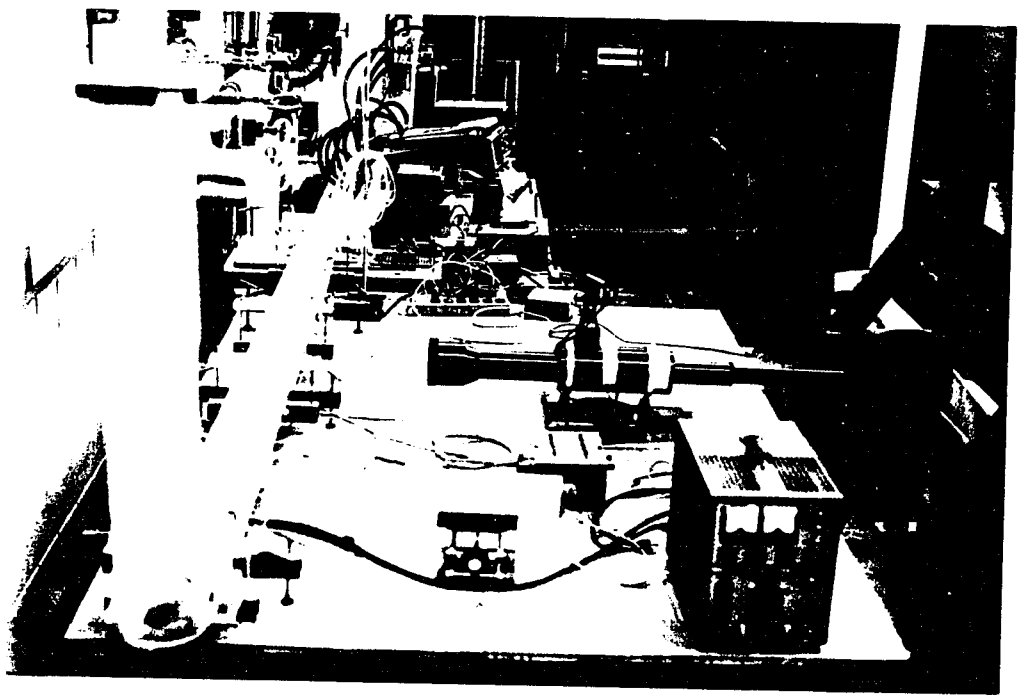

Figure 4.2. Experimental set up

oscillation is considered, one can conclude that fully developed flow in the presence of oscillating particles can never be attained. The particles were driven to oscillate between the lower and the upper plates of the duct by applying a DC voltage difference to the electrodes. The DC voltage was generated by a 230-6P-R&D high volt DC power supply.

4.2. Measurements of the Vertical Velocity of Electrically Driven Particles in a Totally Confined Volume

The vertical velocity of the electrically driven particles was measured in a confined volume using a Laser Doppler Anemometer. The test secton Figure 4.3 consisted of two brass electrodes with a separation distance of 16 mm and an internal volume defined by glass walls. The internal horizontal cross section measured 15 x 5.25 cm. The test section was horizontally leveled, and the laser beams measuring the particle velocity were directed to the center of the test section. Tables 4.1 and 4.2 give the particle vertical velocity v_p at different electric field strengths for copper and glass particles respectively for particle diameters of (37-44, 44-63, 63-74, and 74-88 μm). The glass particle vertical velocities at various electric field strengths are presented in Figure 4.4.a. An error of about 5% may be expected for the velocity measurements, due to reading from the screen of the oscilliscope. The following general observations can be seen from the results tabulated in Tables 4.1 and 4.2.

1. The particle vertical velocity increases with an increase in the electric field strength.

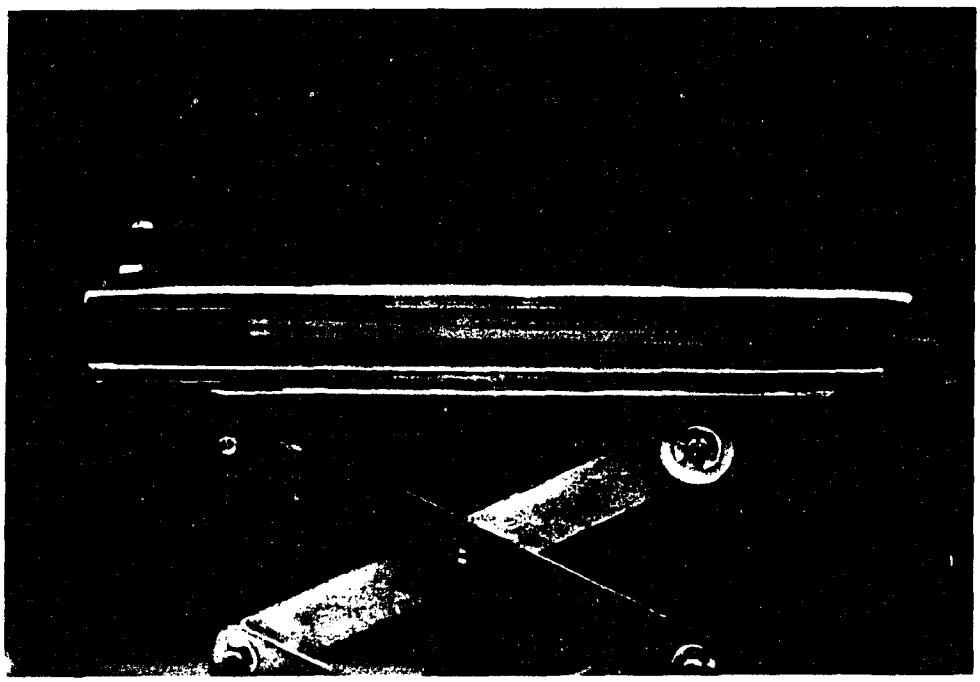

Figure 4.3. Closed volume test section for calibration of the particle vertical velocity using a LDA, plate separation distance 1.6 cm

Table 4.1. Vertical velocity of copper particles[a]

Electric field strength	Vertical Velocity (m/s)			
	37 - 44 (μ m)	44 - 63 (μ m)	63 - 74 (μ m)	74 - 88 (μ m)
1.875	-	-	-	-
2.500	-	-	-	-
3.125	-	-	-	-
3.750	0.70	0.75	0.80	0.80
4.375	0.90	0.90	0.90	0.90
5.000	1.0	1.0	1.0	1.0
5.625	1.0	1.0	1.0	1.0
6.250	1.0	1.0	1.0	1.0
6.875	1.0	1.0	1.0	1.0
7.500	1.0	1.0	1.0	1.0
8.125	Break - Down			

[a]An error of about 5% may be expected for the velocity measurements, due to reading from the screen of the oscilliscope.

Table 4.2. Vertical velocity of glass particles[a]

Electric field strength	Vertical Velocity (m/s)			
	37 - 44 (μm)	44 - 63 (μm)	63 - 74 (μm)	74 - 88 (μm)
1.875	-	-	-	-
2.500	0.95	1.1	1.2	1.2
3.125	1.25	1.25	1.25	1.25
3.750	1.4	1.35	1.35	1.35
4.375	1.5	1.5	1.5	1.5
5.000	1.7	1.7	1.7	1.7
5.625	1.8	1.8	1.8	1.8
6.250	1.85	1.85	1.85	1.9
6.875	1.85	1.85	1.85	1.9
7.500	1.85	1.85	1.85	1.9
8.125	1.85	1.85	1.85	1.9
8.750	1.85	1.85	1.85	1.9

[a]An error of about 5% may be expected for the velocity measurements, due to reading from the screen of the oscilliscope.

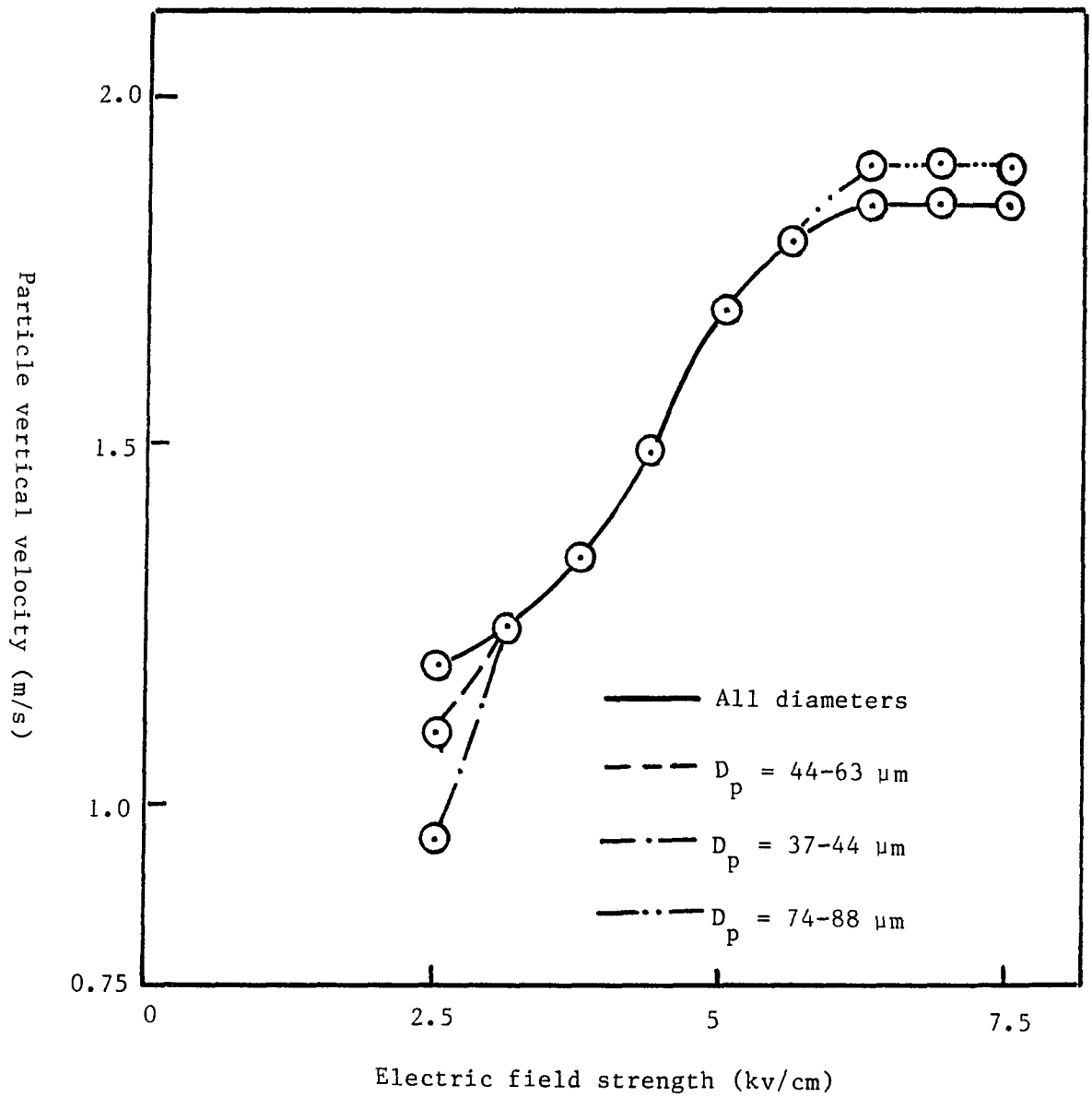

Figure 4.4.a. Glass particle vertical velocity versus electric field strength

2. The vertical velocity is a function of the electric field and the material of the particle but not of the particle diameter within the range of measured particles.
3. Particles began to move between the electrodes at some minimum electric field strength Equation (3.7) with corresponding minimum velocity Equation (3.5) as it was predicted by Colver [4].
4. Small particles began their motion at a lower minimum velocity than the bigger ones. This can be explained by the greater adhesion force between the smaller particles, which produces an additional force opposing to the motion of the particles.
5. There is some upper limiting vertical velocity corresponding to an upper limiting electric field strength. Above this value the increase of the electric field strength does not increase the mean vertical velocity, but rather the particle number density will be increased and the velocity fluctuation around its mean valve will be decreased. This can be observed on Figure 4.4.b for glass particle with diameter (44-63) μm where at a. E = 6.25 kv/cm and at b. E = 7.5 kv/cm. The experimentally measured upper limiting particle vertical velocity cannot be predicted, using the single particle model (see Equations 3.1 and 3.2).

4.3. Measurement of the Minimum Lifting Air Velocity in a Rectangular Duct

The minimum lifting air velocity in a rectangular duct for both glass and copper particles having diameters of (44-63, 6-374 and 74-88) μm was measured by filling the particle feeder by the tested particles to be in

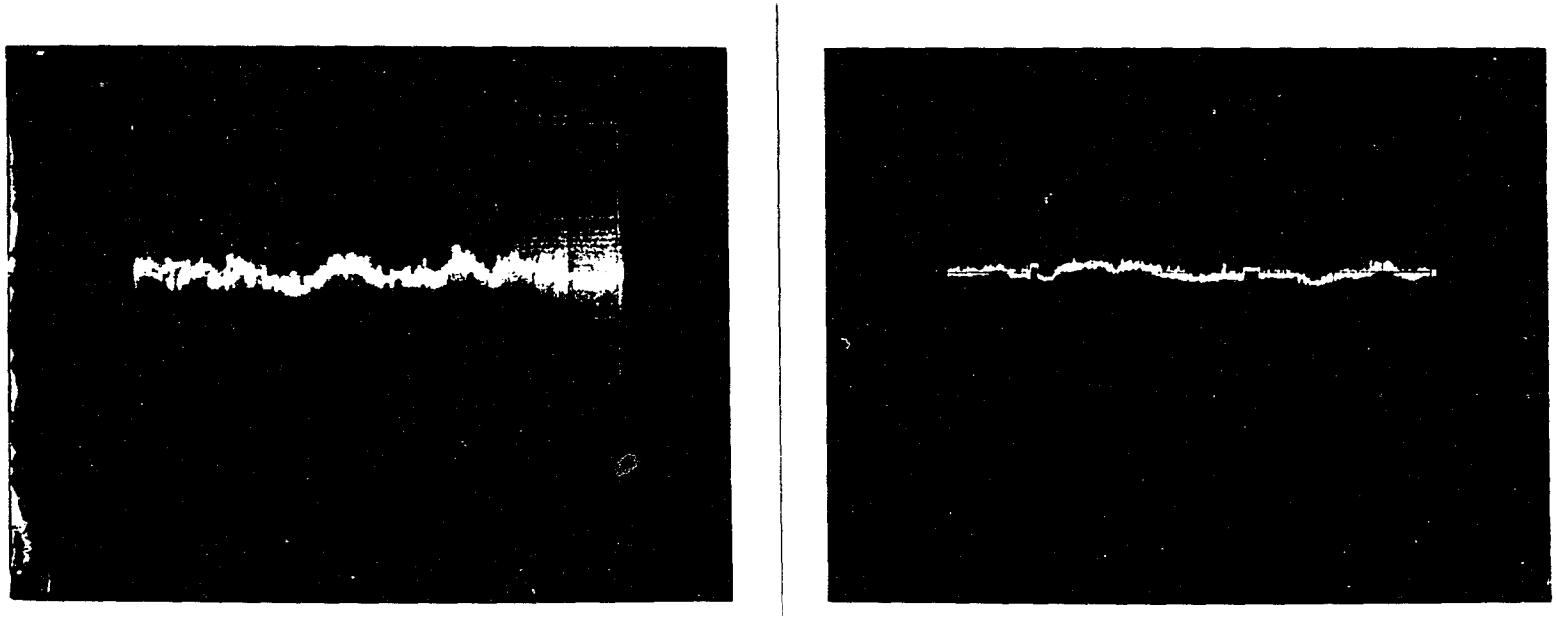

Figure 4.4.b. Particle vertical velocity measured by a LDA and displayed on an oscilliscope. (a) E = 6.25 kv/cm, (b) E = 7.5 kv/cm

Table 4.3. Measured minimum lifting air velocity $u_{a,min}$ and its corresponding particle velocity u_p

Particle diameter	Copper		Glass	
(μ m)	$u_{a,min}$ (m/s)	u_p (m/s)	$u_{a,min}$ (m/s)	u_p (m/s)
74 - 88	2.05	1.5	1.78	1.40
63 - 74	1.95	1.45	1.75	1.41
44 - 63	1.85	1.45	1.71	1.42

the same level of the lower plate of the test duct. The air velocity was increased gradually until air lifted particles were detected by the LDA Beam, located at a distance of 75 cm from the duct inlet. In the same time the particle velocity was also measured. The test was repeated for each particle size of the copper and glass. The measured values are presented in Table 4.3.

The minimum lifting air velocity was calculated according to Zenz's method [61] for each particle. Taking into consideration that the solid-gas flow was very diluted in the present tests, the minimum lifting air velocity can be compared with the case of the single particle solution with a correction for the hydraulic duct diameter. The particle velocity of the measured minimum lifting air velocity of each particle was also calculated by Arastoopour Equation (3.22). Results of the calculation are

are tabulated in Table 4.4. Comparing the calculated values with the measured ones, one can infer the following:

1. Arastoopour's Equation [57] is an accurate expression for the particle velocity as a function of the air velocity for both copper and glass particles.
2. Zenz's method [61] is not accurate particularly for copper, i.e., the method loses its accuracy for particle of materials having high mass density.

4.4. Measurements of the Pressure Drop of the Air Flow Along the Test Duct

The pressure drop of an air flow without particles was measured along the duct for different air flow bulk velocities u_a, namely (7.98, 6.37, 4.06, 3.19, 2.32, 1.466, 1.19, and 0.827) m/s. These air flow velocities give Reynolds numbers referred to the hydraulic diameter of the duct having values of (12551, 10017, 6394, 3663, 2304, 1872 and 1300) respectively. The air flow bulk velocities were chosen so that the first three values cover the turbulent flow regime. The second two values cover the transient flow regime and the last three values cover the lamenar flow regime. The bulk air flow velocities were measured by a system of rotameters and control valves. The static pressure drop Δp_a of the air flow was measured along the duct in 13 points located along the duct, taking the first point as a reference. The absolute static pressure of the first point p_1 and the rotameters static pressure p_m were also measured for each test. Test data of pressure drop corresponding to the eight selected velocities are

Table 4.4. Calculated minimum lifting air velocity $u_{a,min}$ and its corresponding particle velocity u_p

Particle diameter	Copper		Glass	
(μ m)	$u_{a,min}$[a] (m/s)	u_p[b] (m/s)	$u_{a,min}$[a] (m/s)	u_p[b] (m/s)
74 - 88	3.7535	1.544	2.295	1.4818
63 - 74	3.674	1.506	2.295	1.491
44 - 63	3.635	1.4968	2.295	1.507

[a]Zenz's method [61].

[b]Arastoopour's equation [57].

summarized in Table 4.5. The pressure reading values located along the duct are given in torr, while the rotameters pressure are reported in inches of mercury. The air flow Reynolds number referred to the duct hydraulic diameter Re_D is expressed as

$$Re_D = \frac{u_a D_H}{\nu} \tag{4.1}$$

where u_a air flow bulk velocity (m/s)

D_H hydraulic diameter of the duct (m)

ν kinematic viscosity of air (m^2/s)

The data in Table 4.5 can be analyzed to get a plot of the air friction factor against the flow Reynolds number in log-log scale (Mody diagram) Figure 4.5 where the friction factor f is defined as

Table 4.5. Pressure drop along the duct without particles

u_a(m/s)	7.98	6.37	4.06	3.1955	2.3298	1.466	1.19	0.82766
Re_D	12551	10017	6394.4	5023	3664	2304	1872	1300
p_m [a]	8.6	5.5	2.1	1.35	0.7	0.25	0.2	0.15
p_1 [b]	0.665	0.445	0.2	0.135	0.075	0.039	0.035	0.02
$_1\Delta p_2$ [b]	0.06	0.04	0.02	0.0043	0.0023	0.002	0.0016	0.0013
$_1\Delta p_3$	0.1	0.065	0.035	0.016	0.0083	0.0055	0.0036	0.003
$_1\Delta p_4$	0.14	0.095	0.045	0.025	0.016	0.009	0.0058	0.0046
$_1\Delta p_5$	0.18	0.12	0.055	0.033	0.021	0.0105	0.0077	0.0059
$_1\Delta p_6$	0.24	0.16	0.075	0.044	0.026	0.0135	0.01	0.0072
$_1\Delta p_7$	0.28	0.19	0.085	0.053	0.031	0.0160	0.013	0.0083
$_1\Delta p_8$	0.32	0.215	0.095	0.060	0.035	0.0180	0.015	0.0093
$_1\Delta p_9$	0.34	0.23	0.105	0.067	0.039	0.020	0.017	0.01

[a] Rotameters pressures are given in inches of mercury.

[b] Duct flow static pressures are given in torr.

Table 4.5. Continued

u_a(m/s)	7.98	6.37	4.06	3.1955	2.3298	1.466	1.19	0.82766
$_1\Delta p_{10}$	0.415	0.28	0.12	0.076	0.0445	0.022	0.0185	0.011
$_1\Delta p_{11}$	0.44	0.3	0.13	0.087	0.0500	0.024	0.020	0.012
$_1\Delta p_{12}$	0.48	0.32	0.14	0.97	0.055	0.026	0.0215	0.013
$_1\Delta p_{13}$	0.525	0.355	0.16	0.11	0.059	0.028	0.0228	0.014

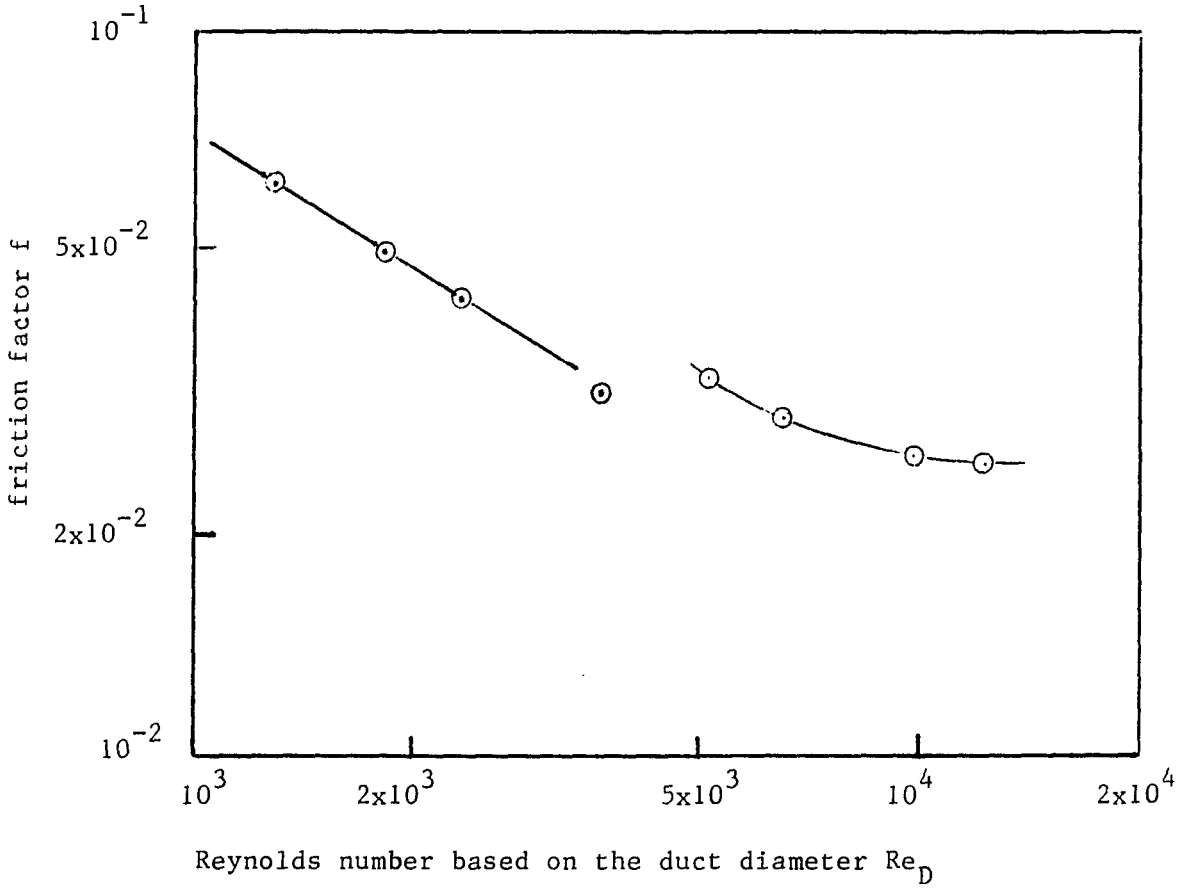

Figure 4.5. Friction factor f versus duct Reynolds number Re_D without particles

$$f = \frac{\Delta p_a}{1/2\ \rho\ u^2_a\ (L/D_H)} \qquad (4.2)$$

where as

Δp_a static pressure drop between point 1 and 13 (Pa)

ρ specific mass of air (kg/m^3)

u_a bulk velocity of air (m/s)

L distance between the measuring points 1 and 13 (m)

D_H hydraulic diameter of the duct

4.5. Measurement of the Solid-Air Flow Parameters Along the Duct (at constant electric field strength)

The effect of electrically driven particles in a duct flow was experimentally investigated for copper and glass particles with diameters of (63-74 and 74-88) μm and (44-63, 63-74, and 74-88) μm respectively. For each particle size the flow parameters were measured along the duct for bulk flow velocities of (7.89, 6.37, 4.06, 3.1955, 2.3298, 1.466, 1.19 and 0.82766) m/s. The particles were fed to the duct by a particle feeder (Appendix A) in a controlled and constant rate for each test. The air was also fed to the duct at a constant mass flow rate in each test. A total of 13 measuring points were located along the duct Figure (4.1) the following parameters were measured:

1. The static pressure of the solid-air flow (Δp_{s-a}) taking the first point as a reference.
2. The particle velocity u_s in the x-direction along the axis of the duct.
3. The absolute value of the particle vertical velocity v_s.

4. The particle number density n was calculated for each point using the particle continuity Equation

$$n\ A_D\ u_s = G_s\ N \qquad (4.3)$$

where

A_D the cross-section area of the duct.

G_s the volumetric feeding rate of the particles.

N number of particles per unit volume.

The electric field strength E = 5 kv/cm was kept constant at all tests which gave particle vertical velocities of (1.0 and 1.7) m/s for the copper and glass particles respectively. Test data are given in Appendix E.

4.5.1. Analysis of the test data

The obtained test data can be analyzed to give a graphical representation of the following relation:

1. The pressure gradient of the solid-air flow and of the solids only per unit mass flow rate of conveyed particles

$$\left[\frac{\Delta p_{s-a}/L_{ss}}{\dot{m}_s}\right] \text{ and } \left[\frac{\Delta p_s/L_{ss}}{\dot{m}_s}\right] \text{ vs duct Reynolds number } Re_D$$

where

L_{ss} length of the duct, where steady state velocity of the particles can be observed. Measured from the point of steady state particle velocity to the point of the last pressure tap (13).

Δp_{s-a} the static pressure drop of the solid-air flow in $[P_a]$ corresponding to L_{ss}.

Δp_s the static pressure drop of the solids only in $[P_a]$ corresponding to L_{ss}.

$\dot{m}_s$ mass flow rate of the conveyed particles.

2. The friction factor of the solid-air flow and of the solids only per unit mass flow rate of conveyed particles $\bar{f}_{s-a}$ and $\bar{f}_s$ vs duct Reynolds number Re_D

where

$$\bar{f}_{s-a} = \frac{(\Delta p_{s-a}/L_{ss})\cdot D_H}{1/2\ \rho\ u_a^2 \dot{m}_s} \qquad (4.4.a)$$

$$\bar{f}_s = \frac{(\Delta p_s/L_{ss})\cdot D_H}{1/2\ \rho\ u_a^2 \dot{m}_s} \qquad (4.4.b)$$

Values of the (pressure gradient and friction factor) of the solid-air flow per unit mass flow rate of the conveyed particles are presented in Tables (4.6-4.10) for copper particles having diameters of (63-74 and 74-88) μm and glass particles having diameters of (44-63, 63-74 and 74-88) μm respectively. Pressure gradient of the solid-air flow per unit mass flow rate of conveyed particles vs Re_D for copper and glass particles are plotted in Figures 4.6 and 4.7, respectively. While the friction coefficient of the solid-air flow per unit mass flow rate of the conveyed particles $\bar{f}_{s-a}$ vs Re_D for copper and glass particles are plotted in log-log scale Figures 4.8 and 4.9, respectively.

3. The apparent drag coefficient of the solid particle. The term apparent drag is adapted here to include the effect of particle momentum exchange with the upper and lower walls of the duct due to the vertical motion of the particles and the particle-particle interaction (as explained in

Table 4.6. Pressure gradient and friction factor per unit mass flow rate of the conveyed particles vs. the duct Reynolds number[a]

u_a (m/s)	Re_D	L_{ss} (m)	$\Delta p_{s-a}/L_{ss}\dot{m}_s$ ($s^{-1}\ m^{-2}$)	$\Delta p_s/L_{ss}\dot{m}_s$ ($s^{-1}\ m^{-2}$)	$\bar{f}_{s-a}$ (s/kg)	$\bar{f}_s$ (s/kg)
7.98	12,551	0.9	10,135	2,832	6.599	1.843
6.37	10,017	1.05	7,793	2,811	7.959	2.872
4.06	6,394	1.35	5,067	2,782	12,747	6,998
3.1955	5,024	1.5	4,686	3,005	19,029	12.200
2.3298	3,663	1.65	4,520	3,598	34.5299	27.487
1.466	2,304	1.65	4.333	3.651	83.61	70.043
1.19	1,872	1.65	4,881	4,012	142.9	117.4
0.82766	1,300	1.65	4,510	4,196	273.1	253.99

[a]Copper spherical particles with diameters of 63-74 μm.

Table 4.7. Pressure gradient and friction factor per unit mass flow rate of the conveyed particles vs. the duct Reynolds number[a]

u_a (m/s)	Re_D	L_{ss} (m)	$\Delta p_{s-a}/L_{ss}\dot{m}_s$ ($s^{-1}\ m^{-2}$)	$\Delta p_s/L_{ss}\dot{m}_s$ ($s^{-1}\ m^{-2}$)	$\bar{f}_{s-a}$ (s/kg)	$\bar{f}_s$ (s/kg)
7.98	12,551	0.9	10434	3130	6.79	2.037
6.37	10,017	1.05	8180	3194	8.356	3.26
4.06	6,394	1.35	5326	3040	13.395	7.6454
3.1955	5,024	1.5	5008	3326	20.318	13.5023
2.3298	3,663	1.65	4829	3907	36.87955	29.838
1.466	2,304	1.65	4359	3677	84.095	70.923
1.19	1,872	1.65	4922	4052	144.08	118.615
0.82766	1,300	1.65	4763	4.237	288.232	256.40

[a]Copper spherical particles with diameters of 74-88 μm.

Table 4.8. Pressure gradient and friction factor per unit mass flow rate of the conveyed particles vs. the duct Reynolds number[a]

u_a (m/s)	Re_D	L_{ss} (m)	$\Delta p_{s-a}/L_{ss}\dot{m}_s$ ($s^{-1}\ m^{-2}$)	$\Delta p_s/L_{ss}\dot{m}_s$ ($s^{-1}\ m^{-2}$)	$\bar{f}_{s-a}$ (s/kg)	$\bar{f}_s$ (s/kg)
7.98	12,551	1.50	31,105	2,978	20.25	001.939
6.37	10,017	1.65	21,960	3,008	22.439	3.07
4.06	6,394	1.65	12,454	4,031	31.326	10.139
3.1955	5,024	1.65	10,168	3,808	41.285	15.463
2.3298	3,663	1.65	11,467	5,957	87.593	45.503
1.466	2,304	1.65	12,704	8,757	245.084	168.95
1.19	1,872	1.65	13,053	9,830	382.016	287.9
0.82766	1,300	1.65	16,088	14,161	973.0	857.112

[a]Glass spherical particles with diameters of 44-63 μm.

Table 4.9. Pressure gradient and friction factor per unit mass flow rate of the conveyed particles vs. the duct Reynolds number[a]

u_a (m/s)	Re_D	L_{ss} (m)	$\Delta p_{s-a}/L_{ss}\dot{m}_s$ ($s^{-1}\ m^{-2}$)	$\Delta p_s/L_{ss}\dot{m}_s$ ($s^{-1}\ m^{-2}$)	$\bar{f}_{s-a}$ (s/kg)	$\bar{f}_s$ (s/kg)
7.98	12,551	1.50	31,502	3,375	20.511	2.197
6.37	10,017	1.65	22,862	3,910	23.361	3.996
4.06	6,394	1.65	12,754	4,331	32.082	10.896
3.1955	5,024	1.65	10,227	3,869	41.530	15.708
2.3298	3,663	1.65	11,662	6,151	89.070	46.989
1.466	2,304	1.65	14,722	10,776	284.02	207.890
1.19	1,872	1.65	14,570	11,352	426.51	332.400
0.82766	1,300	1.65	16,240	14,313	982.96	866.298

[a]Glass spherical particles with diameters of 63-74 μm.

Table 4.10. Pressure gradient and friction factor per unit mass flow rate of the conveyed particles vs. the duct Reynolds number[a]

u_a (m/s)	Re_D	L_{ss} (m)	$\Delta p_{s-a}/L_{ss}\dot{m}_s$ ($s^{-1}\ m^{-2}$)	$\Delta p_s/L_{ss}\dot{m}_s$ ($s^{-1}\ m^{-2}$)	$\bar{f}_{s-a}$ (s/kg)	$\bar{f}_s$ (s/kg)
7.98	12,551	1.50	32,090	3,970	20.839	2.585
6.37	10,017	1.65	23,463	4,510	23.973	4.608
4.06	6,394	1.65	13,837	5,414	34.803	13.618
3.1955	5,024	1.65	10,589	4,230	42.994	17.173
2.3298	3,663	1.65	11,953	6,443	91.312	49.215
1.466	2,304	1.65	14,722	10,776	284.023	207.890
1.19	1,872	1.65	15,481	12,776	453.272	359.046
0.82766	1,300	1.65	16,392	14,464	993.728	876.760

[a]Glass spherical particles with diameters of 74-88 μm.

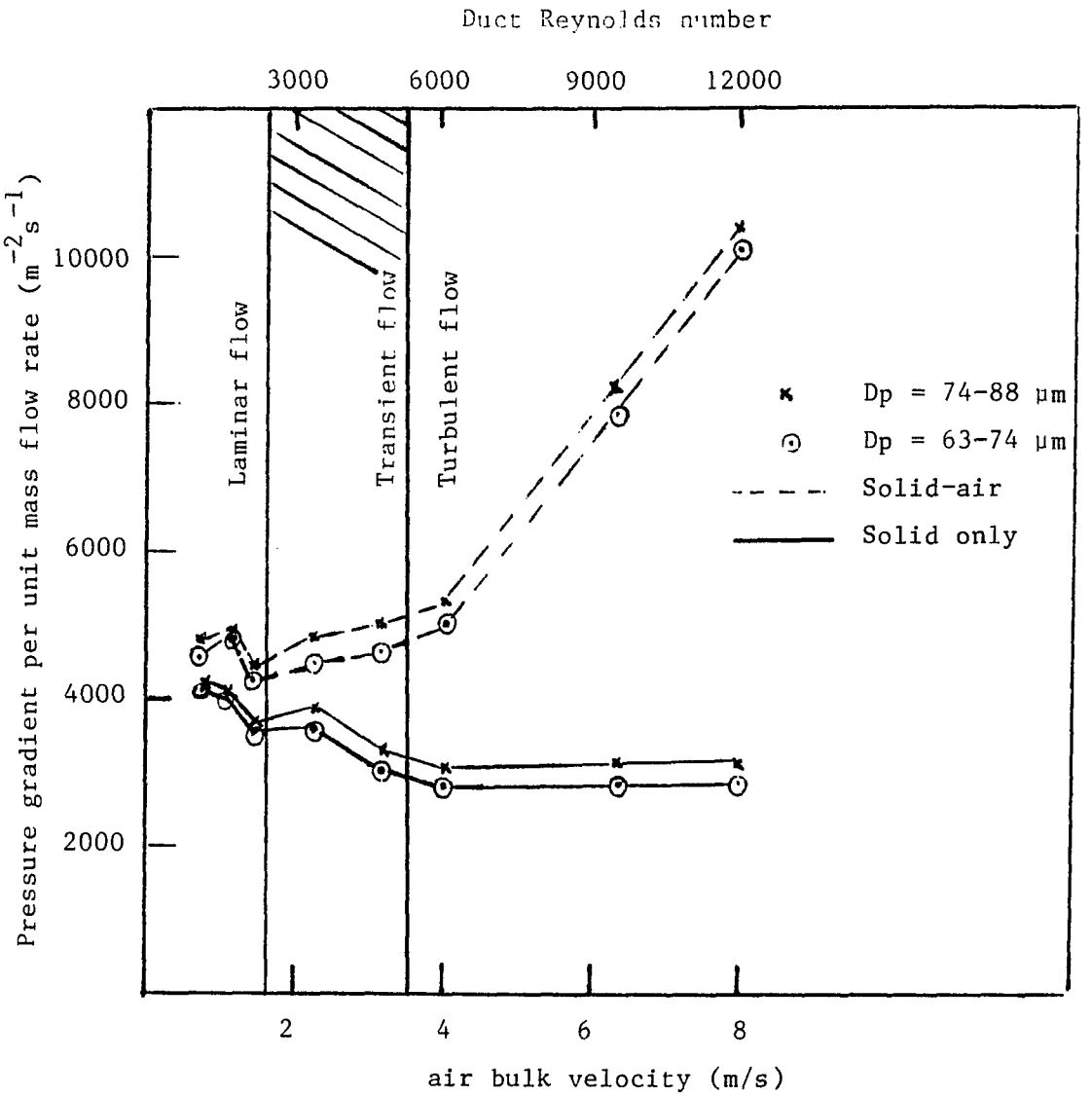

Figure 4.6. Effect of particles on the pressure gradient per unit mass flow rate of the copper particles (hatch area shown for particle free flow)

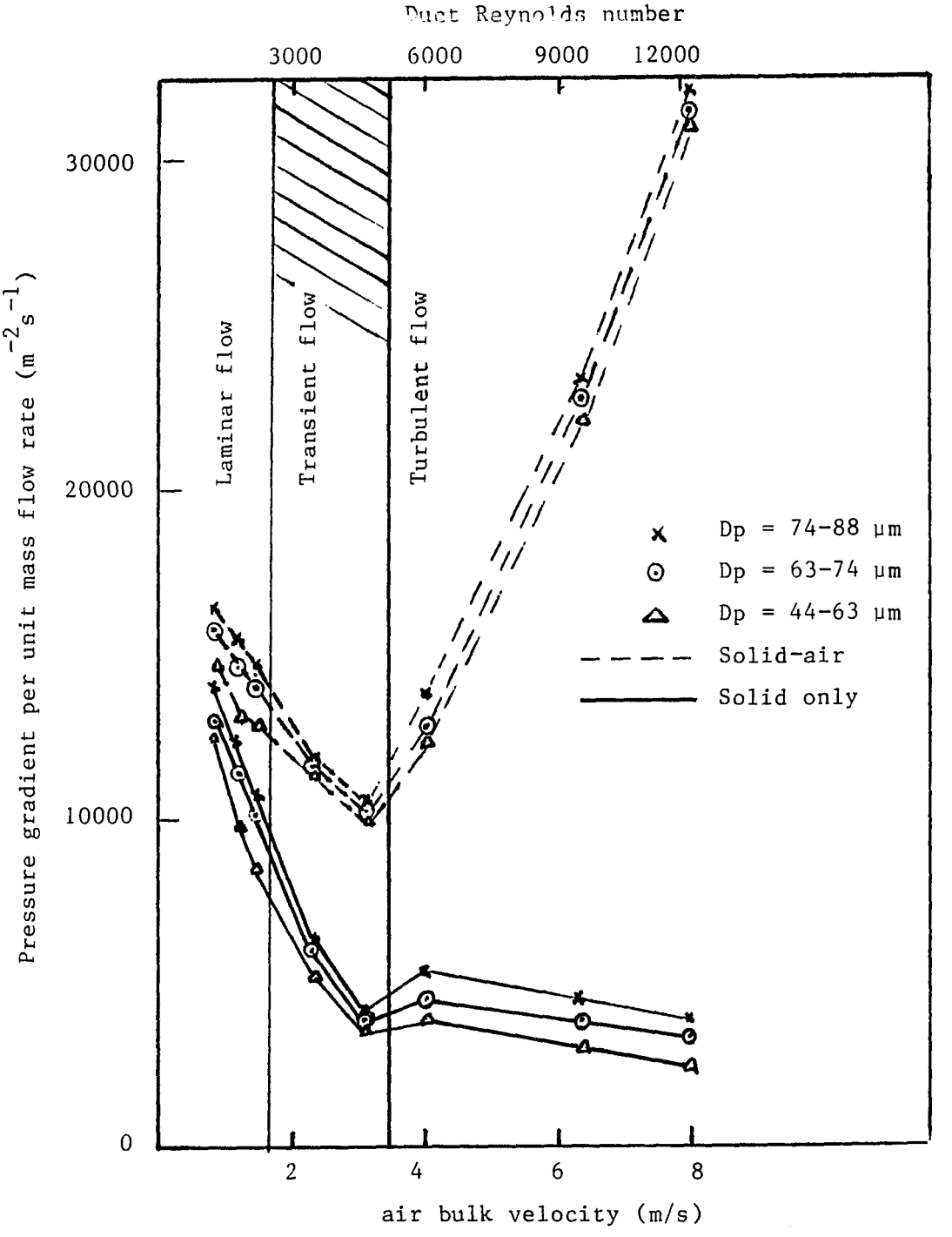

Figure 4.7. Effect of particles on the gradient per unit mass flow rate of glass particles (hatch area shown for particle free flow)

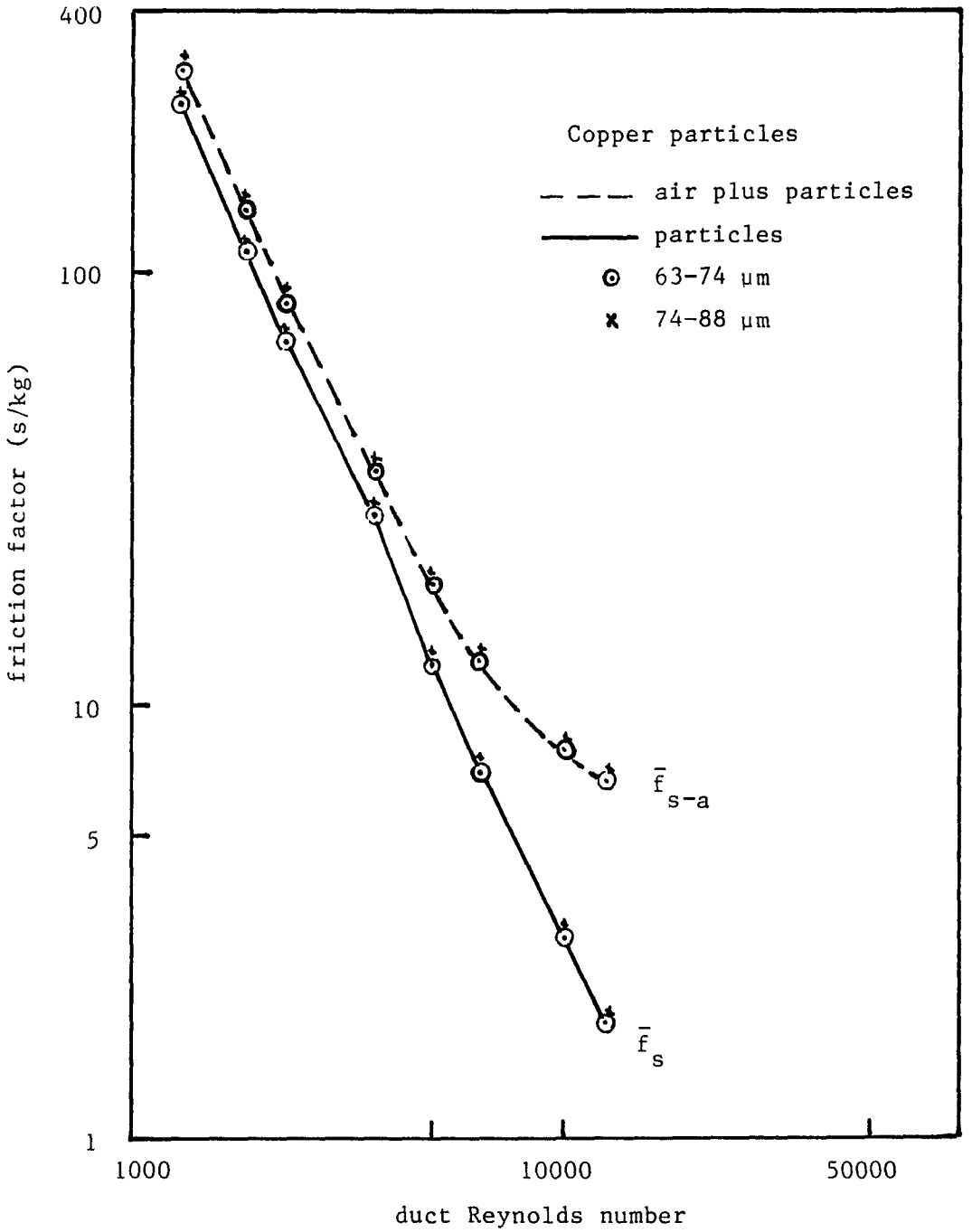

Figure 4.8. Friction factor $\bar{f}_{s-a}$ (total, particles plus air) and $\bar{f}_s$ (particles) versus duct Reynolds number

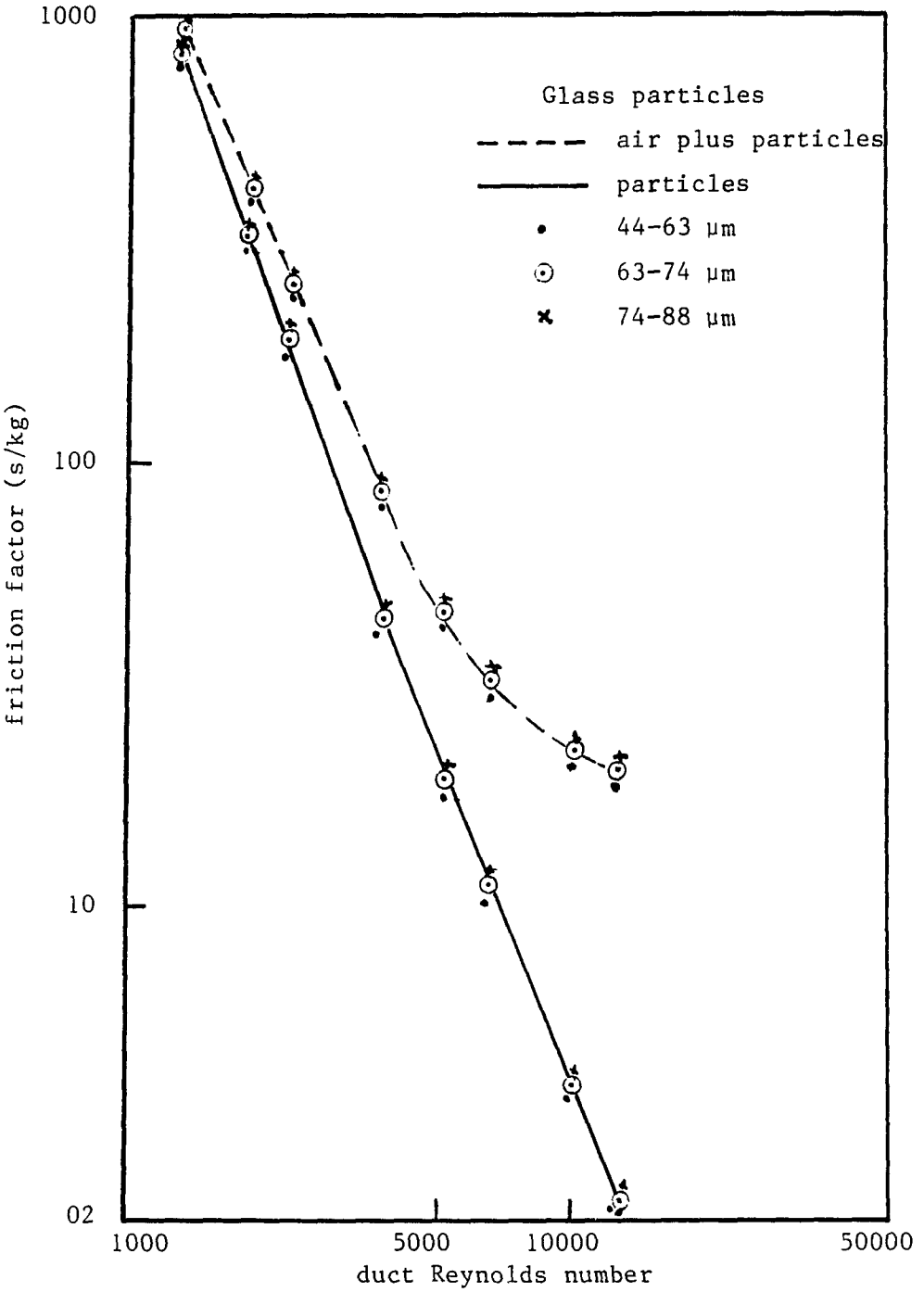

Figure 4.9. Friction factor $\bar{f}_{s-a}$ (total, particles plus air) and $\bar{f}_{s}$ (particles) versus duct Reynolds number

Chapter 3). Since both the mass density and the vertical velocity of the particles are not the same for copper and glass, different curves should be expected for the two kinds of material. Also it should be expected that a single curve would be found for particles of different sizes but of the same material and at the same electric field strength (i.e., the same vertical velocity).

Calculated data of the apparent drag coefficient $\bar{C}_D$ based on the obtained data of Tables 13.1-13.40 are presented in Tables 4.11-4.15 for copper particles having diameters of (63-74 and 74-88) μm and glass particles having diameters of (44-63, 63-74 and 74-88) μm respectively. Figures (4.11 and 4.12) are a plot of the apparent drag coefficient $\bar{C}_D$ vs the particle Reynolds number Re_p for copper and glass respectively where the particle Reynolds number is defined as

$$Re_p = \frac{V_r D_p}{\nu} \tag{4.5}$$

D_p average diameter of the particles.

V_r relative air to particle velocity.

$$V_r^2 = (u_a - u_s)^2 + v_s^2 \tag{4.6}$$

Make reference to Figure 4.10. The drag coefficient for the particle were calculated for the portion of the duct in which the particles had steady state velocity as follows

$$\Delta p_s = F_p \; n \; L_{ss} \cos \psi \tag{4.7}$$

where

The pressure drop due to the presence of the particles corresponding to a the length of the duct L_{ss}.

Table 4.11. Apparent drag coefficient $\bar{C}_D$ vs. particle Reynolds number Re_p[a]

u_a (m/s)	u_s (m/s)	$\bar{V}_r$ (m/s)	cos θ	Re_p	L_{ss} (m)	ΔP_s (Pa)	$nx10^{-8}$ (m^{-3})	$\bar{C}_D$
7.98	2.65	5.4229	0.9828	23.980	0.90	12.667	1.466	1.502
6.37	2.1	4.3855	0.9736	19.397	1.05	14.667	1.829	1.844
4.06	1.35	2.8886	0.9382	12.776	1.35	18.667	2.845	2.807
3.1955	1.05	2.3671	0.9063	10.470	1.50	22.400	3.658	3.634
2.3298	0.77	1.8520	0.8418	8.195	1.65	29.507	4.989	5.620
1.466	0.48	1.4040	0.7021	6.211		18.533	4.954	7.449
1.19	0.39	1.2800	0.6247	5.664		13.040	3.904	8.938
0.82766	0.27	1.1449	0.4870	5.064		13.640	5.639	9.979

[a]Copper spherical particles with diameters of 63-74 μm. Particle vertical velocity of 1.0 m/s.

Table 4.12. Apparent drag coefficient $\bar{C}_D$ vs. particle Reynolds number Re_p[a]

u_a (m/s)	u_s (m/s)	$\bar{V}_r$ (m/s)	cos θ	Re_p	L_{ss} (m)	ΔP_s (Pa)	$nx10^{-8}$ (m^{-3})	$\bar{C}_D$
7.98	2.05	6.0186	0.9861	31.259	0.90	14.000	1.158	1.234
6.37	1.63	4.844	0.9784	25.153	1.05	16.667	1.457	1.558
4.06	1.05	3.171	0.9490	16.468	1.35	20.400	2.261	2.299
3.1955	0.82	2.577	0.9217	13.380	1.50	24.80	2.895	3.062
2.3298	0.60	1.998	0.8657	10.374	1.65	23.040	3.957	4.660
1.466	0.38	1.476	0.7356	7.665	1.65	18.667	3.868	5.989
1.19	0.31	1.332	0.6606	6.916	1.65	13.173	3.036	7.363
0.82766	0.22	1.170	0.5193	6.075	1.65	13.773	4.278	8.9935

[a]Copper spherical particles with diameters of 74-88 μm. Particle vertical velocity of 1.0 m/s.

Table 4.13. Apparent drag coefficient $\bar{C}_D$ vs. particle Reynolds number Re_p[a]

u_a (m/s)	u_s (m/s)	$\bar{V}_r$ (m/s)	cos θ	Re_p	L_{ss} (m)	Δp_s (Pa)	$nx10^{-8}$ (m^{-3})	$\bar{C}_D$
7.98	5.2	3.2580	0.8531	11.279	1.5	6.000	1.536	2.0916
6.37	4.15	2.7960	0.7939	9.678	1.65	6.667	1.925	2.2895
4.06	2.65	2.2080	0.6384	7.640	1.65	8.933	3.015	4.2895
3.1955	2.3	1.9200	0.4660	6.651	1.65	8.440	3.474	6.3276
2.3298	1.5	1.8917	0.4386	6.548	1.65	8.173	3.298	7.0745
1.466	0.94	1.7790	0.2954	6.159	1.65	7.693	3.370	10.9217
1.19	0.77	1.7510	0.2398	6.060	1.65	8.640	4.125	12.7428
0.82766	0.53	1.7258	0.1721	5.970	1.65	12.440	5.994	18.1104

[a]Glass spherical particles with diameters of 44-63 μm. Particle vertical velocity of 1.7 m/s.

Table 4.14. Apparent drag coefficient $\bar{C}_D$ vs. particle Reynolds number Re_p[a]

u_a (m/s)	u_s (m/s)	$\bar{V}_r$ (m/s)	cos θ	Re_p	L_{ss} (m)	Δp_s (Pa)	$nx10^{-8}$ (m^{-3})	$\bar{C}_D$
7.98	3.950	4.3700	0.9213	19.346	1.50	6.780	0.972	1.197
6.37	3.150	3.6410	0.88432	16.100	1.65	8.667	1.219	1.661
4.06	2.000	2.6700	0.77128	11.810	1.65	9.600	1.920	2.491
3.1955	1.750	2.2310	0.6477	9.870	1.65	8.573	2.195	3.318
2.3298	1.150	2.690	0.57015	9.153	1.65	8.440	2.068	4.582
1.466	0.725	1.8544	0.39957	8.200	1.65	9.467	2.100	8.988
1.19	0.590	1.8027	0.3328	7.970	1.65	9.973	2.580	9.786
0.82766	0.409	1.7508	0.23912	7.740	1.65	12.573	3.723	12.625

[a]Glass spherical particles with diameters of 63-74 μm. Particle vertical velocity of 1.7 m/s.

Table 4.15. Apparent drag coefficient $\bar{C}_D$ vs. particle Reynolds number Re_p[a]

u_a (m/s)	u_s (m/s)	$\bar{V}_r$ (m/s)	cos θ	Re_p	L_{ss} (m)	Δp_s (Pa)	$nx10^{-8}$ (m^{-3})	$\bar{C}_D$
7.98	3.05	5.215	0.9453	27.07	1.5	8.000	0.778	0.8747
6.37	2.40	4.3186	0.91926	22.42	1.65	10.000	0.989	1.1726
4.06	1.550	3.0315	0.82796	15.74	1.65	12.000	1.532	2.0482
3.1955	1.400	2.472	0.72615	12.83	1.65	9.373	1.695	2.4746
2.3298	0.900	2.221	0.6417	11.532	1.65	8.840	1.637	3.3843
1.466	0.600	1.907	0.45391	9.906	1.65	9.467	1.567	7.0877
1.19	0.455	1.8521	0.3968	9.617	1.65	10.773	2.068	7.610
0.82766	0.316	1.775	0.2876	9.216	1.65	12.707	2.946	9.458

[a]Glass spherical particles with diameters of 74-88 μm. Particle vertical velocity of 1.7 m/s.

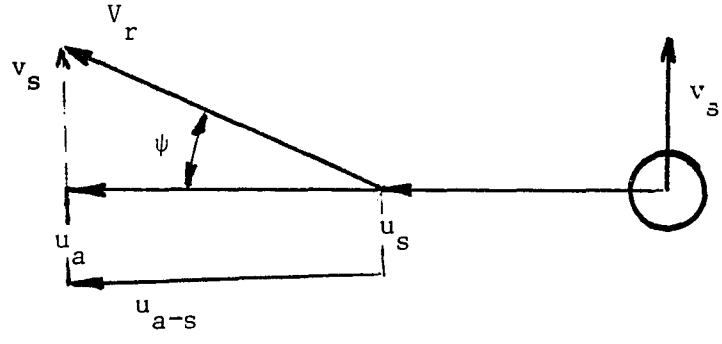

Figure 4.10. Diagram of air and particle velocities

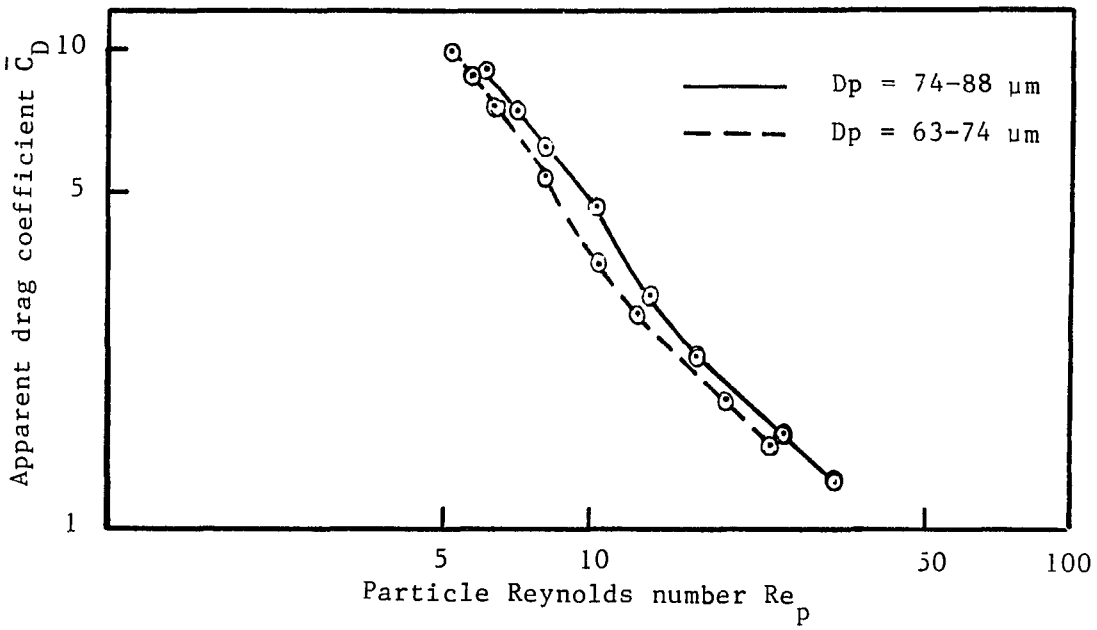

Figure 4.11. Apparent drag coefficient of copper particles versus particle Reynolds number

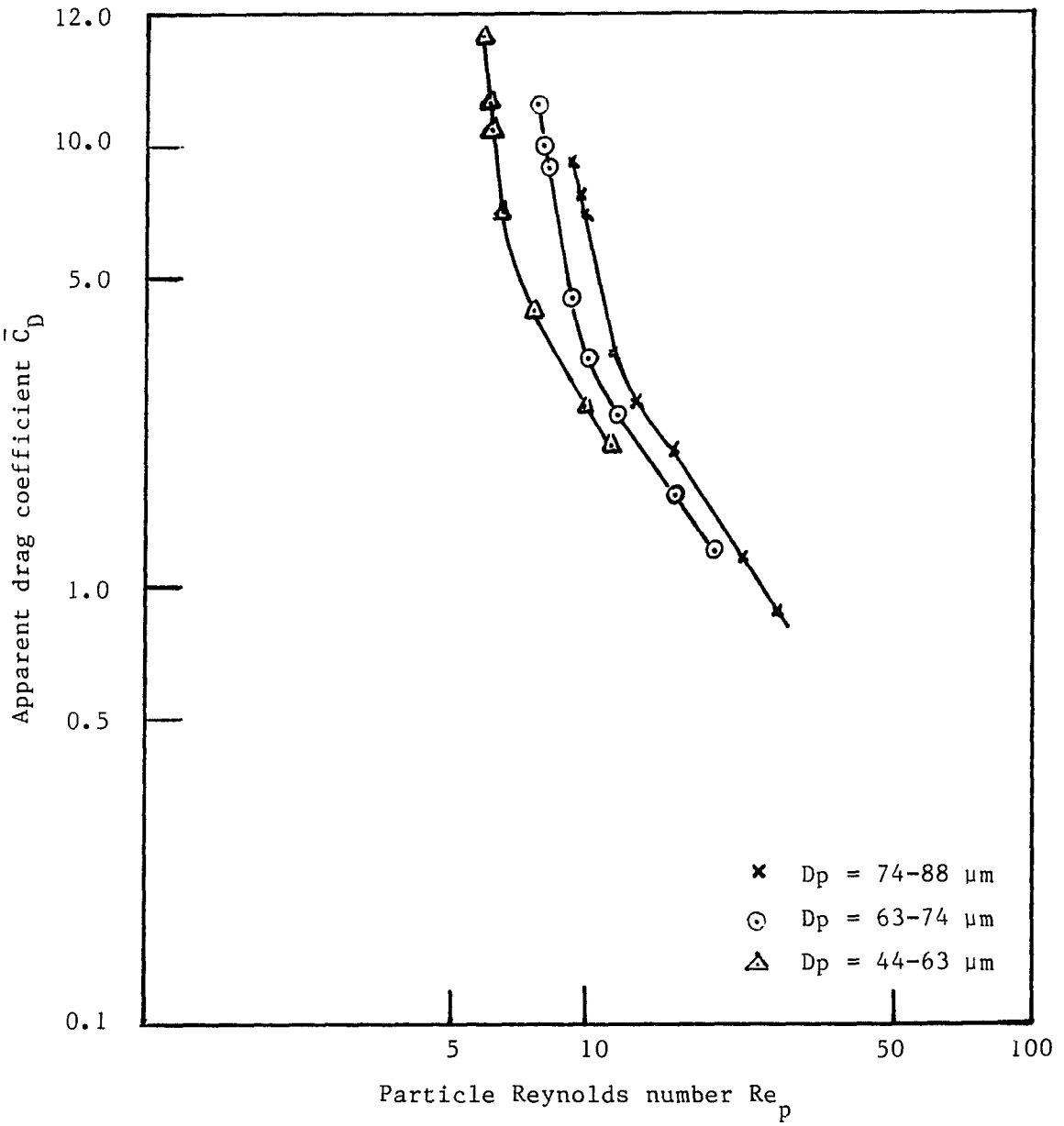

Figure 4.12. Apparent drag coefficient of glass particles versus particle Reynolds number

$\Delta p_s = \Delta p_{s-a} - \Delta p_a$

F_p force per particle

ψ angle of the particle velocity vector with horizontal axes.

$$F_p = \frac{1}{2} \rho_a V_r^2 \bar{C}_D S \tag{4.8}$$

S is a reference area. In this analysis the cross section area of the particle is taken as a reference area.

The apparent drag coefficient of particles with different sizes but the same material at the same electric field strength, can be reduced to a single curve by using the definition of $\bar{R}e_p$ as

$$\bar{R}e_p = Re_p - Re_{p,lim} \tag{4.9}$$

where

$Re_{p,lim}$ is the limiting value of the particle Reynolds number as the air velocity tends to zero

$$Re_{p,lim} = \frac{V_s D_p}{\nu}$$

Values of apparent drag coefficient $\bar{C}_D$ versus the newly defined Reynolds number $\bar{R}e_p$ are presented in Tables 4.16 and 4.17 for copper and glass particles respectively.

A computer code RCURV was used to obtain correlations of the data for both copper and glass particles as a polynomial curve of the second degree with the least squares technique. Correlations were obtained in both linear and log-log scale. The following are the obtained correlations.

The correlation found for the apparent drag coefficient $\bar{C}_D$ of the copper particle vs $\bar{R}e_p$ in a linear and log-log scale respectively give

Table 4.16. Apparent drag cofficient $\bar{C}_D$ of Copper particles vs. the modified Reynolds number $\bar{Re}_p$ [a]

Re_p	$\bar{Re}_p$	$\bar{C}_D$
23.980	19.557	1.502
19.397	14.974	1.844
12.776	8.353	2.807
10.470	6.047	3.634
8.195	3.772	5.620
6.211	1.788	7.449
5.664	1.241	8.938
5.064	0.641	9.979
31.251	26.058	1.234
25.153	19.961	1.558
16.468	11.276	2.299
13.380	8.188	3.062
10.374	5.182	4.660
7.665	2.473	5.989
6.916	1.724	7.363
6.075	0.883	8.9935

[a] Re_{Lim} of particles with diameters of 63-74 μm = 4.423. Re_{Lim} of particles with diameters of 74-88 μm = 5.192.

Table 4.17. Apparent drag cofficient $\bar{C}_D$ of Copper particles vs. the modified Reynolds number $\bar{Re}_p$ [a]

Re_p	$\bar{Re}_p$	$\bar{C}_D$
11.278	5.3933	2.092
9.678	3.7933	2.495
7.640	1.7554	4.290
6.651	0.7664	6.328
6.548	0.6633	7.075
6.159	0.2743	10.922
6.060	0.1754	12.743
5.970	0.0854	18.111
19.346	11.8260	1.197
16.100	8.5808	1.661
11.810	4.2908	2.491
9.870	2.3506	3.318
9.153	1.6334	4.582
8.200	0.6808	0.988
7.970	0.4508	9.786
7.740	0.2208	12.625
27.070	18.244	0.875
22.420	13.594	1.173

[a] Re_{Lim} of particles with diameters of 44-63 μm = 5.885. Re_{Lim} of particles with diameters of 63-74 μm = 7.519. Re_{Lim} of particles with diameters of 74-88 μm = 8.826.

Table 4.17. Continued

Re_p	$\bar{R}e_p$	$\bar{C}_D$
15.740	6.914	2.048
12.83	3.974	2.475
11.532	2.706	3.384
9.906	1.080	7.088
9.617	0.791	7.610
9.216	0.390	9.458

$$\bar{C}_D = 9.185820 - 0.911086\ \bar{R}e_p + 0.024662\ \bar{R}e_p^{\,2} \qquad (4.10)$$

$$\text{Log}\ \bar{C}_D = 0.9556583 - 0.299262\ \text{Log}\ \bar{R}e_p - 0.2312489\ (\text{Log}\ \bar{R}e_p)^2 \qquad (4.11)$$

Similarly, the correlations apparent drag coefficient $\bar{C}_D$ found for the glass particles vs $\bar{R}e_p$ in a linear and log-log scale respectively.

$$\bar{C}_D = 10.33640 - 2.03288\ \bar{R}e_p + 0.090086\ \bar{R}e_p^{\,2} \qquad (4.12)$$

$$\text{Log}\ \bar{C}_D = 0.792739285 - 0.5407780\ \text{log}\ \bar{R}e_p - 0.09990713\ (\text{log}\ Re_p)^2 \qquad (4.13)$$

The obtained data for copper and glass particles compared to its coressponding correlation are plotted in a log-log scale Figures 4.13 and 4.14 respectively.

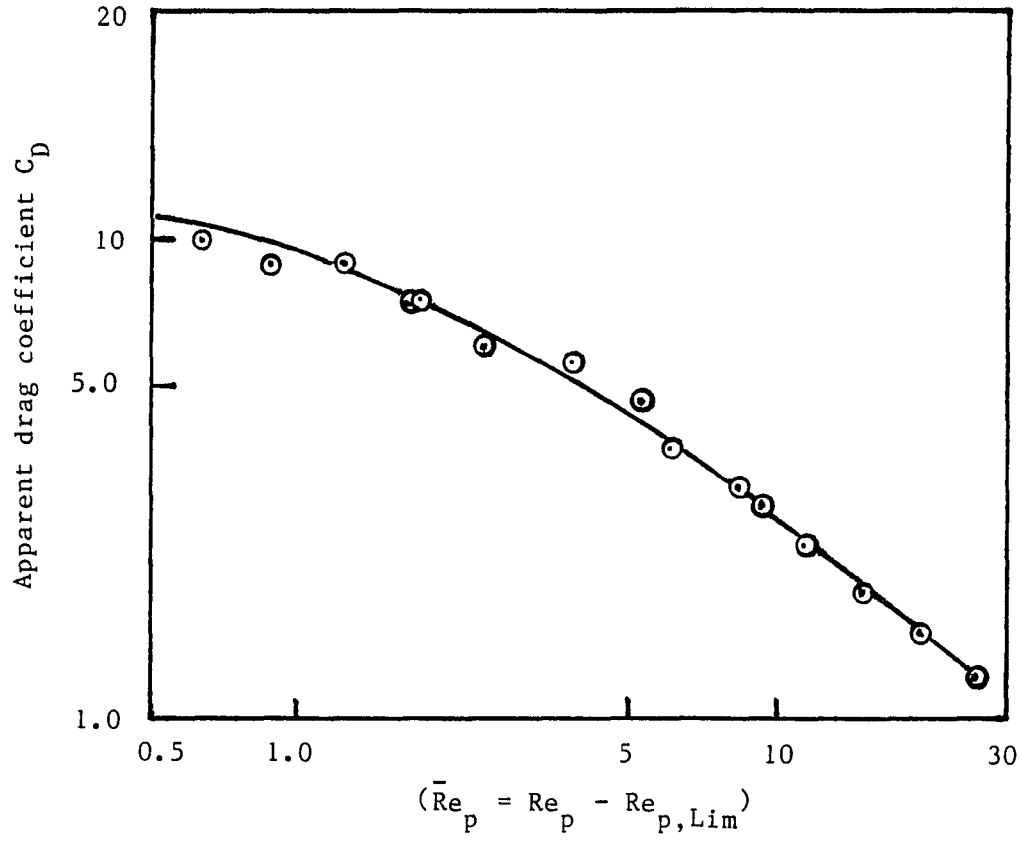

Figure 4.13. Apparent drag coefficient $\bar{C}_D$ of the copper particles versus the modified Reynolds number $\bar{Re}_p$

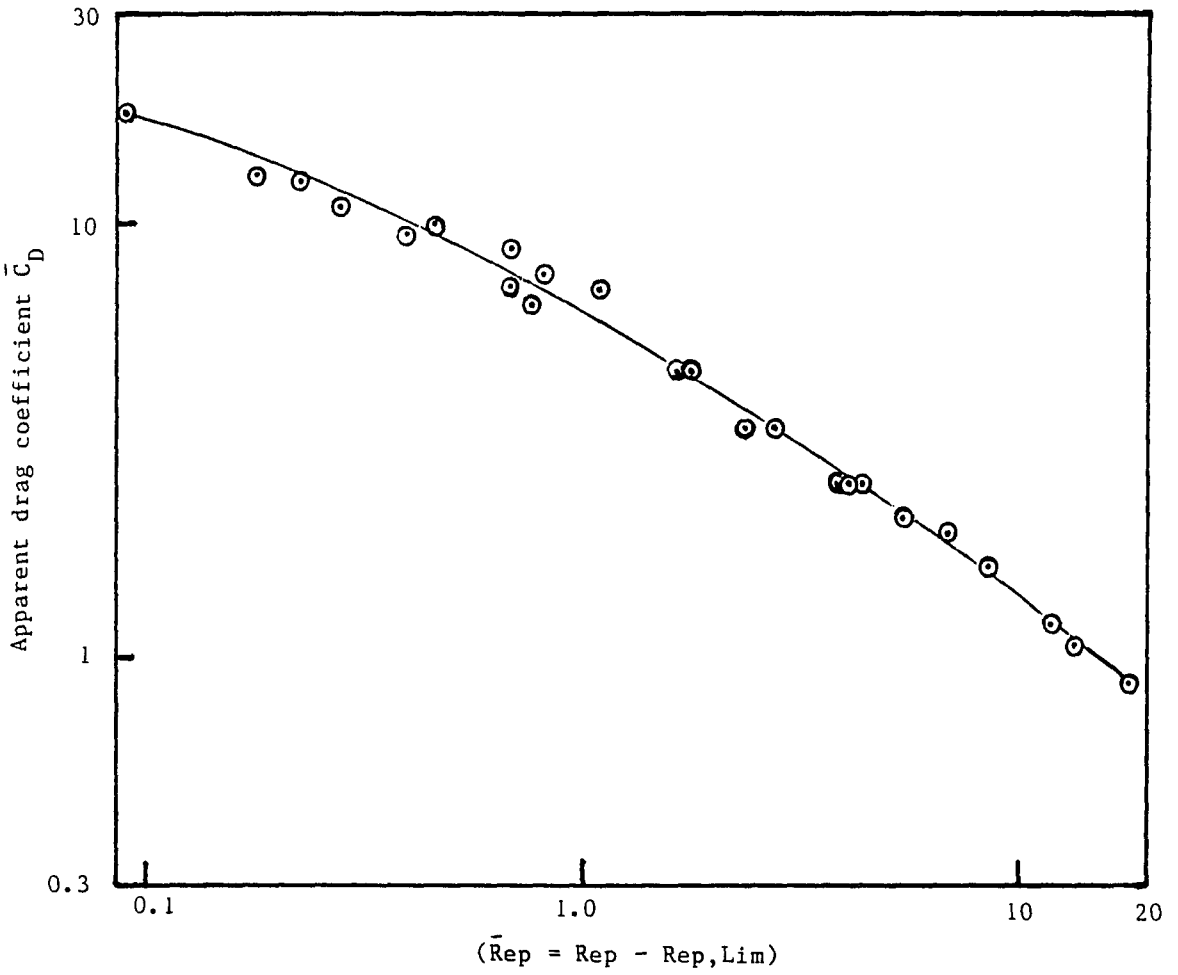

Figure 4.14. Apparent drag coefficient $\bar{C}_D$ of the glass particles versus modified Reynolds number $\bar{R}e_p$

4.6. Measurement of the Solid-Air Flow Parameters in a Duct at Different Values of Electric Field Strength

The following work is an experimental investigation into the effect of the electric field strength on the static pressure drop of a solid-air flow Δp_{s-a} in a duct. Glass particles were selected for these tests for the following reasons:

1. Glass particles have low electric conductivity which allowed the increase of the electric field strength up to 6.25 kv/cm without causing electric breakdown.
2. Glass particles begin to oscillate at electric field strength of 2.5 kv/cm.
3. The glass particle vertical velocity is increasing with the increase of the electric field strength in this possible range of investigation (see Table 4.2).

The experiment was carried out by feeding the glass particle to the duct at a constant and measured volumetric rate of 0.555 cc/s in each test. The volumetric feeding rate was chosen so that all the fed particles could oscillate between the electrodes in all the tested range of the electric field strength. The test was done for glass particles having diameters of 44-63, 63-74 and 74-88 μm. Each particle size was tested at air bulk velocities of 7.89, 6.37, 4.06, and 3.1955 m/s. For each air bulk velocity the static pressure drop due to the solid-air flow, across a distance of 1.8 m of the duct was measured at electric field strength of 0, 2.5, 3.75, 5, and 6.25 kv/cm. It was noticed that for air bulk velocities less than 3.19 m/s and an electric field strength less than 5 kv/cm the glass

particles began to accumulate in the feeder, threfore, data of these air bulk velocities were ignored.

The test data are presented in Tables 4.18, 4.19 and 4.20 for glass particles of diameters 44-63, 63-74 and 74-88 μm respectively.

4.6.1. Analysis of test data

The effect of the electric field strength on the solid-air flow will be demonstrated using the particle size of (74-88) μm as an example. Test data of Table 4.20 can be plotted as follows:

1. Solid-air pressure drop as a function of air flow bulk velocity taking E as a parameter (see Figure 4.15).
2. Solid-air pressure drop as a function electric field strength taking u_a as a parameter (see Figure 4.16).

Figure 4.15 shows that for all the tested regime of air conveying speeds the solid-air pressure drop have a minimum value at E = 2.5 kv/cm then it increases by the increase of the electric field strength.

Figure 4.16 shows that for all the tested range of electric field strength, the pressure drop decreases by the decrease of the speed of the conveying air. Making use of Figure 4.7 for E = 5 kv/cm it can be seen that the pressure drop increases again in the laminar flow regime.

The pressure drop due to the solid part only Δp_s can be expressed as

$$\Delta p_s = \Delta p_{s-a} - \Delta p_a$$

where

Δp_a is the pressure drop due to an air flow without particle (see Table 4.5 for ${}_1\Delta p_{13}$).

Δp_{s-a} see Table 4.20.

Table 4.18. Pressure drop of solid-air flow ΔP_{s-a} versus electric field strength E and air buk velocity u_a[a]

	ΔP_{s-a} (torr)				
u_a (m/s)	E = 6.25 $\frac{kv}{cm}$	E = 5 $\frac{kv}{cm}$	E = 3.75 $\frac{kv}{cm}$	E = 2.5 $\frac{kv}{cm}$	E = 0.0 $\frac{kv}{cm}$
7.98	0.615	0.59	0.567	0.545	0.55
6.37	0.445	0.425	0.405	0.385	0.39
4.06	0.277	0.247	0.217	0.187	0.197
3.1955	0.223	0.203	0.173	0.153	0.158

[a]Glass spherical particles with diameters of 44-63 μm.

Table 4.19. Pressure drop of solid-air flow ΔP_{s-a} versus electric field strength E and air buk velocity u_a[a]

	ΔP_{s-a} (torr)				
u_a (m/s)	E = 6.25 $\frac{kv}{cm}$	E = 5 $\frac{kv}{cm}$	E = 3.75 $\frac{kv}{cm}$	E = 2.5 $\frac{kv}{cm}$	E = 0.0 $\frac{kv}{cm}$
7.98	0.618	0.593	0.57	0.578	0.553
6.37	0.460	0.44	0.420	0.4	0.405
4.06	0.282	0.252	0.222	0.192	0.202
3.1955	0.235	0.215	0.185	0.165	0.170

[a]Glass spherical particles with diameters of 63-74 μm.

Table 4.20. Pressure drop of solid-air flow ΔP_{s-a} versus electric field strength E and air buk velocity u_a[a]

	ΔP_{s-a} (torr)				
u_a (m/s)	E = 6.25 $\frac{kv}{cm}$	E = 5 $\frac{kv}{cm}$	E = 3.75 $\frac{kv}{cm}$	E = 2.5 $\frac{kv}{cm}$	E = 0.0 $\frac{kv}{cm}$
7.98	0.63	0.605	0.582	0.560	0.565
6.37	0.475	0.455	0.435	0.415	0.42
4.06	0.30	0.27	0.24	0.21	0.22
3.1955	0.23	0.21	0.18	0.16	0.165

[a]Glass spherical particles with diameters of 74-88 μm.

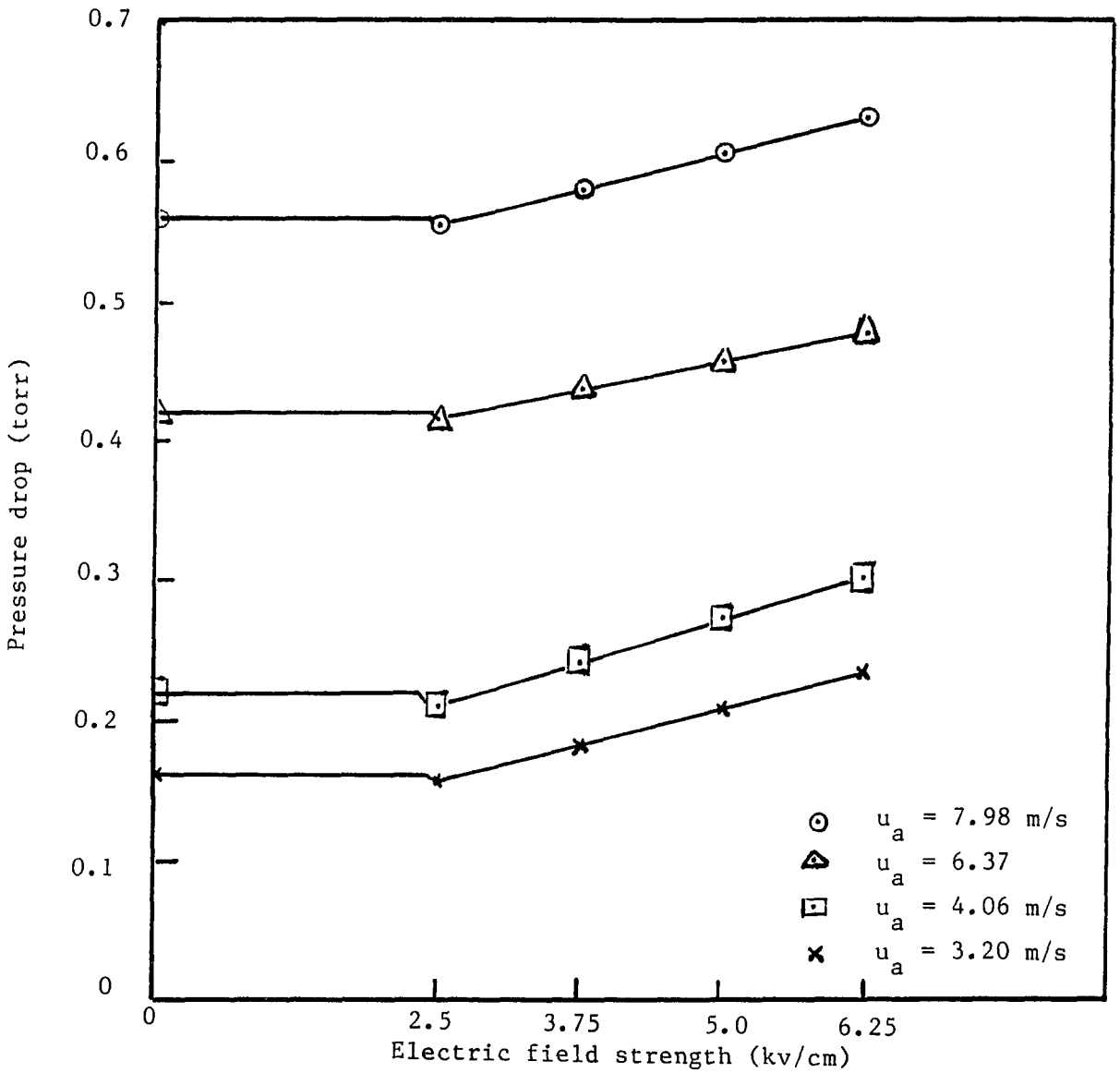

Figure 4.15. Pressure drop of solid-air flow versus electric field strength for various air velocities (G = 0.55 cc/s)

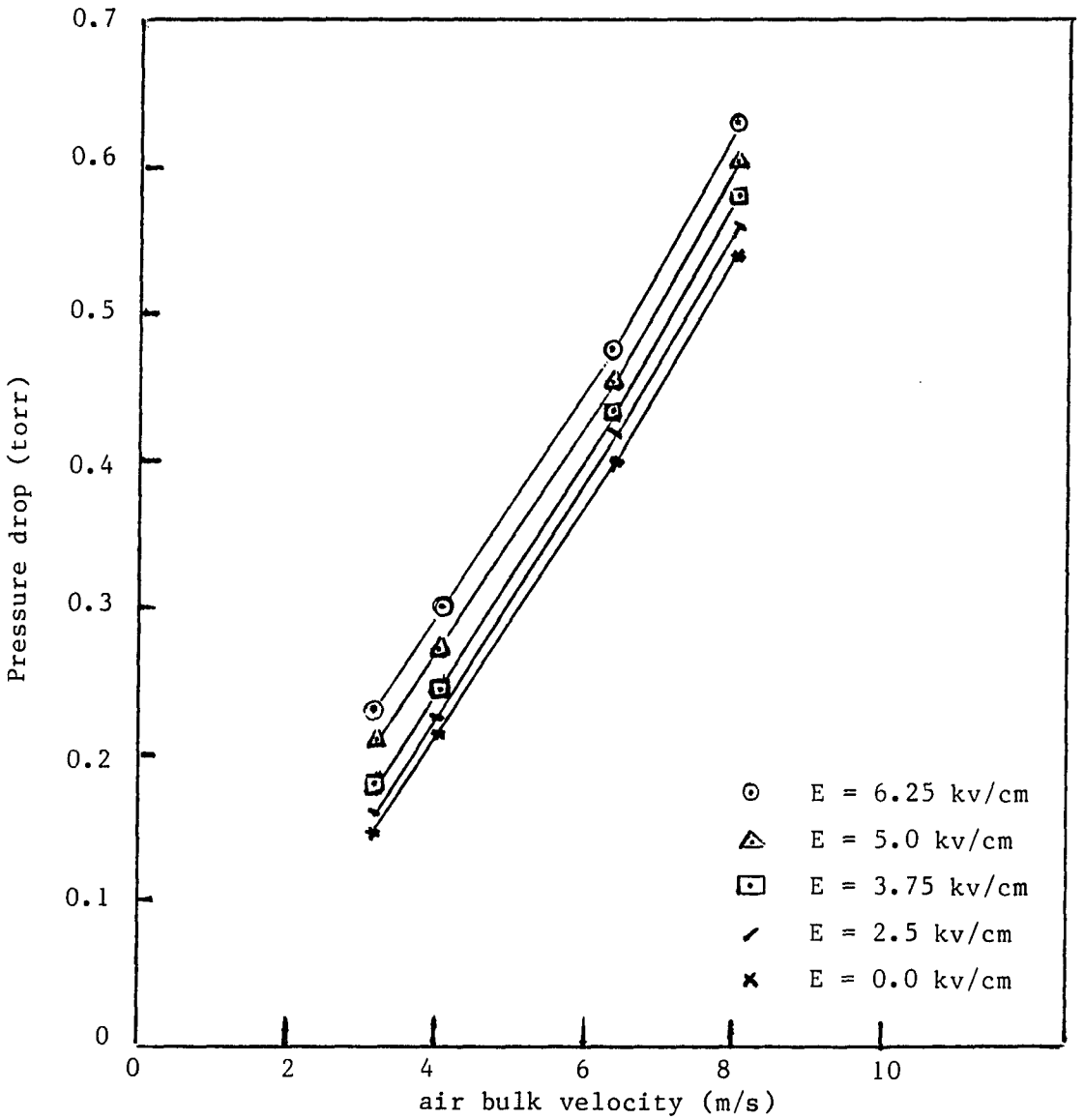

Figure 4.16. Pressure drop of solid-air flow versus air bulk velocity for various electric field strengths (G = 0.55 cc/s)

Values of Δp_s for different electric field strength and different conveying air bulk velocity for glass having diameter of (74-88) μm are summarized in Table 4.21.

Data of Table 4.20 plotted in Figure 4.17 show that the pressure drop due to the particle only has a minimum value at E = 2.5 kv/cm.

4.7. Measurement of the Pressure Drop of a Solid-Air Flow at Various Electric Field Strength and Mass Flow Rate of the Conveyed Particles

The following work is directed at the experimental determination of the change of the pressure gradient of solid-air flow in a duct, due to the change of the conveyed particle mass flow rate and/or the strength of the electric field. The experiment was carried out by feeding glass particles having diameters of 74-88 μm with steady state and constant mass flow rate of 0.0, 0.5324, 0.8315, and 1.3431 grm/s for each test respectively. These mass flow rates were a result of supplying the D.C servometer by voltage of 0, 10, 15, 23.3 V respectively. An air was fed to the duct with constant bulk velocity of 7.88 m/s in all tests. The pressure drop across a distance of 1.8 m of the duct due to the solid-air flow corresponding to electric field strengths of 0, 2.5, 3.75, 5, 6.25, and 7.5 kv/cm. The test was repeated for each value of the premeasured flow rates.

Particles of glass were used in this experiment because of the wide range of the change of the particle vertical velocity corresponding to the change of the electric field strength (see Table 4.2). In order to minimize the predicted error in the pressure drop measurements, the velocity of the conveying air was chosen to be the maximum measurable value by the available rotameters. Also the particle diameter was chosen to be

Table 4.21. Pressure drop due to particles only at different air velocity and electric field strength[a]

u_a (m/s)	ΔP_s (torr) E = 6.25 $\frac{kv}{cm}$	E = 5 $\frac{kv}{cm}$	E = 3.75 $\frac{kv}{cm}$	E = 2.5 $\frac{kv}{cm}$	E = 0.0 $\frac{kv}{cm}$
7.98	0.105	0.08	0.057	0.035	0.04
6.37	0.12	0.1	0.08	0.06	0.065
4.06	0.14	0.11	0.08	0.05	0.06
3.1955	0.12	0.1	0.07	0.05	0.055

[a]Glass spherical particles with diameters of 74-88 μm.

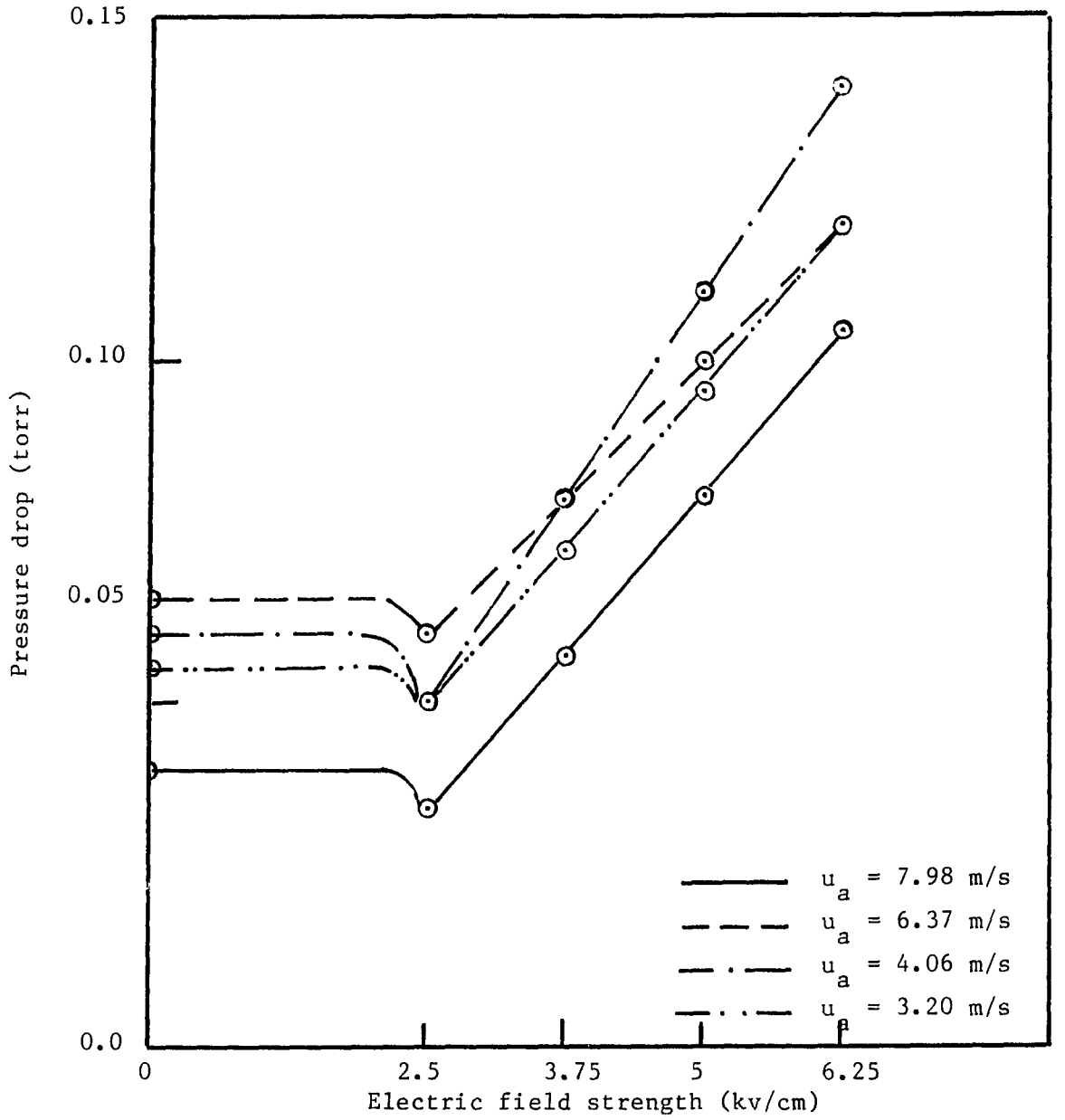

Figure 4.17. Pressure drop due to particles only versus electric field strength at various air bulk velocities (G = 0.55 cc/s)

the biggest available size, expecting a similar trend for the other diameters and air bulk velocities.

The test data are summarized in Table 4.22 and plotted in Figures 4.18 and 4.19. While the data of the pressure gradient due to the solid flow only per unit mass flow rate of the conveyed glass particles vs mass flow rate of the conveyed glass particles and the electric field strength are summarized in Table 4.23.

4.7.1. Analysis of the test data

Figure 4.18 shows that, the pressure drop of the solid-air flow corresponding to different mass flow rates of glass particles having diameters of 74-88 μm, and conveyed by an air having a bulk velocity of 7.98 m/s has a minimum at E = 2.5 kv/cm. Combining this conclusion with conclusions obtained from Figure 4.15 and Tables 4.18 and 4.19 one can conclude the following. For all sizes of the tested spherical glass particles at all speeds of the conveying air and all mass flow rates of the conveyed particles, the corresponding minimum pressure loss is obtained at E = 2.5 kv/cm. The only restriction to this fact is that the solid-air flow should be a diluted mixture.

Figure 4.19 shows the following for glass particles with diameters of 74-88 μm: The static pressure drop of solid-air flow increases linearly with the increase of mass flow rate of the conveyed glass particles at any fixed electric field strength; the slope of this linear relation depends on the strength of the electric field; the minimum slope corresponds to an electric field strength of 2.5 kv/cm.

Table 4.22. Summary of test data pressure drop vs. $\dot{m}_s$, E[a]

Electric field Strength E (kv/cm)	Pressure drop of solid-air flow ΔP_{s-a} (torr)			
	$\dot{m}_s = 0$	$\dot{m}_s = 0.5324$ (grm/s)	$\dot{m}_s = 0.8315$ (grm/s)	$\dot{m}_s = 1.3431$ $(\frac{grm}{f})$
0	0.525	0.543	0.553	0.57
2.5	0.525	0.540	0.547	0.56
3.75	0.525	0.548	0.560	0.582
5	0.025	0.557	0.575	0.605
6.25	0.525	0.570	0.595	0.640
7.5	0.525	0.578	0.607	0.657

[a]Glass spherical particles with diameters of 74-88 μm.

Table 4.23. Pressure gradient due to solid flow only per unit mass flow rate of conveyed glass $[\frac{\Delta P_s}{L \dot{m}_s}]$ vs. electric field strength E and mass flow rate of glass particles

Electric field Strength E (kv/cm)	Pressure gradient due to glass particles per unit mass flow rate of the particles $[S^{-1} m^{-2}]$		
	$\dot{m}_s = 0.5314$ (kg/s)	$\dot{m}_s = 0.8315$ (kg/s)	$\dot{m}_s = 1.3431$ (kg/s)
0	2504.3	2488.8	2481.7
2.5	2086.6	1959.2	1925.8
3.75	3199.9	3117.7	3143.55
5	4452.1	4467.3	4411.7
6.25	6260.7	6235.77	6243.69
7.5	7373.8	7304.2	7279.8

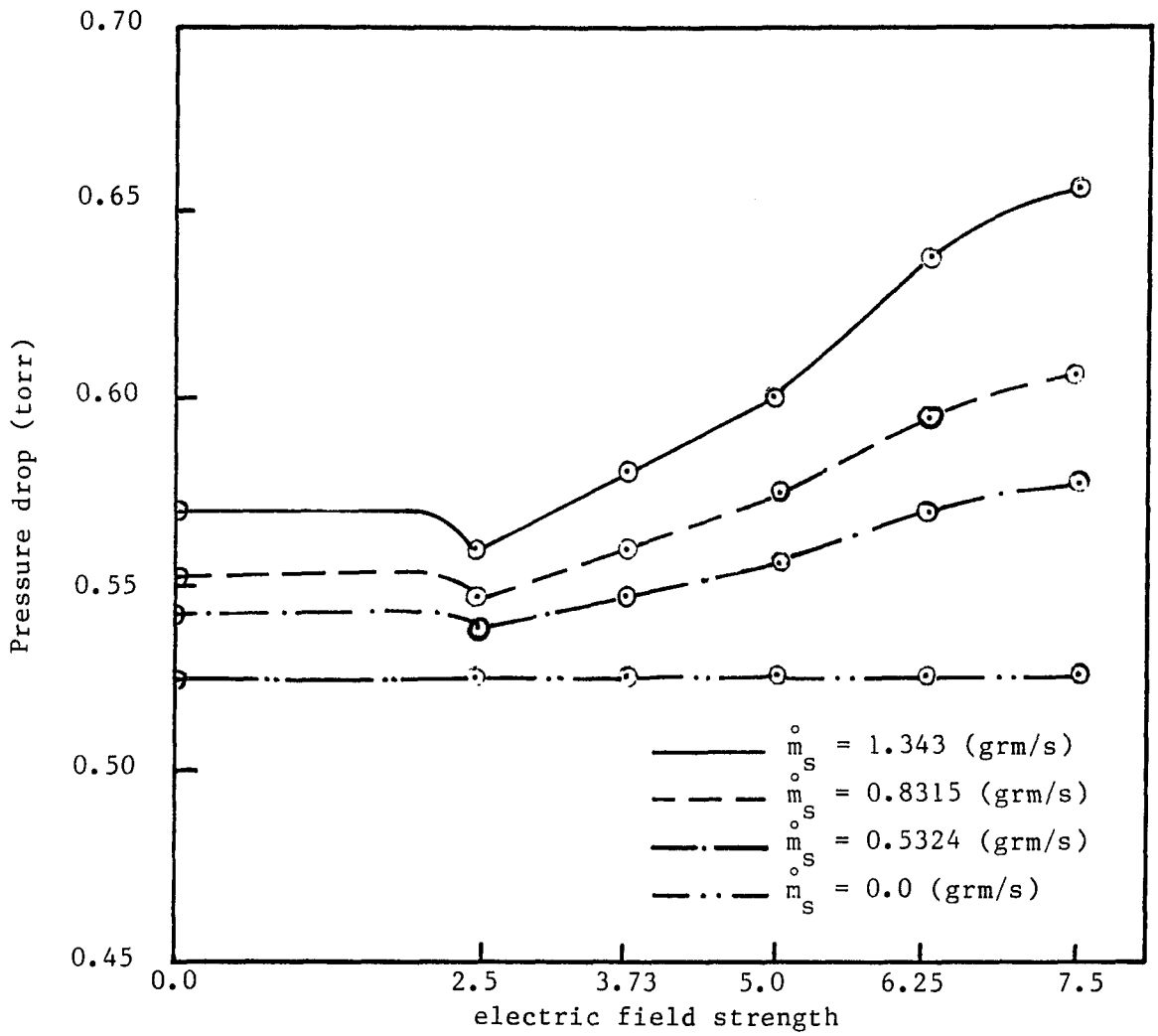

Figure 4.18. Pressure drop of solid-air flow versus electric field strength at various mass flow rates

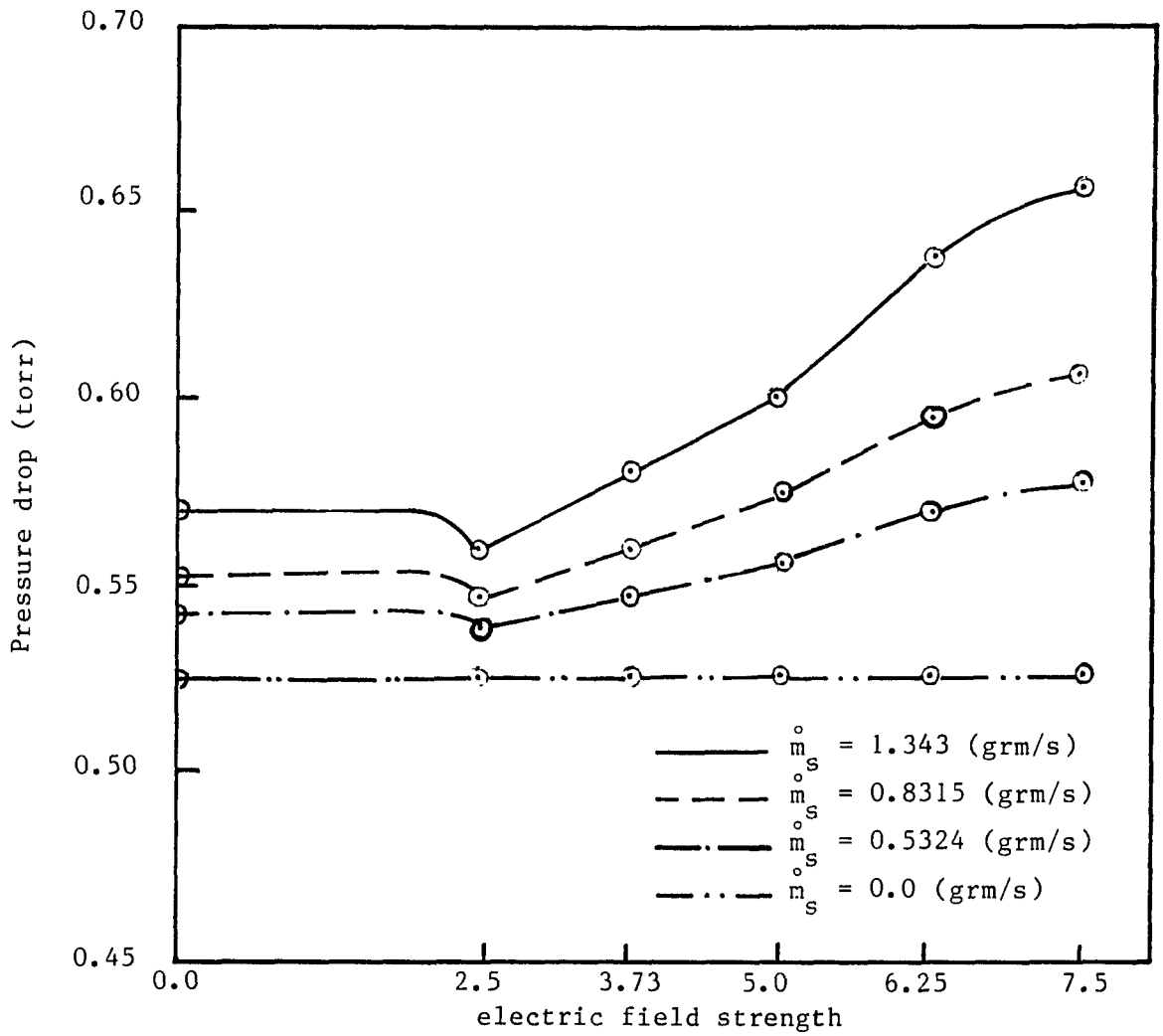

Figure 4.18. Pressure drop of solid-air flow versus electric field strength at various mass flow rates

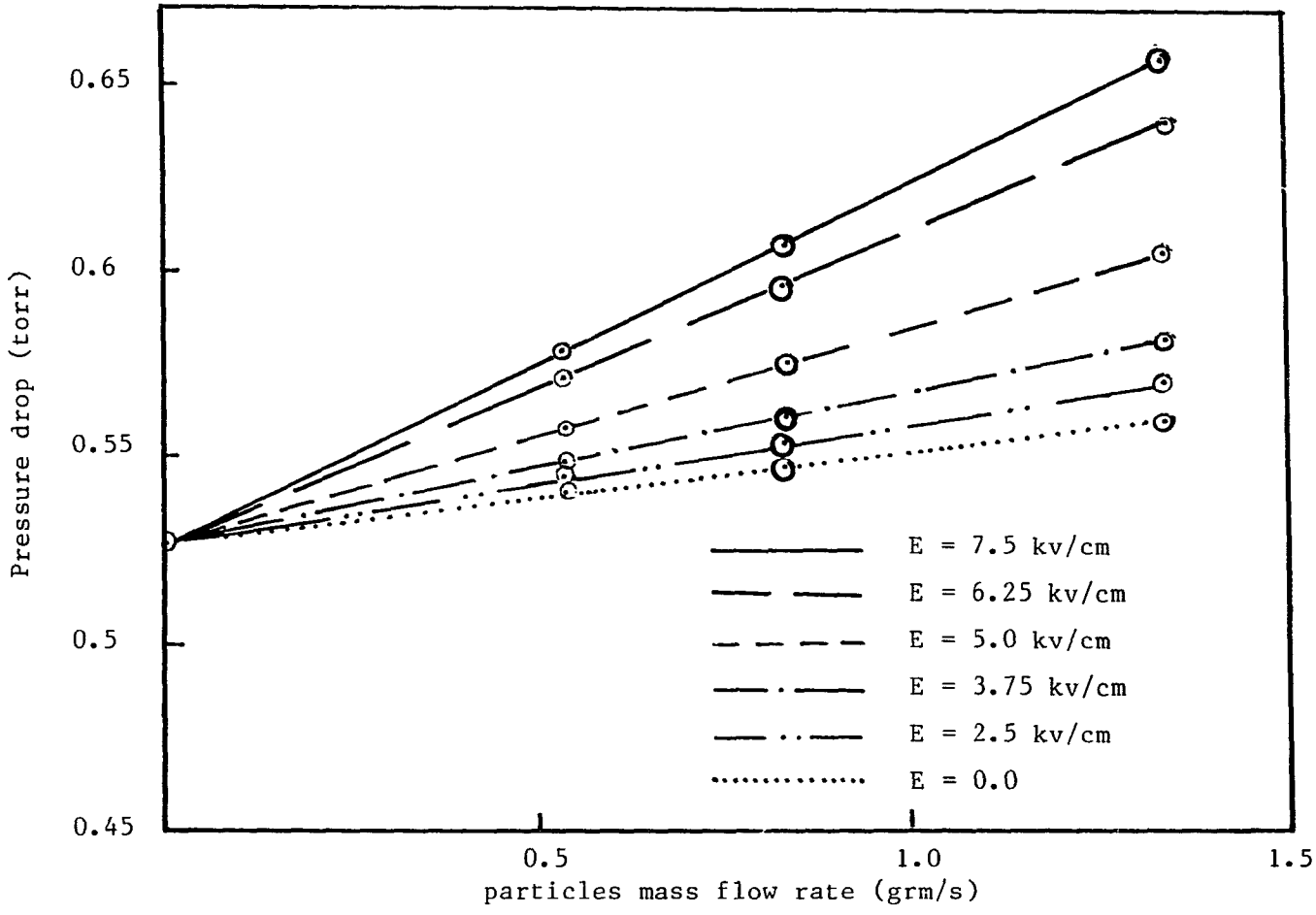

Figure 4.19. Pressure drop of solid-air flow versus particle mass flow rate at various electric field strengths

Results of Table 4.23 shows that the pressure drop Δp_s of the glass particle per unit length of the duct and per unit mass flow rate of the particle, has an almost fixed value [independent of the mass flow rate of the conveyed particles (for diluted mixture) and depends on the strength of the electric field]. Consequently, the friction factor $\bar{f}_s$ of the solid particles per unit mass flow rate of the conveyed particle, depends on the electric field strength regardless to the mass flow rate of the conveyed particles (for the diluted mixtures).

5. SEMI-THEORETICAL ANALYSES

The analytical model of a particle sticking a wall introduced by Cotroneo and Colver [7] was analyzed using the measured particle and air velocity to get a slip coefficient β for both copper and glass particles. The diameters of tested particles for copper and glass were 74-88 and 63-74 μm, and 74-88, 63-74, and 44-63 μm respectively. The slip coefficient for each particle size was calculated for an air bulk velocities of (1.966, 1.19, and 0.82766) m/s. The calculated values of the slip coefficient were used to calculate the steady state pressure gradient ($\Delta p_s/L$) due to the presence of oscillating particles in a duct at different velocities of lamenar air flow.

5.1. Calculation of the Slip Coefficient β

The horizontal particle motion in a duct, conveyed by a laminar air flow, introduced by Catroneo and Colver [7] is given by Equation [3.15].

$$m_p\left(\frac{d\bar{u}}{dt}\right) = 3\pi\mu D_p u_r (1+3D_p V_r/16\mu)^{1/2} + \frac{\pi}{8} D^3_p \rho\omega v_p$$

$$- m_p \left[\frac{2(1+\alpha)\beta/5}{1+(1+\alpha)\beta/5}\right] \frac{u_p v_p}{\ell}$$

The right hand side terms are, respectively, the fluid drag force, fluid lift force (magnus effect), and the wall drag force. The left hand side term equals zero at steady state. By substituting by the measured values of u_s, v_s, u_a in Equation (3.15), the corresponding value of β could be calculated for each particle size and air speed. Calculated values of the slip coefficient β are given in Tables (5.1-5.5) for copper and glass

Table 5.1. Slipping coefficient of copper particles D_p = 74 - 88 μm, v_s = 1.0 m/s

u_a (m/s)	u_s (m/s)	u_r (m/s)	V_r (m/s)	β
1.466	0.38	1.086	1.4762	0.6853
1.19	0.31	0.88	1.332	0.6553
0.82766	0.22	0.60766	1.170	0.6068

Table 5.2. Slipping coefficient of copper particles D_p = 63 - 74 μm, v_s = 1.0 m/s

u_a (m/s)	u_s (m/s)	u_r (m/s)	V_r (m/s)	β
1.466	0.48	0.986	1.404	0.6668
1.19	0.39	0.8	1.280	0.6459
0.82766	0.27	0.5576	1.1449	0.6298

Table 5.3. Slipping coefficient of glass particles D_p = 74 - 88 μm, v_s = 1.7 m/s

u_a (m/s)	u_s (m/s)	u_r (m/s)	V_r (m/s)	β
1.466	0.6	0.866	1.907	1.371
1.19	0.455	0.753	1.85208	1.5925
0.82766	0.316	0.5106	1.775	1.56156

Table 5.4. Slipping coefficient of glass particles D_p = 63 - 74 μm, v_s = 1.7 m/s

u_a (m/s)	u_s (m/s)	u_r (m/s)	V_r (m/s)	β
1.466	0.725	0.741	1.8544	1.3948
1.19	0.59	0.60	1.8027	1.3688
0.82766	0.409	0.41866	1.75029	1.3644

Table 5.5. Slipping coefficient of glass particles D_p = 44 - 63 μm, v_s = 1.7 m/s

u_a (m/s)	u_s (m/s)	u_r (m/s)	V_r (m/s)	β
1.466	0.94	0.526	1.779	1.3614
1.19	0.77	0.42	1.751	1.3093
0.82766	0.53	0.29766	1.7258	1.3542

particles having diameters of 74-88, 63-74 μm and 74-88, 63-74, and 44-63 μm respectively.

5.2. Calculation of the Pressure Gradient and the Particle Angular Rotation

The horizontal force per unit particle, at steady state, is given by the summation of the first and second terms on the right hand side of Equation (3.23) or by the third term alone. The pressure gradient $\Delta p_s/L_{ss}$ is given by Equation (3.16)

$$\Delta p_s/L_{ss} = n\bar{F}_p$$

The particle angular rotation is given by

$$\|\bar{\omega}\| = \left[\frac{(1+\alpha)\beta}{1+(1+\alpha)\beta/5}\right] u_s/D_p$$

The measured value of the particle number density and the calculated value of the slip coefficient β, corresponding to each case, are used to

calculate the pressure gradient due to the presence of the particles in the air flow and the particle angular rotation.

The calculated values of the particle angular velocity and the calculated pressure gradient compared to the corresponding measured values are presented in Tables 5.6-5.10 for copper and glass particles with diameters of (74-88 and 63-74) μm and (74-88, 63-74 and 44-63) μm respectively. A sample of the copper and glass particles having diameters of 63-74 μm are presented in Figures 5.1, 5.2 respectively.

5.3. Discussion

The calculated pressure gradient due to the presence of oscillating particle in a ducted air flow agrees quite well with the corresponding measured values. The accuracy of this method increases with a decrease in both the particle vertical velocity and number density, i.e., with a decrease in the particle-particle interaction.

The absence of a term expressing the particle-particle interaction may account for the values of the slip coefficient β, in the cases of glass particles, exceed the unity, which is the maximum physical value, expected ($0 \leq \beta \leq 1$). The theoretical model gives an interesting method for calculating the particle angular velocity using the test data in the lamenar air flow regime.

Calculated values for the slip coefficient β, in the cases of copper particles of different sizes, indicate that the value of β increases with a decrease in the incident angle between the particle trajectory and the wall at impact. Consequently β increases with a decrease in the conveying air speed at steady state conditions and at the same electric field strength.

Table 5.6. Pressure gradient and particle angular rotation for copper particles, D = (74 - 88) μm

Measured u_a (m/s)	Measured n (m^{-3} x 10^{-8})	Measured $\Delta P/L$ (N/m^3)	Calculated $\Delta P/L$ (N/m^3)	Calculated ω (rad/s)
1.466	3.8682	10.37011	9.6937	4513.47
1.190	3.036	7.3183	5.98729	3662.82
0.8276	4.278	7.65166	5.62089	2440.322

Table 5.7. Pressure gradient and particle angular rotation for copper particles, D = (63 - 74) μm

Measured u_a (m/s)	Measured n (m^{-3} x 10^{-8})	Measured $\Delta P/L$ (N/m^3)	Calculated $\Delta P/L$ (N/m^3)	Calculated ω (rad/s)
1.466	4.954	10.296	9.12635	6300.566
1.190	3.904	7.24426	5.6924	4983.9298
0.82766	5.6393	7.577	5.5744	3381.077599

Table 5.8. Pressure gradient and particle angular rotation for glass particles D = (74 - 88) μ

Measured u_a (m/s)	Measured n ($m^{-3} \times 10^{-8}$)	Measured $\Delta P/L$ (N/m^3)	Calculated $\Delta P/L$ (N/m^3)	Calculated ω (rad/s)
1.466	1.5686	5.259128	4.82438	13267.3
1.190	2.06848	5.9850	4.38765	9.150.599
0.82766	2.946	7.059	4.28289	6271.155

Table 5.9. Pressure gradient and particle angular rotation for glass particles D = (63 - 74) μm

Measured u_a (m/s)	Measured n ($m^{-3} \times 10^{-8}$)	Measured $\Delta P/L$ (N/m^3)	Calculated $\Delta P/L$ (N/m^3)	Calculated ω (rad/s)
1.466	2.100	5.2591	3.78882	14780
1.180	2.580	5.5406	3.73705	11866
0.82766	3.7227	6.9850	3.7295	8206.4

Table 5.10. Pressure gradient and particle angular rotation for glass particles D = (44 - 63) μm

Measured u_a (m/s)	Measured n ($m^{-3} \times 10^{-8}$)	Measured $\Delta P/L$ (N/m^3)	Calculated $\Delta P/L$ (N/m^3)	Calculated ω (rad/s)
1.466	3.37	4.27396	3.363597	21788
1.180	4.125	4.79988	3.297805	17329
0.82766	5.9935	6.9109	3.359374	12227

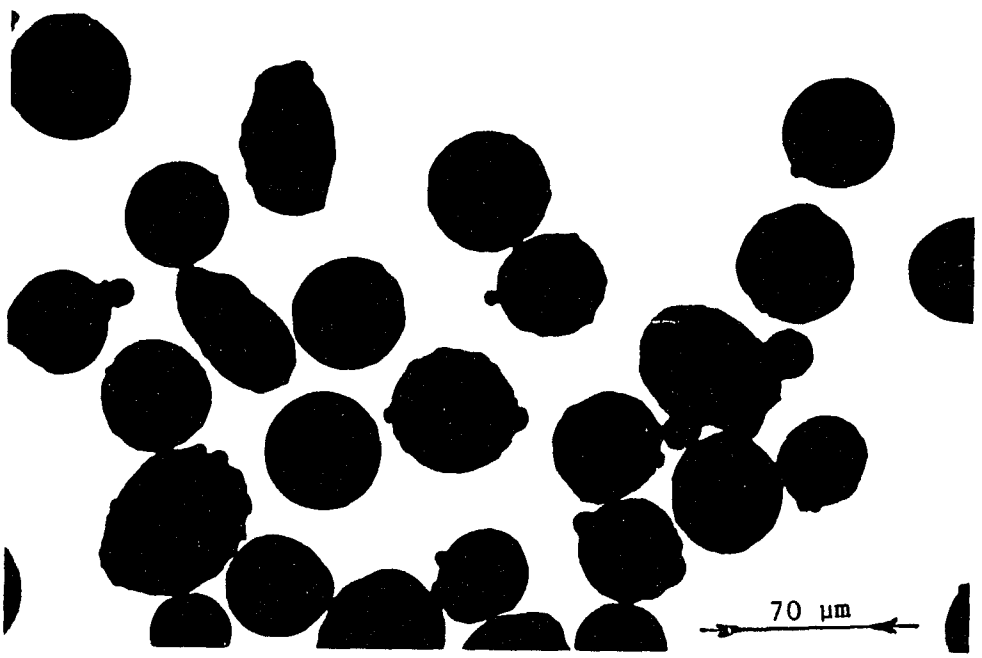

Figure 5.1. Sample of copper particles with diameters of 63-74 µm

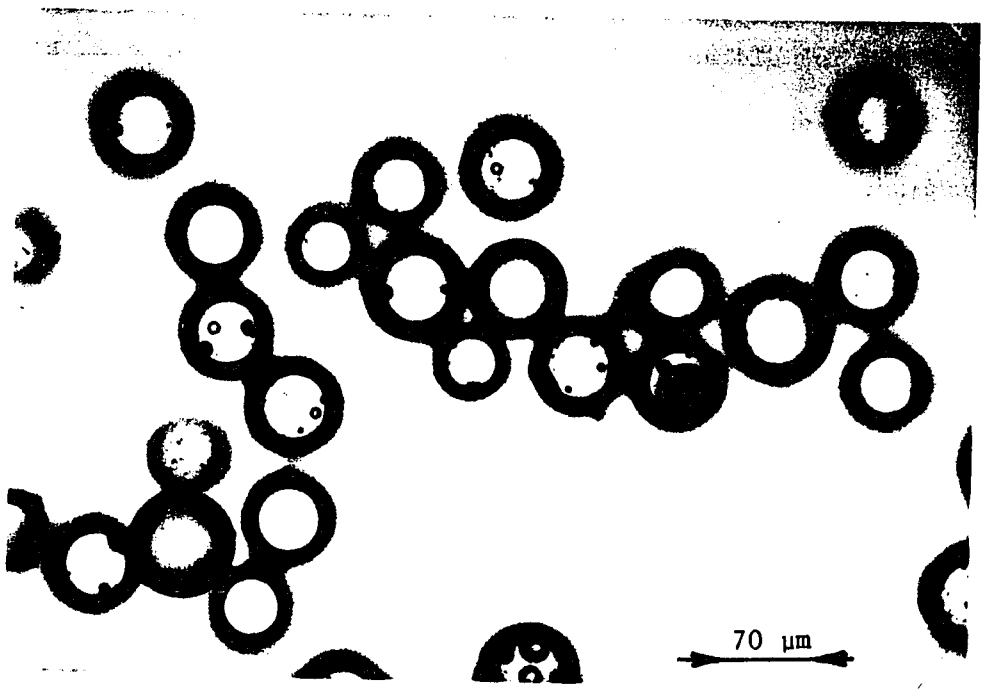

Figure 5.2. Sample of glass particles with diameters of 63-74 µm

6. CONCLUSIONS AND RECOMMENDATIONS

The effect of electrically driven particle on air flow was investigated by supplying particles to a rectangular duct having a cross sectional area measuring 5.25 x 1.6 cm and a length of 225 cm. The upper and lower walls (electrodes) were copper sheets with the side walls of glass acted as insulator to confine the flow. The particles were driven to oscillate vertically between the upper and lower electrodes which were connected to a DC power generator. The air flow through the duct was controlled.

The effect of the particles on the flow was detected by measuring the static pressure drop along the duct. While the effect of the flow on the particles was detected by measuring the velocity of these particles using a laser Doppler anemometer.

The pressure gradient due to the presence of oscillating solid particles, conveyed by a laminar air flow was calculated according to the theoretical model offered by Cotroneo and Colver [7]. The results of the calculation compared favorably to corresponding measured values.

Another series of experiments was carried out to measure the multiple particle vertical velocity in a totally confined volume. The vertical velocity was measured in the cases of copper and glass particles having diameters of (37-44, 44-63, 63-74 and 74-88) μm respectively. The test section consisted of two parallel plates (electrodes) of brass with a separation distance of 1.6 cm, and side walls of glass. The internal volume of the test section was (15 x 5.25 x 1.6) cm. The electrodes were connected to a DC power generator. The particles' vertical velocity was measured by a laser Doppler anemometer.

Results of the multiple particles vertical velocity measurements, for both copper and glass particles with diameters ranging from 37 μm up to 88 μm, indicate the following:

1. A minimum lift-off velocity was measured for both copper and glass particle. This minimum lift-off velocity was theoretically predicted by Colver [4]. The minimum lift-off velocity corresponds to a constant electric field strength for all particle sizes of the same material. In other words the minimum lift-off electric field strength is fixed regardless of the particle size, but it is a function of the particle material.
2. The vertical velocity of the multiple particles increases by increasing the electric field strength up to some limiting value, which is dependent on the material of the particles. The effect of a further increase in the electric field strength will be limited by particle-particle collisions. That leads to a saturation phenomenon of the particle velocity, similar to the phenomenon of the particle number density saturation which was reported by Colver [3, 4].

Measurements of the effect of electrically driven particles on an air flow in a duct show the following:

1. The most economical air flow velocity for conveying both copper and glass particles is in the transient regime of air flow where the pressure drop per unit mass flow rate of conveyed particle has a minimum. The pressure increases by decreasing the air velocity in the laminar regime and also increases by increasing the air flow in the turbulent region.

2. When the effect of the electric field strength on the pressure drop of a solid-air flow was examined for the case of glass particles having diameters of 44-63, 63-74, and 74-88 μm, the test data showed that the pressure drop corresponding to the minimum lift-off electric field strength is the minimum pressure drop and is even less than the pressure drop at zero electric field strength. This minimum corresponds to all tested particle sizes and all tested air flow rates.
3. From the aforementioned two facts, one can generalize the result that the most economical conveying condition of a dilute suspension of glass particles (for all of the all-tested sizes) can be obtained by conveying the particle in air with velocities in the transient regime and electrically augmented by an electric field strength of 2.5 kv/cm (which is the minimum electric field strength to just lift off glass particles).
4. A correlation of the apparent drag coefficient for both copper and glass particle could be obtained for particles driven by an electric field strength of 5 kv/cm, and particle Reynolds number in the range of 0 to 32. The apparent drag coefficient correlation for each particle material accounts for the particle-particle and the particle-wall interactions.
5. Measured values of particle to air velocity ratio for copper and glass particles having diameters of (44-63, 63-74, and 74-88) μm show good agreement with Arastoopour et al. [57] correlation.
6. Measurement of the saltation velocity of copper and glass particle compared to these calculated by Zenz's correlation [61] showed good

agreement for glass particles, but it found to be not accurate for the copper particles. This is probably because Zenz's correlation was obtained from a test data of coal particles, which has mass density closer to that of the glass rather than that of the copper.

7. It was observed, during all of the experiments, that the formation and behavior of the electric suspension was sensitive to the humidity of the air, especially for the long transport lines. If this problem could be overcome, then a new approach is possible for the utilization of the electrically augmented pneumatic conveyors in the industry.
8. The electric suspension of the particle offers a new technique for studying the effect of low velocity air flow (below the saltation velocity) on a cloud of particles. It is also proved to be useful tool for the study of powdered combustion and possibly detonation phenomena of combustable particles.

Calculation of the pressure gradient using a theoretical model for the laminar flow regime, given by Cotroneo and Colver [7] show the following:

1. The slip coefficient for both copper and glass particle can be calculated for different test cases.
2. The good agreement between the calculated pressure gradient and the corresponding measured values for the cases of copper particles indicates that the model is a reasonably accurate description of the particle-wall dynamics.
3. The difference between the measured and calculated pressure gradient in the case of glass particles probably accounts for the large value of the slip coefficient ($\beta > 1$). The difference shows the importance of

adding a term to the particle model which accounts for the particle-particle interaction, particularly for a dense suspension of materials having a low material density. In general it was observed that the accuracy of the model decreases with an increase in the particle number density and with a decrease of the particle specific mass.

4. Calculated values of the slip coefficient β indicate that the value of β increases with an increase in the conveying air speed at steady state condition. Consquently β increases with the decrease of the incident angle of the particle with the wall at impact.
5. The theoretical model, when analyzed with test data in laminar flow, allows one to calculate the angular velocity of the particles.

6.1. Suggestions for Future Work

Several suggestions regarding the extension of this work can be made. These are summarized below.

1. More information on the particle-particle interaction is needed in order to formulate a complete and precise mathematical model prescribing the particle motion in a duct.
2. A laser Dopper anemometer having a longer laser wavelength and connected to a microcomputer is recommended. This would provide the facility for more accurate velocity measurements for particles with diameters greater than 88 μm. Also the particle speed distribution and the root mean square speed could be measured. This would provide more accurate measurement of the average particle speed than that which was

obtained by displaying the output of the LDA on an oscilloscope.

3. The case of a dense suspension should also be investigated. This investigation can be carried out if a particle feeder having a higher volumetric feeding rate is used, and if the window glass which was used as side walls is replaced by pyrex glass, which has higher electric resistivity. In this case the electric field strength could be increased and consequently higher particle number densities can be attained. This in turn would lead to the a greater attenuation of a laser beam for the determination of the particle number density.
4. The study should be extended to cover a wider variety of particle materials.
5. If suggestions 3 and 4 are carried out, it should be possible to find a more general correlation for the drag coefficient of an electrically driven particle in a duct. This correlation could include the effects of the particle mass density, particle electric conductivity, particle number density, and electric field strength as variable parameters in addition to the particle Reynolds number and the limiting particle Reynolds number which are already included in the present correlation. Also if suggestions 3 and 4 are carried out successfully, it should be possible to find the electric field strength which gives the minimum transporting pressure

drop for various other materials. It can also answer the question regarding the most: economical electric field strength for suspending other materials and dense suspensions.

Finally, other studies that can be attempted using the same test facility include:

1. The effect of electrically driven particle on the air flow in a rectangular duct using particles of various other materials (coal, sand, aluminum etc.).
2. Measuring the saltation velocity of particles with other mass density as a mean of extending Zenz's method [61] for materials other than coal.
3. Evaluating the horizontal velocity profile of particle with and without an electric field.
4. Evaluating verticle velocity of the particles at different heights of the test section at various values of the electric field strength.

7. REFERENCES

1. Soo, S. L. "Design of Pneumatic Conveying Systems." J. Powder Bulk Solids Tech. 4, No. 2/3 (1980): 33-43.

2. Colver, G. M. "Mass, Heat, and Charge Transfer in an Electric Particulate Suspension." Symposium on Heat and Mass Transfer, Department of Mechanical and Industrial Engineering, University of Illinois at Urbana-Champaign, September 9, 1987.

3. Colver, G. M. "Electric Suspension Above Fixed Fluidized and Acoustically Excited Beds." J. Powder Bulk Solids Tech. 4, No. 2/3 (1980): 21-31.

4. Colver, G. M. "Dynamics of an Electric (Particulate) Suspension." Pages 355-373. In Trans-Tech. M. Shahinpoor, ed. Advances in the Mechanics and the Flow of Granular Materials. 1st Ed. Vol. 1. Clausthal-Zellerfeld. Federal Republic of Germany; Gulf Pub. Co., Houston, TX, 1983.

5. Colver, G. M. and Howell, D. L. "Particle Diffusion in an Electric Suspension." Proc. IEEE IAS Conf. on Electrostatics, Cincinnati, Ohio (September 29-October 3, 1980): 1056-1062.

6. Colver, G. M., and Ehlinger, L. J. "Particle Speed Distribution Measurement in an Electric Particulate Suspension." IEEE Transaction on Industry Applications 24, No. 4 (July August 1988): 732-739.

7. Cotroneo, J. A. and Colver G. M. "Electrically Augmented Pneumatic Transport of Copper Spheres at Low Particulate and Duct Reynolds Numbers." J. Electrostatics 5 (1978): 205-223.

8. Rudinger, G. Fundamentals of Gas-Particle Flow. Handbook of Powder Technology. Elsevier Scientific Publishing Company, Amsterdam, The Netherlands, 1980.

9. Soo, S. L. Fundamentals of Multiphase Fluid Dynamics. Preliminary Edition. Soo Associates, Urbana-Champaign, Illinois, 1987.

10. Farber, L. "The Venturi as a Meter for Gas-Solids Mixtures." Trans. ASME 75 (1953): 943-951.

11. Wallis, G. B. One-Dimensional Two-Phase Flow. McGraw-Hill Book Co., New York, 1969.

12. Neilson, J. H., and Gilchrist, A. "An Analytical and Experimental Investigation of the Velocities of Particles Entrained by the Gas Flow in Nozzles." J. Fluid Mechanics 33 (1968): 131-149.

13. Hogland, R. F. "Recent Advance in Gas-Particle Nozzle Flows." ARS J. 32 (1962): 662-671.

14. Sharma, M. P. and Crowe, C. T. "A Novel Physico-Computational Model for Quasi One-Dimensional Gas-Particle Flows." J. Fluids Eng. 100 (1978): 343-349.

15. Arastoopour, H., Lin, S., and Weil, S. A. "Analysis of Vertical Pneumatic Conveying of Solids Using Multiphase Flow Models." AIChE J. 28 (1982): 467-473.

16. Arastoopour, H., Wang, C., and Weil, S. A. "Particle-Particle Interaction for a Dilute Gas-Solid System." Chem. Eng. Sci. 37 (1982): 1379-1386.

17. Doss, D. E. "Analysis and Application of Solid-Gas Flow Inside a Venturi with Particle Interaction." Int. J. Multiphase Flow 11, No. 4 (1985): 445-458.

18. Soo, S. L. "Differential-Integral Equations of Multiphase Flow." Fluidization '85 Science and Technology Conference Papers. Second China-Japan Symposium, Kunming, China (April 10-15, 1985): 25-36.

19. Matsumoto, S. "Simulation of Gas-Solid Two-Phase Flow in a Horizontal Pipe." J. Chem. Eng. of Japan 9, No. 1 (February 1976): 23-28.

20. Gasterstadt, J. "Die Experimentelle Untersuchung Des Pneumatischen Fordervorganges." V.D.I. Forsch-Arb, No. 265, 1924.

21. Cramp, W., and Priestly, A. "Pneumatic Grain Conveyers." Engineer (London) 137 (1924):312.

22. Dukler, A. E., Wilkes, M. and Cleveland, R. G. "Frictional Pressure Drop in Two-Phase Flow." AIChE J. 10 (1964): 38-45.

23. Hariu, O. H. and Molstad, M. C. "Pressure Drop in Vertical Tubes in Transport of Solids by Gases." Ind. Eng. Chem. 41 (1949): 1148.

24. Konno, H. and Saito, S. "Pneumatic Conveying of Solids Through Straight Pipes." J. Chem. Eng. Japan 2(2) (1969): 211.

25. Capes, C. E. and Nakamura, K. "Verticla Pneumatic Conveying - an Experimental Study with Particles in the Intermediate and Turbulent Flow Regimes." Can. J. Chem. Eng. 51 (1973): 31.

26. Yousfi, Y. and Gau, G. "Aerodynamics of the Vertical Flow of Concentrated Gas-Solids Suspensions. I. Flow Regimes and Aerodynamic Stability." (Aerodynamique de L'ecoulement vertical

de suspensions concentrees gaz-solides. I. Regimes D'ecoulement et stabilite aerodynamique.), Chem. Eng. Sci. 29 (1974): 1939. (In French).

27. Hinkle, B. L. "Acceleration of Particles and Pressure Drops Encountered in Horizontal Pneumatic Conveying." Ph.D. Thesis, Georgia Institute of Technology, 1953.

28. Wen, C. Y., and Galli, A. F. Dilute Phase Systems. In Davidson and Harrison, ed. Fluidization. Academic Press, New York, 1971.

29. Yang, W. C. "Estimating the Solid Particle Velocity in Vertical Pneumatic Conveying Lines." Ind. Eng. Chem. Fundamentals 12 (1973): 349.

30. Yang, W. C. "Correlations for Solid Friction Factors in Vertical and Horizontal Pneumatic Conveyings." AIChE J. 20 (1974): 605.

31. Yang, W. C., and D. L. Keairns. "Estimating the Acceleration Pressure Drop and the Particle Acceleratin Length in Vertical and Horizontal Pneumatic Transport Lines." Proc. Pneumotransport 3. Organized by BHRA Fluid Engrg., Bath, England, 1976.

32. Yang, W. C. "A Unified Theory on Dilute Phase Pneumatic Transport." Proceedings of the International Conference on Powder and Bulk Solids Handling and Processing, Chicago, Illinois, May 1976.

33. Yang, W. C. "A Correlation for Solids Frictin Factor in Vertical Pneumatic Conveying Lines." Paper presented at the International Powder and Bulk Solids Handling and Processing Conference, Chicago, May 1977.

34. Vogt, E. G. and White, R. R. "Friction in the Flow of Suspensions." Ind. Eng. Chem. 40 (1948): 1731-38.

35. Belden, D. H. and Kassel, L. S. "Pressure Drops Encountered in Conveying Particles of Large Diameter in Vertical Transfer Lines." Ind. Eng. Chem. 41 (1949): 1174-1178.

36. Korn, A. M. "How Solids Flow in Pneumatic Handling Systems." Chem. Eng. (1950): 108-111.

37. Mehta, N. C., Smith, J. M. and Comings, E. W. "Pressure Drop in Air-Solid Flow Systems." Ind. Eng. Chem. 49 (1957): 986-992.

38. Razumov, I. M. "Calculating Pneumatic Transport of Solid Catalysts." Int. Chem. Eng. 2 (1962): 539-543.

39. Stemerding, S. "The Pneumatic Transport of Cracking Catalyst in Vertical Risers." Chem. Eng. Sci. 17 (1962): 599-608.

40. Engineering Equipment User's Association, Pneumatic Handling of Powdered Materials. EEUA Handbook No. 15. Constable, London (1963).

41. Chowdhury, S. B., Banerjee, S. and Lahiri, A. "Studies on Pneumatic Transport of Coal." Indian J. Tech. 5 (1967): 384-87.

42. Boothroyd, R. G. "Pressure Drop in Duct Flow of Gaseous Suspensions of Fine Particles." Trans. Instn. Chem. Engrs. 44, T306-T313 (1966): 913-822).

43. Jones, J. H., Braun, W. C., Daubert, T. E. and Allendorf, H. D. "Estimation of Pressure Drop for Vertical Pneumatic Transport of Solids." AIChE J. 13 (1967): 608-111.

44. Curran, F. P. and Gorin, E. "Studies on Mechanics of Fluo-Solids Systems." Prepared for Office of Coal Research, Contract No. 14-01-001-415, Interim Report No. 3, Book 1. Washington, D.C., 1968.

45. Rose, H. E. and Duckworth, R. A. "The Fluid Transport of Powdered Materials in Pipelines." Inst. Chem. Eng. Symposium Series, 27 (1968): 53-63.

46. Richards, P. C. and Wiersma, S. "Pressure Drop in Vertical Pneumatic Conveying." Paper presented at Pneumotransport 2, A1-1-15, Guildford, England, September 5-7, 1973.

47. Khan, J. I. and Pei, D. C. "Pressure Drop in Vertical Solid-Gas Suspension Flow." Ind. Eng. Chem. Process Des Develop 12 (1973): 428-431.

48. Knowlton, T. M. and Bachovchin, D. M. "The Determination of Gas-Solids Pressure Drop and Choking Velocity as a Function of Gas Density in a Vertical Pneumatic Conveying Line." Paper presented at the International Conference on Fluidization, Pacific Grove, Calif., June 15-20, 1975.

49. Leung, L. S. and Wiles, R. J. "Design of Vertical Pneumatic Conveying Systems." Paper presented at Penumotransport 3, C4-47-58, University of Bath, England, April 7-9, 1976.

50. Modi, M. V., Talwalkar, A. T., and Punwani, D. V. "Pressure-Drop Correlation for Designing Vertical Dilute-phase Gas-solids Lift-lines for Materials Used in Coal Conversion Processes." Paper presented at the International Powder and Bulk Solids

Handling and Processing Conference, Chicago, Illinois, May 16-18, 1978.

51. Konchesky, J. L., George, T. J. and Craig, J. G. "Air and Powder Requirements for the Pneumatic Transport of Crushed coal in Vertical Pipelines." ASME 97 (1975): 101-106.

52. Lapple, C. E. Fluid and Particle Dynamics. University of Delaware, Newark, Delaware, 1951.

53. Culgan, J. M. "Pneumatic Conveying of Materials of Unit Density in a Three-Inch Pipe." Ph.D. Thesis, Georgia Institute of Technology, May 1952.

54. Clark, R. H., Charles, D. E., Richardson, T. F., and Newitt, D. M. "Pneumatic Conveying, Part I, The Pressure Drop During Horizontal Conveyance." Trans. Instn. Chem. Engrs. 30 (1952): 209-224.

55. Richardson, J. F., and McLeman, M. "Pneumatic Conveying, Part II, Solids Velocities and Pressure Gradients in a One-Inch Horizontal Pipe." Trans. Inst. Chem. Engrs. 38 (1960): 257-266.

56. Duckworth, R. A., and Kokka, R. S. "The Influence of Particle Size on the Frictional Pressure Drop Caused by the Flow of Solid-Gas Suspension in a Pipe." Paper presented at Pneumotransport 1, C3, Churchill College, Cambridge, England, September 6-8, 1971.

57. Arastoopour, H., Modi, M. V., Punwani, D. V., and Talwalkar, A. T. "A Review of Design Equations for Dilute Phase Gas-Solids Horizontal Conveying Systems for Coal and Related Materials." Paper presented at Powder and Bulk Solids Conference/Exhibition, Philadelphia, Pennsylvania, May 15-17, 1979.

58. Doing, I. D., and Roper, G. H. "The Minimum Gas Rate for Dilute-Phase Solids Transportation in a Gas Stream." Australian Chem. Eng. 1 (January 1963): 9-19.

59. Matsumoto, S., Hara, M., Saito, S., and Maeda, S. "Minimum Transport Velocity for Horizontal Pneumatic Conveying." J. Chem. Eng. of Japan 7, No. 6 (1974): 425-430.

60. Thomas, D. G. "Transport Characteristics of Suspensions: Part VI. Minimum Transport Velocity for Large Particle Size Suspension in Round Horizontal Pipes." AIChE J. (July 1962): 373-378.

61. Zenz, F. A. "Conveyability of Materials of Mixed Particle Size." IfEC Fund 3 (February 1964): 65-75.

62. Sutton, O. G. Micrometeorology. McGraw-Hill Book Co., New York, 1962.

63. Stern, A. D. Air Pollution. Vol. 1. Second Edition. Academic Press, New York, 1974.

64. Noll, E. Kenneth and Fang, Y. P. Kenneth. "Development of a Dry Deposition Model for Atmospheric Coarse Particles." Atmospheric Environment 23, No. 3 (1989): 585-594.

65. McCready, D. I. "Wind Tunnel Modeling of Small Particle Deposition." Aersol Sci. Technol. 5 (1986): 301-312.

66. Cheng, Lung. "Collection of Airborne Dust by Water Sprays." Industrial and Engineering Chemistry, Process Design and Development, 12, No. 3 (July 1973): 221-225.

67. Rietema, K. "On Interaction Between Fluid and Particles." Proc. Symp. Instn. Chem. Engrs., London, 1962.

68. Maxwell, J. C. A Treatise on Electricity and Magnetism. 3rd ed. Vol. 1. Dover Pub., New York, NY, 1954.

69. Colver, G. M. "Dynamic and Stationary Charging of Heavy Metallic and Dielectric Particles Against a Conducting Wall in the Presence of a DC Applied Electric Field." J. Appl. Phys. 47, No. 11 (November 1976): 4839-4849.

70. Johnson, T. W. and Melcher, J. R. "Electromechanics of Electrofluidized Beds." Ind. Eng. Chem. (Fundam.) 14, No. 3 (1975): 143-156.

71. Dietz, P. W. "Ectrofluidized Bed Mechanics." Ph.D. Thesis, M.I.T., Cambridge, Mass., 1976.

72. Timoshenko, S. and Goodler, J. N. Theory of Elasticity. McGraw-Hill, New York, NY, 1951.

73. Clover, G. M. "Spark Breakdown of Particulate Clouds, A Review." 13th Annual Meeting, Fine Particle Soc., Chicago, 1982.

74. Hara, M. and Akazaki, M. "A Method for Prediction of Gaseous Discharge Threshold Voltage in the Presence of a Conducting Particle." J. Electrostatics 2 (1976/77): 223-239.

75. Lebedev, N. N. and Skal'skaya, I. P. "Force Acting on a Conducting Sphere in the Field of a Parallel Plate Condenser." Sov. Phys., Tech. Phys. 7, No. 3 (1962): 258-270.

76. Colver, G. M. and Howell, D. L. "Particle Diffusion in an Electric Suspension." Proc. IEEE-IAS Conf. on Electrostatics, Cincinnati, Ohio, September 29-October 3, 1980.

77. Hewitt, G. F. "Developing Annular Flow." Multiphase Science and Technology 3 (1985): 163-183.

78. Lombardi, C. and Perdrocchi, E. "A Pressure Drop Correlation in Two-Phase Flow." Energia Nucleare (Milan) 19, No. 2 (February 1972): 91-99.

79. Ingebo, R. D. "Drag Coefficients for Droplets and Solid Spheres in Clouds Accelerated in Air Streams." NACA TN3762 (1956).

80. Rudinger, G. "Experiments on Shock Relaxation in Particle Suspensions in a Gas and Preliminary Determination of Particle Drag Coefficients." N.J. Lipstein (Ed.). Multi-Phase Flow Symposium. ASME, New York, 1963.

81. Rudinger, G. "Effective Drag Coefficient for Gas-Particle Flow in Shock Tubes." Trans. ASME, J. Basic Eng. 92D (1970): 165-172.

82. Rowe, P. N., and Henwood, G. A. "Drag Force in a Hydraulic Model of a Fluidized Bed." Trans. Inst. Chem. Eng. 39 (1961): 43-54.

83. Hewitt, G. F. "Developing Annular Flow." Multiphase Science and Technology 3 (1985): 163-182.

84. Hewitt, G. F., and Owen, D. G. "Pressure Drop and Entrained Fraction in Fully Developed Flow." Multiphase Science and Technology 3 (1985): 145-155.

85. Camberland, D. J., and Crawford, R. J. The Packing of Particles. Handbook of Powder Technology, Elsevier Science Publishers B. V., Amsterdam, Netherlands, 1987.

86. Desai, C. J. "Heat Transfer to a Stationary and Moving Sphere Immersed in a Fluidized Bed." Ph.D. Dissertation, Iowa State University, Ames, Iowa, 1989.

87. Beckwith, T. G., Buck, N. L., and Marangoni, R. D. Mechanical Measurements. Third edition. Addison-Wesley Publishing Company, Inc., Philippines, 1982.

88. Shigley, J. E., and Mischke, C. R. Standard Handbook of Machine Design. McGraw-Hill Book Co., New York, NY, 1986.

8. ACKNOWLEDGMENTS

The author would like to express his deepest gratitude and sincerest appreciation to Dr. Gerald M. Colver, his thesis advisor and committee chairman, for his invaluable help, guidance, and advice.

The author is deeply indebted to his doctoral committee, Dr. Lennox N. Wilson, Dr. George H. Junkhan, Dr. Robert C. Brown, Dr. Bruce R. Munson, and Dr. Alric P. Rothmayer, for their interest, help and encouragement during the course of the study.

The author would especially like to thank Dr. Bruce R. Munson for his interest, invaluable advice, and for supplying the Laser Doppler Anemometer and the precision pressure sensor.

The author would like to express his gratitude to Mr. Hap Steed, Mr. Jim J. Dautremont, Mr. Gaylord Scandrett for offering advice and help throughout the construction of the experimental system.

Finally, the author would like to thank his sons, Saad El-Din and Mohamed, and his wife, Eman Sliem for her patience, understanding and unfailing encouragement. Without her help, the conclusion of this work would have been impossible. This thesis is dedicated to her.

9. APPENDIX A: PARTICLE FEEDER

The particle feeding system consisted of a DC servomotor (produced by Electro-Craft Corporation EC), reduction gears, and an Augar. The motor speed was controlled by connecting it to Micranta 278S DC power supply. The volumetric feeding rate G_p of the feeder was calibrated by using an electric stopwatch to measure the time to feed 300 ml of a well shaken copper powder, corresponding to a motor DC line voltage of 5, 10, 15 and and 23.3 volt respectively. The results are presented in Table 9.1.

The volumetric rates presented in Table 9.1. are powder volumetric rates which is the volumetric rate of the solid particles of the copper and the volumetric rate of free space occupying the gaps between the packed spherical copper particles. To get the volumetric rates of the solid particles, the randum packing coefficient of a well shaked spherical particles[1] was experimentally determined using the copper as a reference. This was carried out by taking the average weight of ten consecutive well shaked samples each of 200 ml of copper powder. The average mass was 1.1202 kg with maximum error of 0.1% referred to the average mass. Knowing that the mean density of copper is 8954 kg/m^3. The corresponding voluem of the solids is 125.106 ml giving a packing coefficient of a well shaked randum packing equal to 0.6255. This agrees with a value of 0.63 as a maximum possible packing coefficient for random packing of mono-size spheres in a cylinder of infinite length and diameter compared to the diameter of the packed spheres, given by Camberland and Crawford [85].

---

[1]Defined as the ratio of the volume of the solid parts to the total volume of the powder.

Table 9.1. Results of feeder calibration

Voltage (V)	Volume (ml)	Time (S)	Feeding Rate (CC/S)
5	300	1160	0.2586
10	300	853	0.35170
15	300	546	0.54945
23.3	300	338	0.88757

Using the value of 0.6255 for the packing coefficient, it gives volumetric rates of the solid part of the particles G_s equal to (0.16, 0.22, 0.3436 and 0.555) cc^3/s corresponding to motor DC voltage of (5, 10, 15, 23.3) volt respectively. The dependence of the volumetric rates on the motor DC volt is presented in Figure 9.1.

To determine experimentally the mass density of the glass particles, the mass of a well shaken 200 ml glass spherical powder was measured, and the average mass of ten well shaken samples each of 200 ml was found to be 0.303 kg with a maximum error of 0.3% referred to the average mass. This gives a specific mass of the glass particles equal to 2422 kg/m^3.

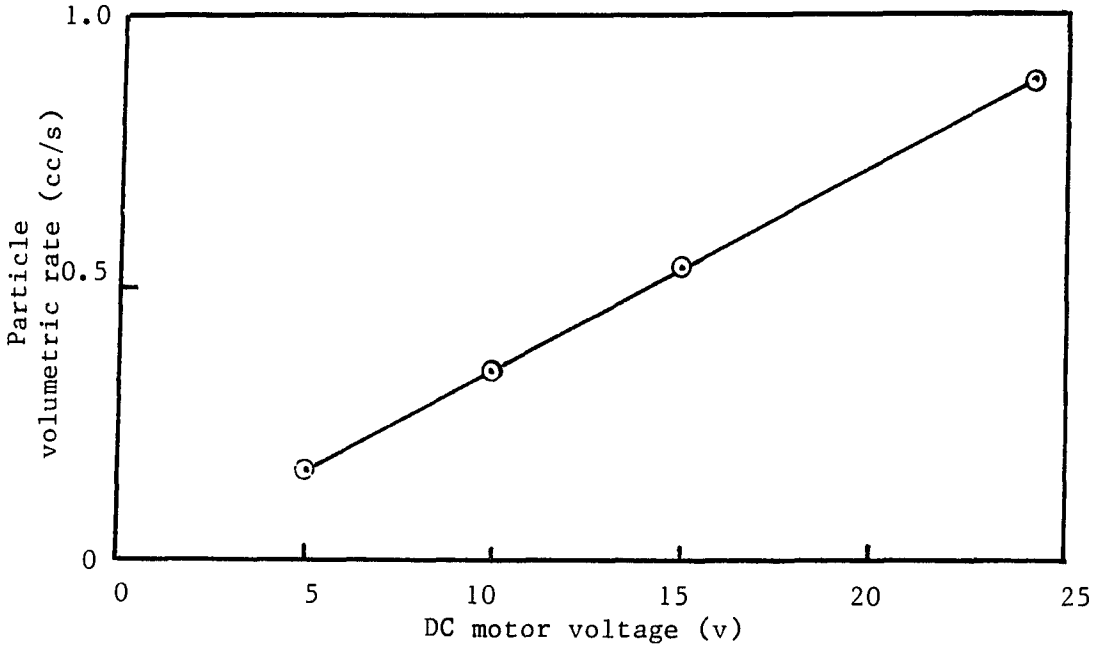

Figure 9.1. Calibration of particle feeder, particle volumetric rates versus DC voltage

10. APPENDIX B: ROTAMETERS

The air flow bulk velocity in the duct was measured using a system of six rotameters connected in parallel as shown in Figure 10.1. The rotameters were previously calibrated for flow rate by Desai [86] using a wet test meter and air meter. The calibration equation of each rotameter is listed in Table 10.1. A mercury manometer was used to measure the flow static pressure of the rotameters. The air volumetric flow rate, G_a, at pressure, p, can be obtained from the calibrated one G_{ast} at standard condition using the relation

$$G_a/G_{a,st} = [\frac{\rho_{a,st}}{\rho_a}]^{1/2} \qquad 10.1$$

where

ρ the specific mass of air at pressure p

$\rho_{a,st}$ the specific mass of air at standard condition of calibration.

From the continuity equation

$$G_a \rho_a = A_D \rho_{a,D} u_{a,D} \qquad 10.2$$

where

A_D cross sectional area of the duct

$\rho_{a,D}$ specific mass of air in the duct

$u_{a,D}$ bulk speed of air in the duct

From Equation (10.1 and 10.2) one can get

$$u_{a,D} = \frac{G_{a,st}}{A_D} (\frac{\rho_{a,st}}{\rho_a})^{1/2} (\frac{\rho_a}{\rho_{a,D}}) \qquad 10.3$$

Taking in consideration that $\rho_{a,D} = \rho_{a,st}$ so Equation (10.3) can be written as

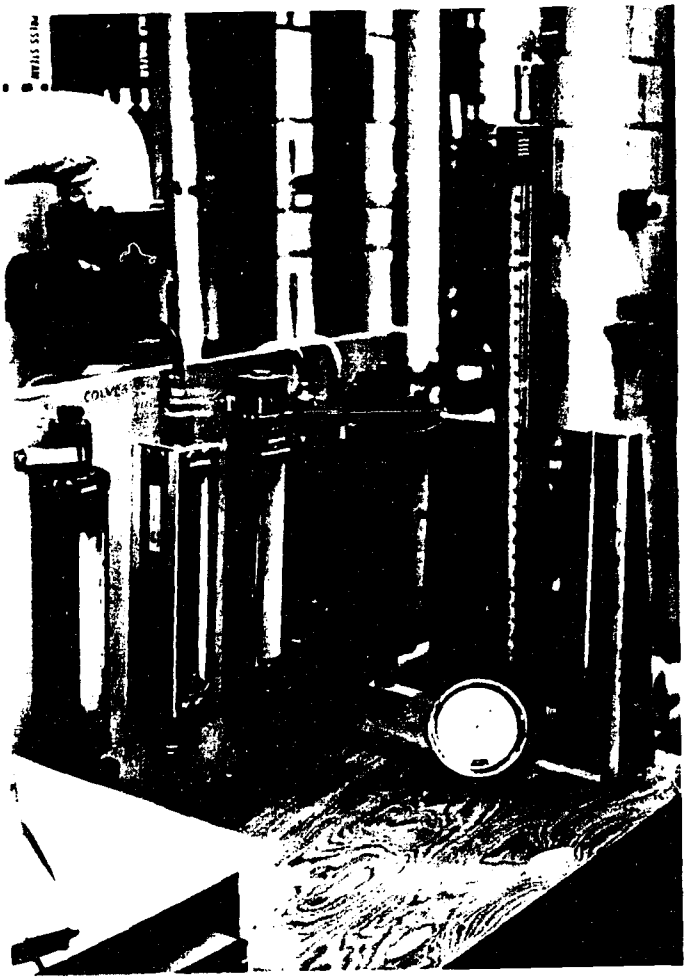

Figure 10.1. Rotameters

Table 10.1. List of rotameters calibration equations

Rotameter type	Range in CC/S	Calibration equation CC/S[a]
Brooks Instruments, Division of Emerson Co. Model No. 1110-01A1V1A	50 to 700	$G_{st} = 26.6588R + 23.4293$
Brooks Instruments, Division of Emerson Co. Model No. 1114-08H2G1A	137 to 998	$G_{st} = 9.6269R + 23.4293$
Brooks Instruments Division of Emerson Co. Model No. 7710H42053	80 to 713	$G_{st} = 7.1395R - 4.0646$
Devco Tube, Cat. No. 250-8	33 to 694	$G_{st} = 27.939R - 6.9009$
Lab Crest Div. Fond P Co., Meter Tube Cat. No. 450 - 700	10 to 230	$G_{st} = 1.5929R - 13.9910$
Schtt and Koerting Co.	750 to 2794	$G_{st} = 9.7284R + 440.9542$

[a] R - range of the float.

$$u_{a,D} = \frac{G_{a,st}}{A_D} \left[\frac{\rho_a}{\rho_{a,st}}\right]^{1/2} \qquad 10.3.a$$

For an adiabatic flow

$$\rho_a/\rho_{a,st} = [p/p_{st}]^{1/\gamma} \qquad 10.4$$

where γ is the specific heats ratio of air. From Equation (10.4) and Equation (10.3.1)

$$u_{a,D} = \frac{G_{a,st}}{A_D} \left[\frac{p}{p_{st}}\right]^{1/2\gamma} \qquad 10.5$$

The measuring inaccuracy of each rotameter is in the order of 1% which would have led to an error of 6% in the air speed measurement. To reduce this error or at least to keep it constant in each test having the same air speed, especial care was given to the pressure reading of the mercury manometer and it was held constant for every test having the same air flow speed. Besides, each rotameter was used either to measure its full volumetric rate or it was off except for the rotameter number six which was used to measure an intermediate value. A list of the calibration equation of each used rotameters is given in Table 10.1.

11. APPENDIX C: LASER DOPPLER ANEMOMETER LDA

A Dantec 55X laser Doppler anemometer LDA was used to measure the particle velocity. The LAD uses the Doppler shift of light scattered by moving particles to determine the particle velocity. The principle of this technique is shown in Figure 11.1. A beam splitter and lens produce two narrow light beams which intersect at the test point at an angle θ, and the light scattered from the particle is focused by a second lens on a photomultiplier. The two intersecting beams forms a small test volume that is filled with parallel interference fringes. The Doppler shift frequency f_D can be expressed as

$$f_D = f_s - f_i = \frac{2\, u_s}{\lambda} \sin(\theta/2) \qquad 11.1$$

where

f_s frequency of scattered light

f_i frequency of incident light

u_s particle velocity along x-axes

λ wavelength of incident light

θ is the angle between the two intersecting beams

The test volume Figure (11.1) is an elipsoid with semi major axes a, b, c in x, y, t axes respectively related to the beam wais diameter d_f of the focused laser beam by

$$2a = \frac{d_f}{\cos(\theta/2)} \qquad 11.2$$

$$2b = d_f \qquad 11.3$$

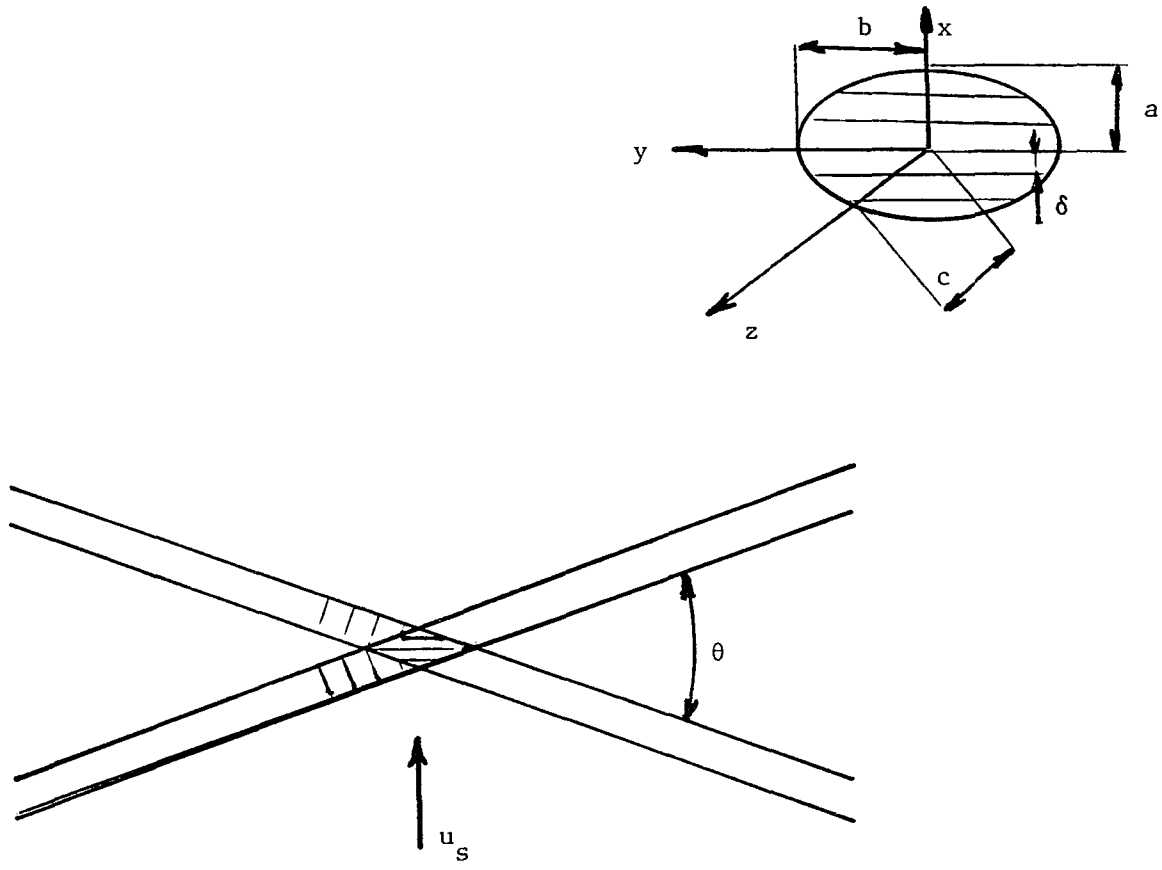

Figure 11.1. Diagram of the LDA laser beams

$$2c = \frac{d_f}{\sin(\theta/2)} \qquad 11.4$$

The fringe spacing ϕ_f is given by

$$\phi_f = \frac{\lambda}{2 \sin(\theta/2)} \qquad 11.4$$

The fringe spacing should be bigger or at least of the same order of the measured particle diameter. To increase the fringe spacing, a lens having focal length of 600 mm was used and to avoid the difficulty of locating the test volume by the photomultiplier, back scattering technique was adapted by mounting the photomultiplier on the LDA modular.

Equation (11.1) can be rearranged to be

$$u_{px} = C\, f_D \qquad 11.5$$

where the calibration factor C is given by

$$C = \frac{\lambda}{2 \sin(\theta/2)} \qquad 11.6$$

The optical system parameters are listed below.

Laser type	124 B
Front lens type	X58
Focal length (mm)	600
Beam diameter (mm)	1.1
Wavelength of laser beam λ(nm)	633
Intersection angle θ (degree)	3.72
Beam waist diameter (mm)	0.44
Fringe space ϕ_f (μm)	9.74
Calibration factor C($m.s^{-1}$/MHz)	9.74

The Laser Doppler Anemometer with back scattering is presented in Figure 11.2.

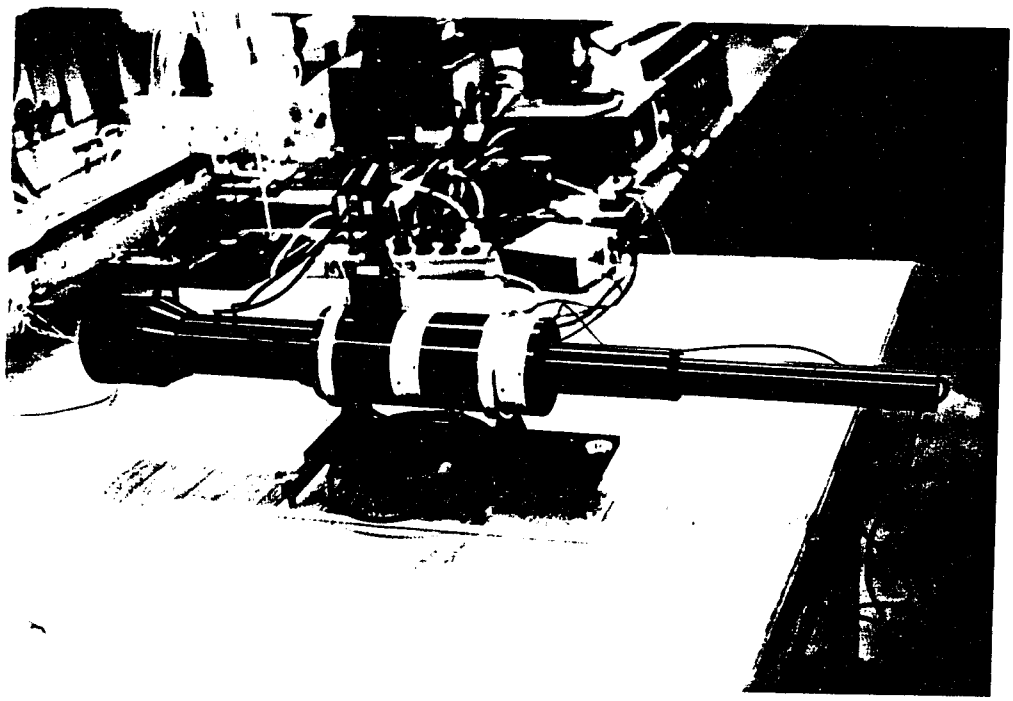

Figure 11.2. Laser Doppler Anemometer with back scattering

12. APPENDIX D: ERROR ANALYSIS

In any experiment, uncertainties in the measured quantities arise as a result of three types of errors: systematic, illegitimate, and random. Systematic errors result from improper experimental procedures. They are characterized by their systematic and consistent nature. These errors can be found and corrected for by proper calibration or warming before using. Illegitimate errors arise from mistakes made in executing the experiment and can be eliminated or avoided by employing proper test procedures, familiarization with the equipment, and repetition of measurements. Random errors, on the other hand, are characterized by their inconsistent and random nature and are inherently present in any laboratory experiment. Random errors are usually estimated using statistical analysis for the uncertainty propagation.

In the present study, illegitimate and systematic errors were avoided by the proper design of the test procedure, calibration, and the repetition of any doubtful measurement.

Measurements are either direct or indirect. In the direct measurements, where the measured parameter is the direct reading of the measuring instrument, the uncertainty of the measured parameter is identical to the uncertainty of the measuring instrument. For the indirect measurements, where the parameters are calculated by the application of an equation containing more than one measured parameter, the uncertainty in the propagation of the errors of these measurements can be predicted. Bechwith et al. [87] and Shigley and Mischke [88] suggested a proper procedure for estimating the uncertainty in a single-sample indirectly

indirectly measured parameter using the pythagorean summation of the discrete uncertainties. As an example, if the indirectly measured parameter X is calculated by the following equation

$$X = \xi\ \eta^a/\zeta^b$$

and the percentage errors of the quantities ξ, η, ζ are $\varepsilon\xi$, $\varepsilon\eta$, ε_ζ respectively. The percentage error ε_x of the quantity x can be calculated as

$$\varepsilon_x^2 = \varepsilon_\xi^2 + (a\varepsilon_\eta)^2 + (b\varepsilon_\zeta)^2 \qquad (12.1)$$

An error estimate of the directly measured data in the present experiment can be made as follows:

1. The error ε_L in measuring the duct lengths in the order of 0.5%.
2. The error ε_D in measuring the particle diameter, is the order of 2.0% (mainly due to the averaging process).
3. The error ε_p in the pressure drop measurements along the duct is about 0.15% as quoted in the instruction manual.
4. The error ε_{us} in the particle velocities (u_s and v_s) measurements by the LDA is estimated to be 5%. This is mianly due to the difficulty of reading from the screen of the oscilliscope.
5. The error ε_{ua} in air flow bulk velocity measurements is estimated by 2%. The inaccuracy of each individual rotameter is about 1% of its full range. However, the overall error of the system was improved by the accurate monitoring of the pressure, proper calibration, and using each tube as a unit (either on or off).
6. The error ε_m, ε_G in measuring the feeded particle mass and volume rates is about 1%.

7. The error ε_v of measuring the DC volt is about 1%.

Error due to uncertainty propagation of the indirectly measured parameters can be estimated as in following list:

1. The error ε_n in the particle number density expressed Equation (4.3) as

$$n = Q_s \; N \; A_D^{-1} \; u_s^{-1}$$

$$\varepsilon_n \% = (\varepsilon_Q^2 + (3 \; \varepsilon_D)^2 + \varepsilon_L^2 + \varepsilon^2_{us})^{1/2}$$

$$= ((1)^2 + (3x2)^2 + (0.5)^2 + (5)^2)^{1/2} = 7.89\%$$

2. The error ε_E in measuring of the electric field strength expressed as E $= V \cdot h^{-1}$

$$\varepsilon_E \% = (\varepsilon_v^2 + \varepsilon_L^2)^{1/2}$$

$$= (1^2 + 0.5^2)^{1/2} = 1.12\%$$

3. The error ε_{ReD} in measuring the duct Reynolds number expressed by

$$Re_D = u_a \; D_H \; \nu^{-1}$$

$$\varepsilon_{ReD}\% = (\varepsilon_a^2 + \varepsilon_L^2)^{1/2}$$

$$= (2^2 + 0.5^2)^{1/2} = 2.06\%$$

where the error of ν is ignored.

4. The error ε_{Rep} in measuring the particle Reynolds number expressed as

$$Rep = V_r \; D_p \; \times^{-1}$$

$$\varepsilon_{Rep}\% = (\varepsilon_{ua} + \varepsilon_{us})^2 + \varepsilon_D^2)^{1/2}$$

$$= ((2+5)^2 + 2^2)^{1/2} = 7.28\%$$

5. The error ε_{Relim} in the measured limiting Reynolds number expressed as

$$Re_{Lim} = v_s \; D_p \; \nu^{-1}$$

$$\varepsilon_{Re,lim} \% = (5^2 + 2^2)^{1/2} = 5.36\%$$

6. The error $\varepsilon_{\bar{Rep}}$ in measuring the newly defined Reynolds number Equation (4.9)

$$\bar{R}_{ep} = R_{ep} - R_{eplim}$$

$$\varepsilon_{\bar{R}ep}\ \% = \varepsilon_{Rep} + \varepsilon_{Replim}$$

$$= 7.28 + 5.36 = 12.64\%$$

7. The error ε_{ps} in measuring the pressure gradient per unit mass flow rate of the conveyed solid particle expressed as

$$\Delta p_{s-a}\ L^{-1}\ \dot{m}_s^{-1}$$

$$\varepsilon_{ps}\ \% = (\varepsilon_p^{\,2} + \varepsilon_L^{\,2} + \varepsilon_{\dot{m}}^{2})^{1/2}$$

$$= (0.15^2 + 0.5^2 + 1^2)^{1/2} = 1.13\%$$

8. The error ε_f in measuring the friction factor per unit mass flow rate of conveyed particles expressed as

$$f = \Delta p_{s-a}\ 2\rho^{-1} u_a^{-2}\ D_H\ L^{-1}$$

$$\varepsilon_f\ \% = (0.15^2 + (2x2)^2 + (2 \times 0.5)^2)^{1/2} = 4.13\%$$

9. The error ε_F in measuring the force per particle expressed as

$$F_p = \Delta p(nL_{ss}\cos\theta)^{-1}$$

$$\varepsilon_F\ \% = (\varepsilon_p^{\,2} + \varepsilon_n^{\,2} + (\varepsilon_L)^2 + \varepsilon_{us}^{\,2})^{1/2}$$

$$= (0.15^2 + (7.89)^2 + (0.5)^2 + 5^2)^{1/2} = 9.355\%$$

where the error of measuring θ is predicted to be of the same order of the error of measuring the particle velocity.

10. The error ε_{CD} in measuring the particle drag coefficient expressed as

$$C_D = F_p\ (\rho u_{a-s}^2\ \frac{\pi}{4}\ D_p^2)^{-1}$$

$$\varepsilon_{CD}\ \% = (\varepsilon_F^{\,2} + (2(\varepsilon_{us} + \varepsilon_a))^2 + \varepsilon_D^{\,2})^{1/2}$$

$$= ((9.355)^2 + (2(5+2))^2 + 2^2)^{1/2} = 16.956\%$$

where the uncertainty of the specific mass of air is ignored. The error in measuring the drag coefficient has the maximum error expectation among all measured parameters.

13. APPENDIX E: TEST DATA

The test data of the solid-air flow pressure drop, particle horizontal and vertical velocities, and particle number density along a rectangular duct at a constant electric field strength of 5 kv/cm and various conveying air speeds are presented in Tables 13.1-13.40.

Table 13.1. Data of solid-air flow parameters along the duct at constant electric field strength[a]

Test point i	Pressure drop $_1\Delta p_i$ (torr)	Particle horizontal velocity u_s (m/s)	Particle number density $n \times 10^{-8}$ $[m^{-3}]$
1	-	1.5	2.590
2	0.120	1.9	2.045
3	0.190	2.1	1.850
4	0.230	2.3	1.689
5	0.305	2.55	1.523
6	0.370	2.65	1.466
7	0.420	2.65	1.466
8	0.375	2.65	1.466
9	0.525	2.65	1.466
10	0.590	2.65	1.466
11	0.665	2.65	1.466
12	0.710	2.65	1.466
13	0.760	2.65	1.466

[a]Copper spherical particles with diameters of 63-74 μm. Air flow bulk velocity of 7.98 m/s. Input volt of the feeder servomotor of 23.3 V. Particle vertical velocity 1.0.

Table 13.2. Data of solid-air flow parameters along the duct at constant electric field strength[a]

Test point i	Pressure drop $_1\Delta p_i$ (torr)	Particle horizontal velocity u_s (m/s)	Particle number density $n \times 10^{-8}$ $[m^{-3}]$
1	-	1.20	3.200
2	0.130	1.50	2.561
3	0.170	1.75	2.195
4	0.228	1.90	2.022
5	0.280	2.10	1.829
6	0.325	2.10	1.829
7	0.370	2.10	1.829
8	0.410	2.10	1.829
9	0.465	2.10	1.829
10	0.505	2.10	1.829
11	0.550	2.10	1.829
12	0.595	2.10	1.829
13	0.630	2.10	1.829

[a]Copper spherical particles with diameters of 63-74 μm. Air flow bulk velocity of 6.37 m/s. Input volt of the feeder servomotor of 23.3 V. Particle vertical velocity 1.0.

Table 13.3. Data of solid-air flow parameters along the duct at constant electric field strength[a]

Test point i	Pressure drop $_1\Delta p_i$ (torr)	Particle horizontal velocity u_s (m/s)	Particle number density $n \times 10^{-8}$ $[m^{-3}]$
1	-	0.80	4.8014
2	0.035	1.15	3.3401
3	0.09	1.30	2.9547
4	0.13	1.35	2.8453
5	0.155	1.35	2.8453
6	0.19	1.35	2.8453
7	0.205	1.35	2.8453
8	0.230	1.35	2.8453
9	0.260	1.35	2.8453
10	0.290	1.35	2.8453
11	0.320	1.35	2.8453
12	0.350	1.35	2.8453
13	0.385	1.35	2.8453

[a]Copper spherical particles with diameters of 63-74 μm. Air flow bulk velocity of 4.06 m/s. Input volt of the feeder servomotor of 23.3 V. Particle vertical velocity 1.0.

Table 13.4. Data of solid-air flow parameters along the duct at constant electric field strength[a]

Test point i	Pressure drop $_1\Delta p_i$ (torr)	Particle horizontal velocity u_s (m/s)	Particle number density $n \times 10^{-8}$ $[m^{-3}]$
1	-	0.75	5.1215
2	0.06	1.0	2.8411
3	0.086	1.05	3.6582
4	0.11	1.05	3.6582
5	0.135	1.05	3.6582
6	0.165	1.05	3.6582
7	0.189	1.05	3.6582
8	0.215	1.05	3.6582
9	0.243	1.05	3.6582
10	0.269	1.05	3.6582
11	0.295	1.05	3.6582
12	0.320	1.05	3.6582
13	0.348	1.05	3.6582

[a]Copper spherical particles with diameters of 63-74 μm. Air flow bulk velocity of 3.1955 m/s. Input volt of the feeder servomotor of 23.3 V. Particle vertical velocity 1.0.

Table 13.5. Data of solid-air flow parameters along the duct at constant electric field strength[a]

Test point i	Pressure drop $_1\Delta p_i$ (torr)	Particle horizontal velocity u_s (m/s)	Particle number density $n \times 10^{-8}$ $[m^{-3}]$
1	-	0.65	5.909
2	0.043	0.77	4.9885
3	0.070	0.77	4.9885
4	0.0915	0.77	4.9885
5	0.118	0.77	4.9885
6	0.144	0.77	4.9885
7	0.170	0.77	4.9885
8	0.195	0.77	4.9885
9	0.220	0.77	4.9885
10	0.245	0.77	4.9885
11	0.270	0.77	4.9885
12	0.295	0.77	4.9885
13	0.321	0.77	4.9885

[a]Copper spherical particles with diameters of 63-74 μm. Air flow bulk velocity of 2.3295 m/s. Input volt of the feeder servomotor of 23.3 V. Particle vertical velocity 1.0.

Table 13.6. Data of solid-air flow parameters along the duct at constant electric field strength[a]

Test point i	Pressure drop $_1\Delta p_i$ (torr)	Particle horizontal velocity u_s (m/s)	Particle number density $n \times 10^{-8}$ $[m^{-3}]$
1	-	0.47	5.059
2	0.025	0.48	4.954
3	0.036	0.48	4.954
4	0.050	0.48	4.954
5	0.067	0.48	4.954
6	0.083	0.48	4.954
7	0.099	0.48	4.954
8	0.115	0.48	4.954
9	0.130	0.48	4.954
10	0.145	0.48	4.954
11	0.160	0.48	4.954
12	0.175	0.48	4.954
13	0.190	0.48	4.954

[a]Copper spherical particles with diameters of 63-74 μm. Air flow bulk velocity of 1.466 m/s. Input volt of the feeder servomotor of 15 V. Particle vertical velocity 1.0 m/s.

Table 13.7. Data of solid-air flow parameters along the duct at constant electric field strength[a]

Test point i	Pressure drop $_1\Delta p_i$ (torr)	Particle horizontal velocity u_s (m/s)	Particle number density $n \times 10^{-8}$ $[m^{-3}]$
1	-	0.35	4.350
2	0.023	0.39	3.904
3	0.034	0.39	3.904
4	0.046	0.39	3.904
5	0.057	0.39	3.904
6	0.060	0.39	3.904
7	0.710	0.39	3.904
8	0.085	0.39	3.904
9	0.096	0.39	3.904
10	0.108	0.39	3.904
11	0.121	0.39	3.904
12	0.131	0.39	3.904
13	0.142	0.39	3.904

[a]Copper spherical particles with diameters of 63-74 μm. Air flow bulk velocity of 1.190 m/s. Input volt of the feeder servomotor of 10 V. Particle vertical velocity 1.0 m/s.

Table 13.8. Data of solid-air flow parameters along the duct at constant electric field strength[a]

Test point i	Pressure drop $_1\Delta p_i$ (torr)	Particle horizontal velocity u_s (m/s)	Particle number density $n \times 10^{-8}$ $[m^{-3}]$
1	-	0.25	6.090
2	0.022	0.27	5.6393
3	0.031	0.27	5.6393
4	0.040	0.27	5.6393
5	0.050	0.27	5.6393
6	0.06	0.27	5.6393
7	0.07	0.27	5.6393
8	0.080	0.27	5.6393
9	0.090	0.27	5.6393
10	0.100	0.27	5.6393
11	0.111	0.27	5.6393
12	0.121	0.27	5.6393
13	0.132	0.27	5.6393

[a]Copper spherical particles with diameters of 63-74 μm. Air flow bulk velocity of 0.82766 m/s. Input volt of the feeder servomotor of 10 V. Particle vertical velocity 1.0 m/s.

Table 13.9. Data of solid-air flow parameters along the duct at constant electric field strength[a]

Test point i	Pressure drop $_1\Delta p_i$ (torr)	Particle horizontal velocity u_s (m/s)	Particle number density $n \times 10^{-8}$ $[m^{-3}]$
1	-	1.0	2.3743
2	0.11	1.3	1.8264
3	0.17	1.55	1.5318
4	0.23	1.75	1.3567
5	0.29	1.9	1.2496
6	0.365	2.00	1.1872
7	0.42	2.5	1.1582
8	0.49	2.5	1.1582
9	0.53	2.5	1.1582
10	0.60	2.5	1.1582
11	0.66	2.5	1.1582
12	0.71	2.5	1.1582
13	0.77	2.5	1.1582

[a]Copper spherical particles with diameters of 74-88 μm. Air flow bulk velocity of 7.98 m/s. Input volt of the feeder servomotor of 23.3 V. Particle vertical velocity 1.0 m/s.

Table 13.10. Data of solid-air flow parameters along the duct at constant electric field strength[a]

Test point i	Pressure drop $_1\Delta p_i$ (torr)	Particle horizontal velocity u_s (m/s)	Particle number density $n \times 10^{-8}$ $[m^{-3}]$
1	-	1.2	1.9785
2	0.11	1.4	1.6959
3	0.17	1.55	1.5318
4	0.23	1.6	1.4839
5	0.284	1.62	1.4656
6	0.33	1.63	1.4566
7	0.38	1.63	1.4566
8	0.42	1.63	1.4566
9	0.474	1.63	1.4566
10	0.52	1.63	1.4566
11	0.565	1.63	1.4566
12	0.61	1.63	1.4566
13	0.65	1.63	1.4566

[a]Copper spherical particles with diameters of 74-88 μm. Air flow bulk velocity of 6.37 m/s. Input volt of the feeder servomotor of 23.3 V. Particle vertical velocity 1.0 m/s.

Table 13.11. Data of solid-air flow parameters along the duct at constant electric field strength[a]

Test point i	Pressure drop $_1\Delta p_i$ (torr)	Particle horizontal velocity u_s (m/s)	Particle number density $n \times 10^{-8}$ $[m^{-3}]$
1	-	0.7	3.3918
2	0.06	0.9	2.6381
3	0.097	1.00	2.3743
4	0.132	1.05	2.2612
5	0.166	1.05	2.2612
6	0.199	1.05	2.2612
7	0.232	1.05	2.2612
8	0.258	1.05	2.2612
9	0.285	1.05	2.2612
10	0.305	1.05	2.2612
11	0.345	1.05	2.2612
12	0.37	1.05	2.2612
13	0.400	1.05	2.2612

[a]Copper spherical particles with diameters of 74-88 μm. Air flow bulk velocity of 4.06 m/s. Input volt of the feeder servomotor of 23.3 V. Particle vertical velocity 1.0 m/s.

Table 13.12. Data of solid-air flow parameters along the duct at constant electric field strength[a]

Test point i	Pressure drop $_1\Delta p_i$ (torr)	Particle horizontal velocity u_s (m/s)	Particle number density $n \times 10^{-8}$ $[m^{-3}]$
1	-	0.7	3.3918
2	0.05	0.8	2.9678
3	0.08	0.82	2.8954
4	0.12	0.82	2.8954
5	0.14	0.82	2.8954
6	0.18	0.82	2.8954
9	0.25	0.82	2.8954
10	0.28	0.82	2.8954
11	0.31	0.82	2.8954
12	0.33	0.82	2.8954
13	0.36	0.82	2.8954

[a]Copper spherical particles with diameters of 74-88 μm. Air flow bulk velocity of 3.1955 m/s. Input volt of the feeder servomotor of 23.3 V. Particle vertical velocity 1.0 m/s.

Table 13.13. Data of solid-air flow parameters along the duct at constant electric field strength[a]

Test point i	Pressure drop $_1\Delta p_i$ (torr)	Particle horizontal velocity u_s (m/s)	Particle number density $n \times 10^{-8}$ $[m^{-3}]$
1	-	0.5	4.74846
2	0.043	0.6	3.95715
3	0.07	0.6	3.95715
4	0.098	0.6	3.95715
5	0.125	0.6	3.95715
6	0.15	0.6	3.95715
7	0.17	0.6	3.95715
8	0.205	0.6	3.95715
9	0.225	0.6	3.95715
10	0.255	0.6	3.95715
11	0.285	0.6	3.95715
12	0.315	0.6	3.95715
13	0.34	0.6	3.95715

[a]Copper spherical particles with diameters of 74-88 μm. Air flow bulk velocity of 2.3298 m/s. Input volt of the feeder servomotor of 23.3 V. Particle vertical velocity 1.0 m/s.

Table 13.14. Data of solid-air flow parameters along the duct at constant electric field strength[a]

Test point i	Pressure drop $_1\Delta p_i$ (torr)	Particle horizontal velocity u_s (m/s)	Particle number density $n \times 10^{-8}$ $[m^{-3}]$
1	-	0.37	3.9727
2	0.024	0.38	3.8682
3	0.034	0.38	3.8682
4	0.047	0.38	3.8682
5	0.058	0.38	3.8682
6	0.07	0.38	3.8682
7	0.084	0.38	3.8682
8	0.096	0.38	3.8682
9	0.115	0.38	3.8682
10	0.135	0.38	3.8682
11	0.15	0.38	3.8682
12	0.175	0.38	3.8682
13	0.190	0.38	3.8682

[a]Copper spherical particles with diameters of 74-88 μm. Air flow bulk velocity of 1.466 m/s. Input volt of the feeder servomotor of 15 V. Particle vertical velocity 1.0 m/s.

Table 13.15. Data of solid-air flow parameters along the duct at constant electric field strength[a]

Test point i	Pressure drop $_1\Delta p_i$ (torr)	Particle horizontal velocity u_s (m/s)	Particle number density $n \times 10^{-8}$ $[m^{-3}]$
1	-	0.30	3.1372
2	0.024	0.31	3.036
3	0.035	0.31	3.036
4	0.046	0.31	3.036
5	0.056	0.31	3.036
6	0.067	0.31	3.036
7	0.078	0.31	3.036
8	0.089	0.31	3.036
9	0.099	0.31	3.036
10	0.111	0.31	3.036
11	0.122	0.31	3.036
12	0.133	0.31	3.036
13	0.166	0.31	3.036

[a]Copper spherical particles with diameters of 74-88 μm. Air flow bulk velocity of 1.19 m/s. Input volt of the feeder servomotor of 10 V. Particle vertical velocity 1.0 m/s.

Table 13.16. Data of solid-air flow parameters along the duct at constant electric field strength[a]

Test point i	Pressure drop $_1\Delta p_i$ (torr)	Particle horizontal velocity u_s (m/s)	Particle number density $n \times 10^{-8}$ $[m^{-3}]$
1	-	0.22	4.278
2	0.024	0.22	4.278
3	0.034	0.22	4.278
4	0.044	0.22	4.278
5	0.055	0.22	4.278
6	0.065	0.22	4.278
7	0.075	0.22	4.278
8	0.085	0.22	4.278
9	0.095	0.22	4.278
10	0.115	0.22	4.278
11	0.115	0.22	4.278
12	0.125	0.22	4.278
13	0.140	0.22	4.278

[a]Copper spherical particles with diameters of 74-88 μm. Air flow bulk velocity of 0.82766 m/s. Input volt of the feeder servomotor of 10 V. Particle vertical velocity 1.0 m/s.

Table 13.17. Data of solid-air flow parameters along the duct at constant electric field strength[a]

Test point i	Pressure drop $_1\Delta p_i$ (torr)	Particle horizontal velocity u_s (m/s)	Particle number density $n \times 10^{-8}$ $[m^{-3}]$
1	-	4.60	1.736
2	0.07	5.10	1.566
3	0.12	5.20	1.536
4	0.16	5.20	1.536
5	0.2	5.20	1.536
6	0.27	5.20	1.536
7	0.31	5.20	1.536
8	0.345	5.20	1.536
9	0.380	5.20	1.536
10	0.43	5.20	1.536
11	0.485	5.20	1.536
12	0.515	5.20	1.536
13	0.59	5.20	1.536

[a]Glass spherical particles with diameters of 44-63 μm. Air flow bulk velocity of 7.98 m/s. Input volt of the feeder servomotor of 23.3 V. Particle vertical velocity 1.7 m/s.

Table 13.18. Data of solid-air flow parameters along the duct at constant electric field strength[a]

Test point i	Pressure drop $_1\Delta p_i$ (torr)	Particle horizontal velocity u_s (m/s)	Particle number density $n \times 10^{-8}$ $[m^{-3}]$
1	-	4.05	1.972
2	0.06	4.15	1.925
3	0.096	4.15	1.925
4	0.125	4.15	1.925
5	0.160	4.15	1.925
6	0.2	4.15	1.925
7	0.23	4.15	1.925
8	0.26	4.15	1.925
9	0.29	4.15	1.925
10	0.32	4.15	1.925
11	0.36	4.15	1.925
12	0.39	4.15	1.925
13	0.425	4.15	1.925

[a]Glass spherical particles with diameters of 44-63 μm. Air flow bulk velocity of 6.37 m/s. Input volt of the feeder servomotor of 23.3 V. Particle vertical velocity 1.7 m/s.

Table 13.19. Data of solid-air flow parameters along the duct at constant electric field strength[a]

Test point i	Pressure drop $_1\Delta P_i$ (torr)	Particle horizontal velocity u_s (m/s)	Particle number density n x 10^{-8} [m^{-3}]
1	-	2.6	3.073
2	0.04	2.65	3.015
3	0.06	2.65	3.015
4	0.08	2.65	3.015
5	0.10	2.65	3.015
6	0.12	2.65	3.015
7	0.14	2.65	3.015
8	0.16	2.65	3.015
9	0.172	2.65	3.015
10	0.19	2.65	3.015
11	0.21	2.65	3.015
12	0.228	2.65	3.015
13	0.247	2.65	3.015

[a]Glass spherical particles with diameters of 44-63 μm. Air flow bulk velocity of 4.06 m/s. Input volt of the feeder servomotor of 23.3 V. Particle vertical velocity 1.7 m/s.

Table 13.20. Data of solid-air flow parameters along the duct at constant electric field strength[a]

Test point i	Pressure drop $_1\Delta p_i$ (torr)	Particle horizontal velocity u_s (m/s)	Particle number density $n \times 10^{-8}$ $[m^{-3}]$
1	-	2.1	3.805
2	0.034	2.3	3.474
3	0.05	2.3	3.474
4	0.065	2.3	3.474
5	0.08	2.3	3.474
6	0.095	2.3	3.474
7	0.11	2.3	3.474
8	0.125	2.3	3.474
9	0.14	2.3	3.474
10	0.156	2.3	3.474
11	0.171	2.3	3.474
12	0.186	2.3	3.474
13	0.203	2.3	3.474

[a]Glass spherical particles with diameters of 44-63 μm. Air flow bulk velocity of 3.1955 m/s. Input volt of the feeder servomotor of 23.3 V. Particle vertical velocity 1.7 m/s.

Table 13.21. Data of solid-air flow parameters along the duct at constant electric field strength[a]

Test point i	Pressure drop $_1\Delta p_i$ (torr)	Particle horizontal velocity u_s (m/s)	Particle number density $n \times 10^{-8}$ $[m^{-3}]$
1	-	1.4	
2	0.02	1.5	3.298
3	0.033	1.5	3.298
4	0.043	1.5	3.298
5	0.054	1.5	3.298
6	0.065	1.5	3.298
7	0.075	1.5	3.298
8	0.085	1.5	3.298
9	0.093	1.5	3.298
10	0.102	1.5	3.298
11	0.112	1.5	3.298
12	0.12	1.5	3.298
13	0.130	1.5	3.298

[a]Glass spherical particles with diameters of 44-63 μm. Air flow bulk velocity of 2,3298 m/s. Input volt of the feeder servomotor of 15 V. Particle vertical velocity 1.7 m/s.

Table 13.22. Data of solid-air flow parameters along the duct at constant electric field strength[a]

Test point i	Pressure drop $_1\Delta P_i$ (torr)	Particle horizontal velocity u_s (m/s)	Particle number density n x 10^{-8} [m^{-3}]
1	-	0.9	3.520
2	0.013	0.94	3.370
3	0.02	0.94	3.370
4	0.028	0.94	3.370
5	0.036	0.94	3.370
6	0.043	0.94	3.370
7	0.051	0.94	3.370
8	0.0585	0.94	3.370
9	0.066	0.94	3.370
10	0.073	0.94	3.370
11	0.081	0.94	3.370
12	0.089	0.94	3.370
13	0.0967	0.94	3.370

[a]Glass spherical particles with diameters of 44-63 μm. Air flow bulk velocity of 1.466 m/s. Input volt of the feeder servomotor of 10 V. Particle vertical velocity 1.7 m/s.

Table 13.23. Data of solid-air flow parameters along the duct at constant electric field strength[a]

Test point i	Pressure drop $_1\Delta p_i$ (torr)	Particle horizontal velocity u_s (m/s)	Particle number density $n \times 10^{-8}$ $[m^{-3}]$
1	-	0.75	4.235
2	0.012	0.77	4.125
3	0.0195	0.77	4.125
4	0.027	0.77	4.125
5	0.034	0.77	4.125
6	0.0385	0.77	4.125
7	0.042	0.77	4.125
8	0.049	0.77	4.125
9	0.057	0.77	4.125
10	0.064	0.77	4.125
11	0.072	0.77	4.125
12	0.080	0.77	4.125
13	0.098	0.77	4.125

[a]Glass spherical particles with diameters of 44-63 μm. Air flow bulk velocity of 1.19 m/s. Input volt of the feeder servomotor of 10 V. Particle vertical velocity 1.7 m/s.

Table 13.24. Data of solid-air flow parameters along the duct at constant electric field strength[a]

Test point i	Pressure drop $_1\Delta P_i$ (torr)	Particle horizontal velocity u_s (m/s)	Particle number density $n \times 10^{-8}$ $[m^{-3}]$
1	-	0.52	6.1087
2	0.0115	0.53	5.9935
3	0.021	0.53	5.9935
4	0.028	0.53	5.9935
5	0.04	0.53	5.9935
6	0.050	0.53	5.9935
7	0.0595	0.53	5.9935
8	0.069	0.53	5.9935
9	0.079	0.53	5.9935
10	0.088	0.53	5.9935
11	0.098	0.53	5.9935
12	0.105	0.53	5.9935
13	0.1175	0.53	5.9935

[a]Glass spherical particles with diameters of 44-63 μm. Air flow bulk velocity of 0.82766 m/s. Input volt of the feeder servomotor of 10 V. Particle vertical velocity 1.7 m/s.

Table 13.25. Data of solid-air flow parameters along the duct at constant electric field strength[a]

Test point i	Pressure drop $_1\Delta p_i$ (torr)	Particle horizontal velocity u_s (m/s)	Particle number density $n \times 10^{-8}$ $[m^{-3}]$
1	-	3.6	1.066
2	0.07	3.85	0.997
3	0.117	3.95	0.927
4	0.16	3.95	0.927
5	0.213	3.95	0.927
6	0.26	3.95	0.927
7	0.31	3.95	0.927
8	0.355	3.95	0.927
9	0.4	3.95	0.927
10	0.45	3.95	0.927
11	0.5	3.95	0.927
12	0.545	3.95	0.927
13	0.593	3.95	0.927

[a]Glass spherical particles with diameters of 44-63 μm. Air flow bulk velocity of 7.89 m/s. Input volt of the feeder servomotor of 23.3 V. Particle vertical velocity 1.7 m/s.

Table 13.26. Data of solid-air flow parameters along the duct at constant electric field strength[a]

Test point i	Pressure drop $_1\Delta p_i$ (torr)	Particle horizontal velocity u_s (m/s)	Particle number density $n \times 10^{-8}$ $[m^{-3}]$
1	-	3.05	1.2593
2	0.06	3.15	1.2194
3	0.095	3.15	1.2194
4	0.13	3.15	1.2194
5	0.164	3.15	1.2194
6	0.198	3.15	1.2194
7	0.233	3.15	1.2194
8	0.267	3.15	1.2194
9	0.300	3.15	1.2194
10	0.336	3.15	1.2194
11	0.37	3.15	1.2194
12	0.405	3.15	1.2194
13	0.44	3.15	1.2194

[a]Glass spherical particles with diameters of 63-74 μm. Air flow bulk velocity of 6.37 m/s. Input volt of the feeder servomotor of 23.3 V. Particle vertical velocity 1.7 m/s.

Table 13.27. Data of solid-air flow parameters along the duct at constant electric field strength[a]

Test point i	Pressure drop $_1\Delta P_i$ (torr)	Particle horizontal velocity u_s (m/s)	Particle number density $n \times 10^{-8}$ $[m^{-3}]$
1	-	1.9	2.021
2	0.04	2.0	1.920
3	0.06	2.0	1.920
4	0.085	2.0	1.920
5	0.10	2.0	1.920
6	0.12	2.0	1.920
7	0.137	2.0	1.920
8	0.157	2.0	1.920
9	0.177	2.0	1.920
10	0.196	2.0	1.920
11	0.214	2.0	1.920
12	0.233	2.0	1.920
13	0.252	2.0	1.920

[a]Glass spherical particles with diameters of 63-74 μm. Air flow bulk velocity of 4.06 m/s. Input volt of the feeder servomotor of 23.3 V. Particle vertical velocity 1.7 m/s.

Table 13.28. Data of solid-air flow parameters along the duct at constant electric field strength[a]

Test point i	Pressure drop $_1\Delta p_i$ (torr)	Particle horizontal velocity u_s (m/s)	Particle number density $n \times 10^{-8}$ $[m^{-3}]$
1	-	1.70	2.2595
2	0.033	1.75	2.1949
3	0.057	1.75	2.1949
4	0.076	1.75	2.1949
5	0.093	1.75	2.1949
6	0.113	1.75	2.1949
7	0.13	1.75	2.1949
8	0.145	1.75	2.1949
9	0.158	1.75	2.1949
10	0.172	1.75	2.1949
11	0.19	1.75	2.1949
12	0.2	1.75	2.1949
13	0.215	1.75	2.1949

[a]Glass spherical particles with diameters of 63-74 μm. Air flow bulk velocity of 3.1955 m/s. Input volt of the feeder servomotor of 23.3 V. Particle vertical velocity 1.7 m/s.

Table 13.29. Data of solid-air flow parameters along the duct at constant electric field strength[a]

Test point i	Pressure drop $_1\Delta p_i$ (torr)	Particle horizontal velocity u_s (m/s)	Particle number density $n \times 10^{-8}$ $[m^{-3}]$
1	-	1.1	2.1618
2	0.022	1.15	2.0678
3	0.037	1.15	2.0678
4	0.049	1.15	2.0678
5	0.06	1.15	2.0678
6	0.072	1.15	2.0678
7	0.084	1.15	2.0678
8	0.095	1.15	2.0678
9	0.105	1.15	2.0678
10	0.115	1.15	2.0678
11	0.127	1.15	2.0678
12	0.132	1.15	2.0678
13	0.142	1.15	2.0678

[a]Glass spherical particles with diameters of 63-74 μm. Air flow bulk velocity of 2.3298 m/s. Input volt of the feeder servomotor of 15 V. Particle vertical velocity 1.7 m/s.

Table 13.30. Data of solid-air flow parameters along the duct at constant electric field strength[a]

Test point i	Pressure drop $_1\Delta p_i$ (torr)	Particle horizontal velocity u_s (m/s)	Particle number density $n \times 10^{-8}$ $[m^{-3}]$
1	-	0.720	2.11474
2	0.015	0.725	2.10016
3	0.024	0.725	2.10016
4	0.033	0.725	2.10016
5	0.042	0.725	2.10016
6	0.051	0.725	2.10016
7	0.060	0.725	2.10016
8	0.069	0.725	2.10016
9	0.078	0.725	2.10016
10	0.087	0.725	2.10016
11	0.096	0.725	2.10016
12	0.104	0.725	2.10016
13	0.112	0.725	2.10016

[a]Glass spherical particles with diameters of 63-74 μm. Air flow bulk velocity of 1.466 m/s. Input volt of the feeder servomotor of 10 V. Particle vertical velocity 1.7 m/s.

Table 13.31. Data of solid-air flow parameters along the duct at constant electric field strength[a]

Test point i	Pressure drop $_1\Delta p_i$ (torr)	Particle horizontal velocity u_s (m/s)	Particle number density $n \times 10^{-8}$ $[m^{-3}]$
1	-	0.58	2.624
2	0.018	0.59	2.580
3	0.026	0.59	2.580
4	0.034	0.59	2.580
5	0.043	0.59	2.580
6	0.051	0.59	2.580
7	0.059	0.59	2.580
8	0.067	0.59	2.580
9	0.078	0.59	2.580
10	0.089	0.59	2.580
11	0.099	0.59	2.580
12	0.109	0.59	2.580
13	0.114	0.59	2.580

[a]Glass spherical particles with diameters of 63-74 μm. Air flow bulk velocity of 1.19 m/s. Input volt of the feeder servomotor of 10 V. Particle vertical velocity 1.7 m/s.

Table 13.32. Data of solid-air flow parameters along the duct at constant electric field strength[a]

Test point i	Pressure drop $_1\Delta p_i$ (torr)	Particle horizontal velocity u_s (m/s)	Particle number density n x 10^{-8} [m^{-3}]
1	-	0.400	3.8067
2	0.02	0.409	3.7227
3	0.029	0.409	3.7227
4	0.039	0.409	3.7227
5	0.049	0.409	3.7227
6	0.058	0.409	3.7227
7	0.068	0.409	3.7227
8	0.078	0.409	3.7227
9	0.088	0.409	3.7227
10	0.097	0.409	3.7227
11	0.107	0.409	3.7227
12	0.117	0.409	3.7227
13	0.127	0.409	3.7227

[a]Glass spherical particles with diameters of 63-74 μm. Air flow bulk velocity of 0.82766 m/s. Input volt of the feeder servomotor of 10 V. Particle vertical velocity 1.7 m/s.

Table 13.33. Data of solid-air flow parameters along the duct at constant electric field strength[a]

Test point i	Pressure drop $_1\Delta P_i$ (torr)	Particle horizontal velocity u_s (m/s)	Particle number density $n \times 10^{-8}$ $[m^{-3}]$
1	-	2.60	0.91318
2	0.070	3.00	0.79142
3	0.120	3.05	0.77845
4	0.168	3.05	0.77845
5	0.215	3.05	0.77845
6	0.265	3.05	0.77845
7	0.310	3.05	0.77845
8	0.363	3.05	0.77845
9	0.411	3.05	0.77845
10	0.459	3.05	0.77845
11	0.508	3.05	0.77845
12	0.555	3.05	0.77845
13	0.605	3.05	0.77845

[a]Glass spherical particles with diameters of 74-88 μm. Air flow bulk velocity of 7.98 m/s. Input volt of the feeder servomotor of 23.3 V. Particle vertical velocity 1.7 m/s.

Table 13.34. Data of solid-air flow parameters along the duct at constant electric field strength[a]

Test point i	Pressure drop $_1\Delta p_i$ (torr)	Particle horizontal velocity u_s (m/s)	Particle number density $n \times 10^{-8}$ $[m^{-3}]$
1	-	2.0	1.18701
2	0.06	2.4	0.98918
3	0.095	2.4	0.98918
4	0.130	2.4	0.98918
5	0.160	2.4	0.98918
6	0.195	2.4	0.98918
7	0.230	2.4	0.98918
8	0.255	2.4	0.98918
9	0.290	2.4	0.98918
10	0.335	2.4	0.98918
11	0.375	2.4	0.98918
12	0.415	2.4	0.98918
13	0.45	2.4	0.98918

[a]Glass spherical particles with diameters of 74-88 μm. Air flow bulk velocity of 6.37 m/s. Input volt of the feeder servomotor of 23.3 V. Particle vertical velocity 1.7 m/s.

Table 13.35. Data of solid-air flow parameters along the duct at constant electric field strength[a]

Test point i	Pressure drop $_1\Delta P_i$ (torr)	Particle horizontal velocity u_s (m/s)	Particle number density $n \times 10^{-8}$ $[m^{-3}]$
1	-	1.25	1.8994
2	0.04	1.55	1.5318
3	0.065	1.55	1.5318
4	0.095	1.55	1.5318
5	0.115	1.55	1.5318
6	0.14	1.55	1.5318
7	0.16	1.55	1.5318
8	0.18	1.55	1.5318
9	0.195	1.55	1.5318
10	0.22	1.55	1.5318
11	0.24	1.55	1.5318
12	0.255	1.55	1.5318
13	0.27	1.55	1.5318

[a]Glass spherical particles with diameters of 74-88 μm. Air flow bulk velocity of 4.06 m/s. Input volt of the feeder servomotor of 23.3 V. Particle vertical velocity 1.7 m/s.

Table 13.36. Data of solid-air flow parameters along the duct at constant electric field strength[a]

Test point i	Pressure drop $_1\Delta p_i$ (torr)	Particle horizontal velocity u_s (m/s)	Particle number density $n \times 10^{-8}$ $[m^{-3}]$
1	-	1.2	1.9775
2	0.034	1.4	1.695
3	0.06	1.4	1.695
4	0.08	1.4	1.695
5	0.095	1.4	1.695
6	0.113	1.4	1.695
7	0.126	1.4	1.695
8	0.140	1.4	1.695
9	0.153	1.4	1.695
10	0.170	1.4	1.695
11	0.183	1.4	1.695
12	0.195	1.4	1.695
13	0.21	1.4	1.695

[a]Glass spherical particles with diameters of 74-88 μm. Air flow bulk velocity of 3.1955 m/s. Input volt of the feeder servomotor of 23.3 V. Particle vertical velocity 1.7 m/s.

Table 13.37. Data of solid-air flow parameters along the duct at constant electric field strength[a]

Test point i	Pressure drop $_1\Delta p_i$ (torr)	Particle horizontal velocity u_s (m/s)	Particle number density $n \times 10^{-8}$ $[m^{-3}]$
1	-	0.8	1.8413
2	0.02	0.9	1.6367
3	0.035	0.9	1.6367
4	0.046	0.9	1.6367
5	0.057	0.9	1.6367
6	0.068	0.9	1.6367
7	0.079	0.9	1.6367
8	0.090	0.9	1.6367
9	0.100	0.9	1.6367
10	0.111	0.9	1.6367
11	0.122	0.9	1.6367
12	0.133	0.9	1.6367
13	0.143	0.9	1.6367

[a]Glass spherical particles with diameters of 74-88 μm. Air flow bulk velocity of 2.3298 m/s. Input volt of the feeder servomotor of 15 V. Particle vertical velocity 1.7 m/s.

Table 13.38. Data of solid-air flow parameters along the duct at constant electric field strength[a]

Test point i	Pressure drop $_1\Delta p_i$ (torr)	Particle horizontal velocity u_s (m/s)	Particle number density $n \times 10^{-8}$ [m^{-3}]
1	-	0.5	1.8823
2	0.015	0.6	1.5686
3	0.024	0.6	1.5686
4	0.033	0.6	1.5686
5	0.04	0.6	1.5686
6	0.05	0.6	1.5686
7	0.059	0.6	1.5686
8	0.067	0.6	1.5686
9	0.076	0.6	1.5686
10	0.085	0.6	1.5686
11	0.094	0.6	1.5686
12	0.103	0.6	1.5686
13	0.112	0.6	1.5686

[a]Glass spherical particles with diameters of 74-88 μm. Air flow bulk velocity of 1.466 m/s. Input volt of the feeder servomotor of 10 V. Particle vertical velocity 1.7 m/s.

Table 13.39. Data of solid-air flow parameters along the duct at constant electric field strength[a]

Test point i	Pressure drop $_1\Delta p_i$ (torr)	Particle horizontal velocity u_s (m/s)	Particle number density $n \times 10^{-8}$ $[m^{-3}]$
1	-	0.45	2.09146
2	0.017	0.455	2.06848
3	0.026	0.455	2.06848
4	0.035	0.455	2.06848
5	0.044	0.455	2.06848
6	0.053	0.455	2.06848
7	0.062	0.455	2.06848
8	0.071	0.455	2.06848
9	0.08	0.455	2.06848
10	0.09	0.455	2.06848
11	0.100	0.455	2.06848
12	0.110	0.455	2.06848
13	0.119	0.455	2.06848

[a]Glass spherical particles with diameters of 74-88 μm. Air flow bulk velocity of 1.19 m/s. Input volt of the feeder servomotor of 10 V. Particle vertical velocity 1.7 m/s.

Table 13.40. Data of solid-air flow parameters along the duct at constant electric field strength[a]

Test point i	Pressure drop $_1\Delta p_i$ (torr)	Particle horizontal velocity u_s (m/s)	Particle number density $n \times 10^{-8}$ $[m^{-3}]$
1	-	0.31	3.003
2	0.017	0.316	2.946
3	0.027	0.316	2.946
4	0.036	0.316	2.946
5	0.046	0.316	2.946
6	0.056	0.316	2.946
7	0.066	0.316	2.946
8	0.075	0.316	2.946
9	0.085	0.316	2.946
10	0.095	0.316	2.946
11	0.105	0.316	2.946
12	0.115	0.316	2.946
13	0.125	0.316	2.946

[a]Glass spherical particles with diameters of 74-88 μm. Air flow bulk velocity of 0.82766 m/s. Input volt of the feeder servomotor of 10 V. Particle vertical velocity 1.7 m/s.